RADC-TR-71-124
Technical Report, June 1971

ANGLE OF ARRIVAL CALCULATIONS AT 10.6μ

Sponsored By
Advanced Research Projects Agency
ARPA Order No. 1279

The Ohio State University

ElectroScience Laboratory

Department of Electrical Engineering
Columbus, Ohio 43212

Contractor: The Ohio State University
ElectroScience Laboratory
Contract Number: F30602-71-C-0132
Effective Date of Contract: 30 December 1970
Contract Expiration Date: 29 December 1971
Progress Code Number: 9E20

Principal Investigator: Dr. Stuart A. Collins, Jr.
Phone: 614-422-5045

Project Engineer: Edward K. Damon
Phone: 614-422-5953

Contracting Engineer: Raymond P. Urtz, Jr.
Phone: 315-330-3443

Rome Air Development Center
Air Force Systems Command
Griffiss Air Force Base, New York

BLANK PAGE

When US Government drawings, specifications, or other data are used for any purpose other than a definitely related government procurement operation, the government thereby incurs no responsibility nor any obligation whatsoever; and the fact that the government may have formulated, furnished, or in any way supplied the said drawings, specifications, or other data is not to be regarded, by implication or otherwise, as in any manner licensing the holder or any other person or corporation, or conveying any rights or permission to manufacture, use, or sell any patented invention that may in any way be related thereto.

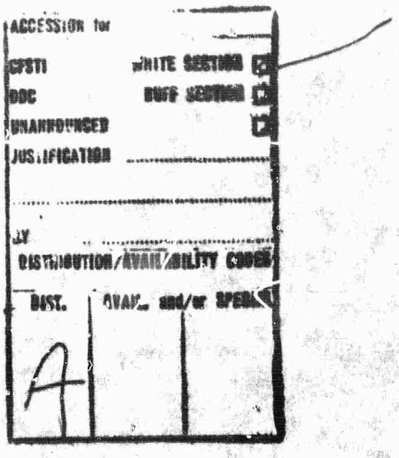

Do not return this copy. Retain or destroy.

UNCLASSIFIED
Security Classification

DOCUMENT CONTROL DATA - R&D

(Security classification of title, body of abstract and indexing annotation must be entered when the overall report is classified)

1. ORIGINATING ACTIVITY *(Corporate author)*: ElectroScience Laboratory, Department of Electrical Engineering, The Ohio State University, Columbus, Ohio 43212

2a. REPORT SECURITY CLASSIFICATION: UNCLASSIFIED

2b. GROUP:

3. REPORT TITLE: ANGLE OF ARRIVAL CALCULATIONS AT 10.6μ

4. DESCRIPTIVE NOTES *(Type of report and inclusive dates)*: Technical Report

5. AUTHOR(S) *(Last name, first name, initial)*: Logan R. Zintsmaster and Stuart A. Collins, Jr.

6. REPORT DATE	7a. TOTAL NO. OF PAGES	7b. NO. OF REFS
June 1971	117	28

8a. CONTRACT OR GRANT NO.: Contract F30602-71-C-0132

b. ARPA Order No. 1279

c.

d.

9a. ORIGINATOR'S REPORT NUMBER(S): ElectroScience Laboratory 3163-1

9b. OTHER REPORT NO(S) *(Any other numbers that may be assigned this report)*: RADC-TR-71-124

10. AVAILABILITY/LIMITATION NOTICES: Approved for Public Release: Distribution Unlimited.

11. SUPPLEMENTARY NOTES: Monitored by Raymond P. Urtz, Jr. 315 330-2122 RADC(OCSE), GAFB, NY 13440

12. SPONSORING MILITARY ACTIVITY: Advanced Research Projects Agency Washington, DC 20301

13. ABSTRACT

This report deals with the specification of the angular position of objects by measurement of the angles of arrival of light beams; and with the measurement uncertainties due to atmospheric turbulence. A survey of the literature is presented showing two approaches to angle of arrival, one for large aperture receivers and one for a single small aperture or a pair of pinholes. Pertinent defining equations are presented for both cases and values are calculated for arrival angle mean square measured with a large aperture and correlation of arrival angles for small apertures. A synonymity between the small correlation function and large aperture mean square angle of arrival is presented and used to present further large aperture mean square values. This provides a significant simplification in calculation and measurement capabilities. Finally the regions of accuracy are presented for the Rytov approximation which forms the basis for the numeric calculations.

DD FORM 1 JAN 64 1473

UNCLASSIFIED
Security Classification

14. KEY WORDS	LINK A		LINK B		LINK C	
	ROLE	WT	ROLE	WT	ROLE	WT
Angle of arrival						
10.6 microns						
Propagation						
Turbulence						
Large aperture						
Small aperture						

INSTRUCTIONS

1. ORIGINATING ACTIVITY: Enter the name and address of the contractor, subcontractor, grantee, Department of Defense activity or other organization *(corporate author)* issuing the report.

2a. REPORT SECURITY CLASSIFICATION: Enter the overall security classification of the report. Indicate whether "Restricted Data" is included. Marking is to be in accordance with appropriate security regulations.

2b. GROUP: Automatic downgrading is specified in DoD Directive 5200.10 and Armed Forces Industrial Manual. Enter the group number. Also, when applicable, show that optional markings have been used for Group 3 and Group 4 as authorized.

3. REPORT TITLE: Enter the complete report title in all capital letters. Titles in all cases should be unclassified. If a meaningful title cannot be selected without classification, show title classification in all capitals in parenthesis immediately following the title.

4. DESCRIPTIVE NOTES: If appropriate, enter the type of report, e.g., interim, progress, summary, annual, or final. Give the inclusive dates when a specific reporting period is covered.

5. AUTHOR(S): Enter the name(s) of author(s) as shown on or in the report. Enter last name, first name, middle initial. If military, show rank and branch of service. The name of the principal author is an absolute minimum requirement.

6. REPORT DATE: Enter the date of the report as day, month, year, or month, year. If more than one date appears on the report, use date of publication.

7a. TOTAL NUMBER OF PAGES: The total page count should follow normal pagination procedures, i.e., enter the number of pages containing information.

7b. NUMBER OF REFERENCES: Enter the total number of references cited in the report.

8a. CONTRACT OR GRANT NUMBER: If appropriate, enter the applicable number of the contract or grant under which the report was written.

8b, 8c, & 8d. PROJECT NUMBER: Enter the appropriate military department identification, such as project number, subproject number, system numbers, task number, etc.

9a. ORIGINATOR'S REPORT NUMBER(S): Enter the official report number by which the document will be identified and controlled by the originating activity. This number must be unique to this report.

9b. OTHER REPORT NUMBER(S): If the report has been assigned any other report numbers *(either by the originator or by the sponsor)*, also enter this number(s).

10. AVAILABILITY/LIMITATION NOTICES: Enter any limitations on further dissemination of the report, other than those imposed by security classification, using standard statements such as:

(1) "Qualified requesters may obtain copies of this report from DDC."

(2) "Foreign announcement and dissemination of this report by DDC is not authorized."

(3) "U. S. Government agencies may obtain copies of this report directly from DDC. Other qualified DDC users shall request through

_____."

(4) "U. S. military agencies may obtain copies of this report directly from DDC. Other qualified users shall request through

_____."

(5) "All distribution of this report is controlled. Qualified DDC users shall request through

_____."

If the report has been furnished to the Office of Technical Services, Department of Commerce, for sale to the public, indicate this fact and enter the price, if known.

11. SUPPLEMENTARY NOTES: Use for additional explanatory notes.

12. SPONSORING MILITARY ACTIVITY: Enter the name of the departmental project office or laboratory sponsoring *(paying for)* the research and development. Include address.

13. ABSTRACT: Enter an abstract giving a brief and factual summary of the document indicative of the report, even though it may also appear elsewhere in the body of the technical report. If additional space is required, a continuation sheet shall be attached.

It is highly desirable that the abstract of classified reports be unclassified. Each paragraph of the abstract shall end with an indication of the military security classification of the information in the paragraph, represented as *(TS), (S), (C), or (U).*

There is no limitation on the length of the abstract. However, the suggested length is from 150 to 225 words.

14. KEY WORDS: Key words are technically meaningful terms or short phrases that characterize a report and may be used as index entries for cataloging the report. Key words must be selected so that no security classification is required. Identifiers, such as equipment model designation, trade name, military project code name, geographic location, may be used as key words but will be followed by an indication of technical context. The assignment of links, rules, and weights is optional.

ANGLE OF ARRIVAL CALCULATIONS AT 10.6μ

Logan R. Zintsmaster
Stuart A. Collins, Jr.

The Ohio State University
ElectroScience Laboratory

This research was supported by the
Advanced Research Projects Agency
of the Department of Defense and was
monitored by Raymond P. Urtz, Jr.
RADC (OCSE), GAFB, NY 13440 under
Contract No. F30602-71-C-0132.

PUBLICATION REVIEW

This technical report has been reviewed and is approved.

Raymond P. Urtz Jr

RADC Project Engineer

ABSTRACT

This report deals with the specification of the angular position of objects by measurement of the angles of arrival of light beams; and with the measurement uncertainties due to atmospheric turbulence. A survey of the literature is presented showing two approaches to angle of arrival, one for large aperture receivers and one for a single small aperture or a pair of pinholes. Pertinent defining equations are presented for both cases and values are calculated for arrival angle mean square measured with a large aperture and correlation of arrival angles for small apertures. A synonymity between the small aperture correlation function and large aperture mean square angle of arrival is presented and used to present further large aperture mean square values. This provides a significant simplification in calculation and measurement capabilities. Finally the regions of accuracy are presented for the Rytov approximation which forms the basis for the numeric calculations.

TABLE OF CONTENTS

I. INTRODUCTION

When optical methods are used to observe an object through the atmosphere, the turbulence in the atmosphere may cause the apparent position of the object to fluctuate. This motion is caused by turbulence-induced fluctuations in the electromagnetic phase of the received wave. The received rays appear to change direction, so that the term angle of arrival fluctuations is used to describe this phenomenon. Knowledge of the angle of arrival fluctuations or its statistical properties is obviously necessary for analysis of systems specifying the accurate location of terrestrial or extraterrestrial object by optical means. It is also conceivable that, since angle of arrival fluctuations are induced by atmospheric turbulence, arrival angle statistics could be used as a convenient tool for study of turbulence characteristics.

The literature on angle of arrival is scattered and offers a wide range of views, approaches, and restrictions. For example there are two general approaches to arrival angle. The first considers the light detected by one or several minute apertures where phase is linear and amplitude is constant across the aperture. The quantities of interest for this approach are the arrival angle variance and correlation function, the mean being easily demonstrated to be zero. Alternatively there is consideration given to a single large aperture where the phase front is crinkled and the amplitude is not at all constant across the aperture. Generally the literature considers only the arrival angle variance for such a situation. For either approach the derivations based on the Rytov, the geometrical optics or other approximation may be given.

It is desirable to be able to predict the angle of arrival observed by both large and small aperture methods in terms of the propagation range, receiver and aperture characteristics, wavelength, and turbulence parameters; outer and inner scale and structure parameter. Some cases have been considered, but most are valid only for restricted ranges of the variables described earlier and all use several approximations.

The original object of this report was to examine the literature, to categorize these different situations and approximations, and to extend the results where feasible. This has been done. Basic extensions involve the computation of arrival angle functions using an index spectrum which accounts for the turbulence inner and outer scales.

In the process of performing these calculations, a synonymity between a small aperture correlation function and large aperture variance function was discovered. This synonymity provides great simplification in the calculation and measurement of these two quantities. The synonymity is presented and derived.

In the balance of the report there is first a general discussion of angle of arrival in Chapter II. This is followed by analytic expressions for angle of arrival statistical functions for first the small aperture approach (Chapter III) and then the large aperture approach (Chapter IV). Numerical results are presented in Chapter V in graphical form for a wide variety of cases along with a discussion of the limits of applicability of the Rytov approximation. Chapter VI deals with the synonymity of the large and small aperture approaches. Finally, the summary appears in Chapter VII.

II. GENERAL DISCUSSION OF ANGLE OF ARRIVAL

In this section we introduce in detail the various concepts and quantities associated with the two major approaches to angle of arrival. First the general measurement situation is considered. The small and large aperture situations are discussed to the extent that typical formulae are presented.

As generally used, the term angle of arrival is concerned with light emitted from an object and detected by a receiver. Pragmatically what is desired is a listing of the angular coordinates of the object with respect to some fixed reference system. In simple minded terms this can be obtained by imaging the object either with a lens (finite aperture) or a pinhole camera (very small aperture) and taking a line from the object through the center of the input aperture. The angular coordinates of the line then define the direction of the object. If there are no intervening refractive index fluctuations then the image of a point object may be a diffraction limited spot with a well defined center. The angular coordinates determined by the spot center can be very precisely chosen in such a case.

Complications arise because of random index fluctuations which cause the image to move around and/or to blur, depending on the physical details of the receiver. Random image motion is then interpreted as random fluctuations in the observed angle of arrival. Further fluctuations in the shape of the received image of a point object also cause fluctuations in the "center of gravity" of the image and may be interpreted as fluctuations of the angle of arrival. It is the statistical description of these random fluctuations in arrival angle caused by refractive index fluctuations that form the basic subject of this report.

It might be noted that the arrival angles measured with an optical instrument might, even in the absence of refractive index fluctuations, not be the true angular coordinates of the object. For example, if there were a refractive index gradient perpendicular to the light path, the light rays would be bent causing an anomolous indication of the true angles. This effect causes the phenomenon of "looming" and causes the sun to be visible after it has in actuality dropped below the horizon. Such effects will not be considered in the present report.

There are various approaches to the measurement and prediction of angle of arrival fluctuations. The measurements are generally categorized by the size of the aperture used for the receiver. Perhaps the cleanest approach involves the use of a very small pinhole sized aperture, as shown in Fig. 1. The pinhole is chosen sufficiently small so as to

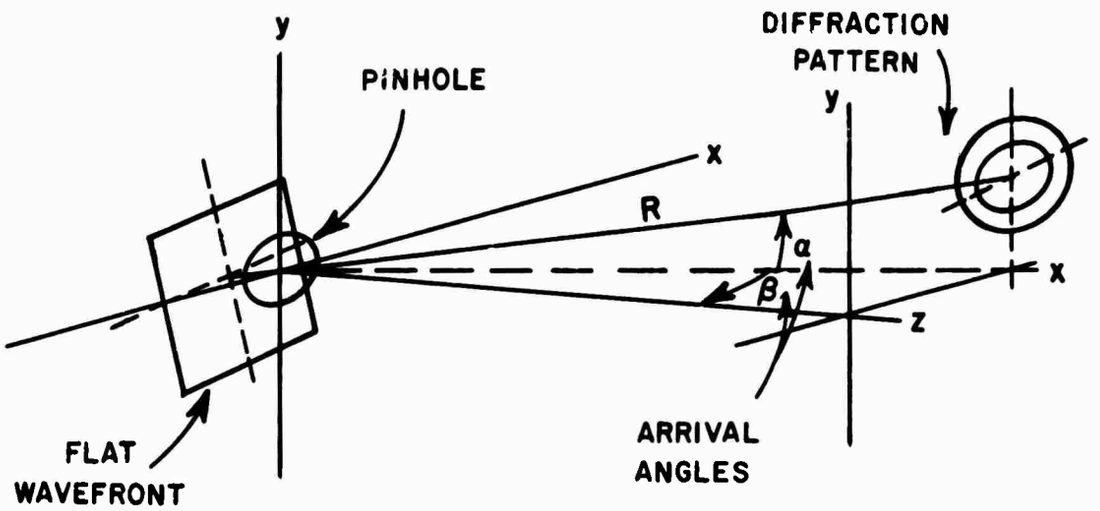

Fig. 1. Definition of small aperture angle of arrival.

be smaller than the spatial extent of any amplitude variation, and so as to contain only a flat wavefront. The displacement, d, of the center of the diffraction pattern in a given direction, then, is related to the angle of arrival, α, by the expression

$$d = R\alpha \tag{1}$$

where R is the distance from pinhole to diffraction pattern. In this situation, motion is caused only by phase fluctuations and not by amplitude fluctuations of the incoming light.

As shown in Fig. 1, two angles of arrival are defined; the elevation angle α, and the azimuth angle, β. One can consider various statistical functions of these angles. The simplest are the variances,* such as $\langle(\alpha-\langle\alpha\rangle)^2\rangle$. (The angular brackets indicate ensemble average.) There are also the two point arrival angle correlation functions for angles of arrival defined at two separate pinholes as shown in Fig. 2. Two such correlation functions exist, differentiated by the relative positions of the pinholes with respect to the direction of motion of the spots, as shown in Fig. 2. These will be discussed in more detail in the next section.

To calculate angle of arrival for a pinhole aperture the wavefront tilt is determined using the optical distance, L, or the equivalent electromagnetic phase shift, $S = k\,L$, along two rays through the turbulent atmosphere from the source to opposite sides of the receiver aperture. As shown in Fig. 3, we have for

$$(2) \qquad \alpha = \lim_{\eta \to 0} \frac{L(y+\eta)-L(y)}{\eta} = \frac{\partial L}{\partial y} = \frac{1}{k}\frac{\partial S}{\partial y}$$

The type of wave, i.e., plane, spherical, etc., will determine the functional form of L. The arrival angle variance $\langle\alpha^2\rangle$ is then expressed as the ensemble average of the square of the average product of two optical phases.

$$(2a) \qquad \langle\alpha^2\rangle = \frac{1}{k^2}\,\frac{\partial^2}{\partial y_1 \partial y_2}\,\langle S(y_1)\,S(y_2)\rangle\Big|_{y_1=y_2}$$

$$(2b) \qquad = \frac{1}{k^2}\,\frac{\partial^2}{\partial y_1 \partial y_2}\,B_s(y_2-y_1)\Big|_{y_1=y_2}$$

$$(2c) \qquad = \frac{-1}{2k^2}\,\frac{\partial^2}{\partial y_1 \partial y_2}\,D_s(y_2-y_1)\Big|_{y_1=y_2} .$$

*The terms angle of arrival variance and mean square value will be used interchangeably. They are identical since the mean is chosen to be zero. Similarily, the terms covariance and correlation function will be used interchangeably.

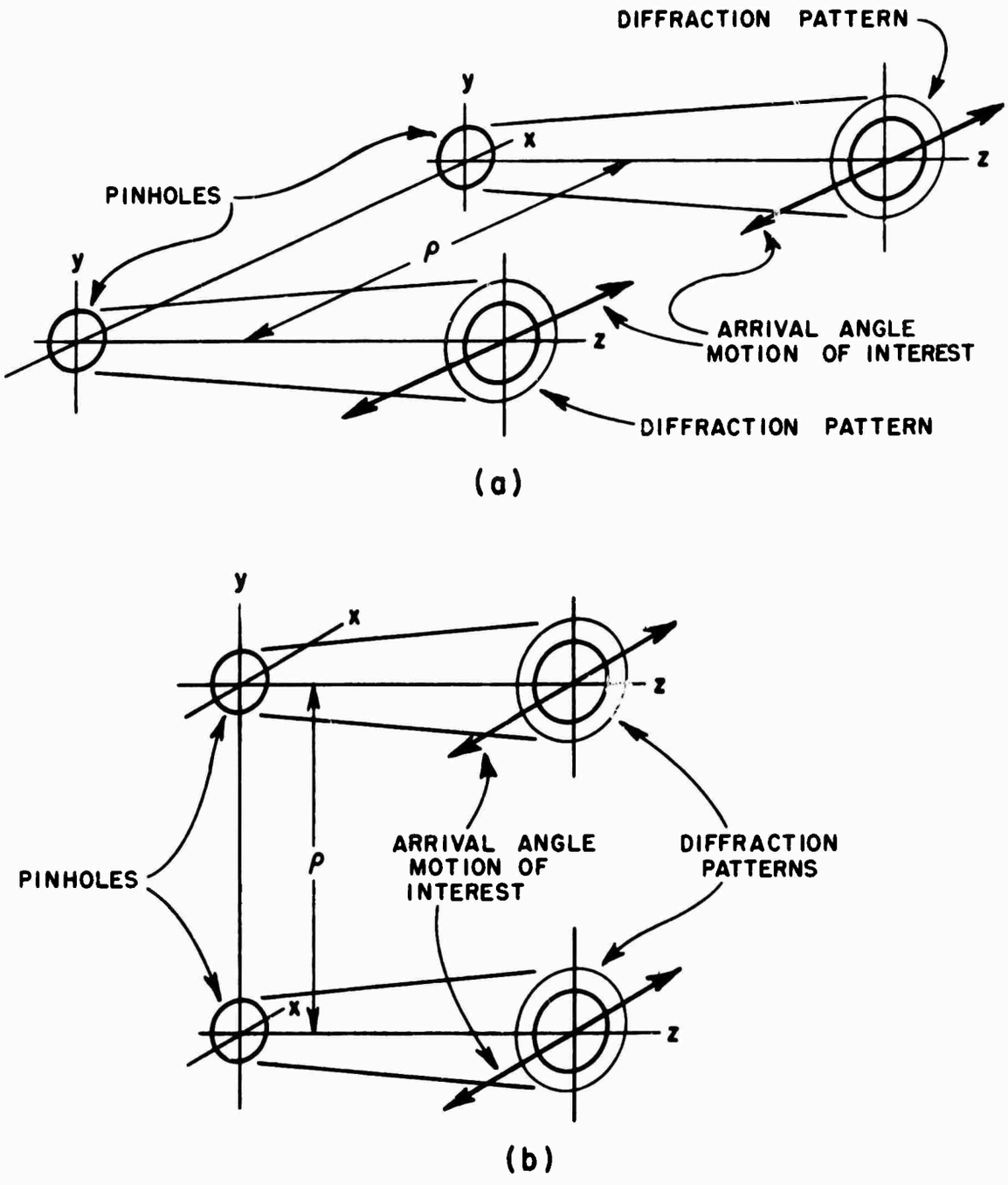

Fig. 2. Definition of small aperture angle of arrival correlation functions.

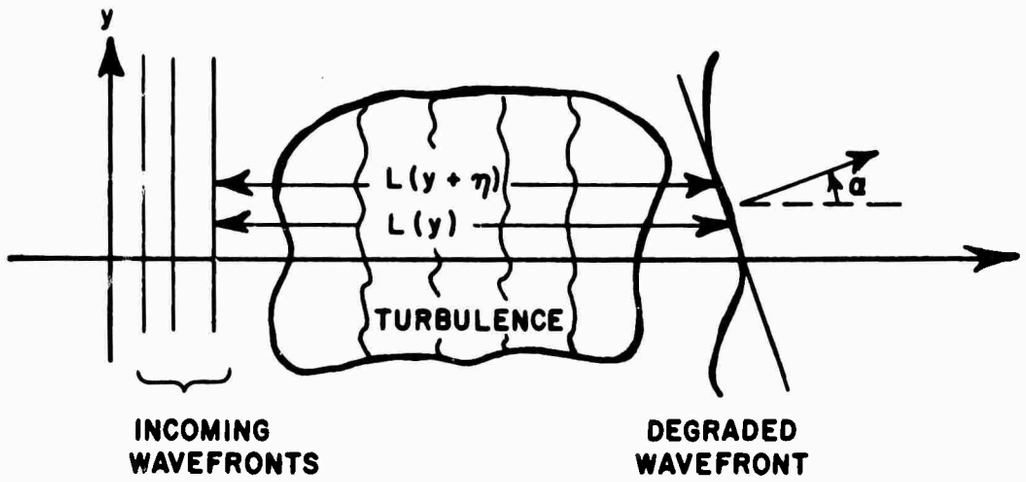

Fig. 3. Example of a small aperture angle of arrival calculation.

Equation (2a) uses the standard form for the phase correlation function

$$B_s(y_2-y_1) = \langle S(y_1)\, S(y_2)\rangle$$

and the associated structure function,

$$D_s(y_2-y_1) = 2\,[B_s(0) - B_s(y_2-y_1)]$$

written for a homogeneous atmosphere. Equations similar to Eq. (2c) will be used subsequently in the report.

Various techniques appear in the literature for the extensions and evaluation of Eq. (2c). They use expressions for the phase correlation or structure functions based on either the eikonal equation approach[1,2,3] of ray optics, or based on the Rytov approximation[4,5,6,7] (which reduces to the eikonal equation approach for short ranges). They also use a variety of correlation functions, structure functions or spatial spectra to represent the atmosphere.

An apparatus using pinhole apertures has one possible drawback as a practical device for angular coordinate measurement. That is the high source signal level required because of the small receiver aperture size. However it does provide a measure of arrival angle variance and correlation functions and, therefore, could be useful under controlled conditions where the source is available. Further the associated analytical calculations of the statistical quantities are simplified by being amplitude independent.

The other approach to arrival angle measurement employs a large aperture receiver with a lens to image the object as shown in Fig. 4.

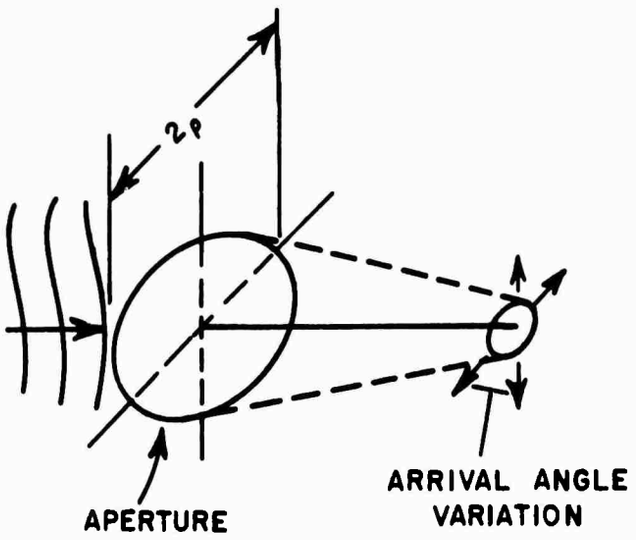

Fig. 4. Definition of large aperture angle of arrival.

This situation is more practical because of its light-gathering ability and subsequent increased sensitivity. However, it is more difficult to work with conceptually because of random spatial wavefront and amplitude fluctuations superimposed upon the no-turbulence fields. Thus, while the wavefront normal provided a reasonable indication of arrival angle for a pinhole aperture, there is very apt to be no unique wavefront normal for a large aperture. One can instead use the focused image, but amplitude and phase fluctuations about the mean wavefront of the incoming light cause motion of the image and deterioration of its shape, thereby increasing measurement uncertainty.

The quantity generally calculated for the large aperture approach is the arrival angle variance. To do this the instantaneous arrival angle is defined using some sort of optimization technique involving either fitting a smooth wavefront to the input fields[8,9] or defining the arrival angle to be that which has the maximum power.[10] These calculations are generally more complex than pinhole aperture calculations because of amplitude fluctuations over the input aperture, and because of the multiple integrations required.

As an indication of the approach to arrival angle calculations for large aperture situations, consider the following approximate calculation from Hufnagel.[8] Assume that to a good degree of approximation the wavefront at any instant can be described by a plane which matches the actual wavefront at four points, the intersection of the transverse coordinate axis with the aperture edge. Then the phase deviation along the x axis will be

$$\phi(\tfrac{D}{2}, 0) - \phi(-\tfrac{D}{2}, 0),$$

the linear variation of the wavefront from the x axis will be

$$[\phi(\tfrac{D}{2}, 0) - \phi(-\tfrac{D}{2}, 0)]/k$$

and the angle of tilt in the x direction will be

$$\alpha_x = [\phi(\tfrac{D}{2}, 0) - \phi(-\tfrac{D}{2}, 0)]/kD. \tag{3a}$$

Assuming that α_x has a zero mean, then its variance will be

$$\langle \alpha_x^2 \rangle = \langle (\phi(\tfrac{D}{2}, 0) - \phi(-\tfrac{D}{2}, 0) \rangle^2 / k^2 D^2 \tag{3b}$$

$$= D_s(D)/k^2 D^2 \tag{3c}$$

$$= 6.88(D/r_o)^{5/3}/k^2 D^2 \tag{3d}$$

$$= 6.88/k^2 r_o^{5/3} D^{1/3} \tag{3e}$$

where the phase structure function, $D_s(\rho)$, has been approximated by

$$D_s(\rho) = 6.88(\rho/r_o)^{5/3}$$

where r_o is Fried's transverse coherence length given by

$$r_o = (6.88/2.91\ k^2 L\ C_N^2)^{3/5}.$$

There are also other approaches to angle of arrival. One is an examination of arrival angle of light from a line source,[11,12] representing an extension of the small aperture approach. Another is a calculation of arrival angle variance using the Fokker-Plank equation[13] which represents a unique approach. These techniques will not be mentioned further. A few experimental measurements have been described by Coulman.[14,15]

To summarize, this section has presented a general discussion of various aspects of angle of arrival work, indicating the sources of uncertainty considered, and discussion of the two models for approaching the subject.

III. SMALL APERTURE ANGLE OF ARRIVAL CALCULATIONS

In this section the exact expression for the small aperture angle of arrival statistical quantities are derived and examined. They include two types of correlation functions and the mean square angle of arrival. The formalism to be presented follows closely that presented by Tatarski [5, section 40]*. As mentioned earlier, the small aperture technique assumes that the aperture is small enough that the aperture size has no effect on the angle of arrival indication. Thus, the phase difference across the aperture is assumed linear and the instantaneous amplitude is assumed to be independent of position in the aperture. Under these conditions the wavefront normal will uniquely define the angle of arrival at any instant of time.

Since the aperture size will not affect the final result, the optical path lengths to pairs of points are considered and the aperture sizes shrink to zero. The situation is shown in Fig. 5a. Using the definition in Eq. (2) we have

*For equations taken from [5], the section number and equation number will be given in parentheses.

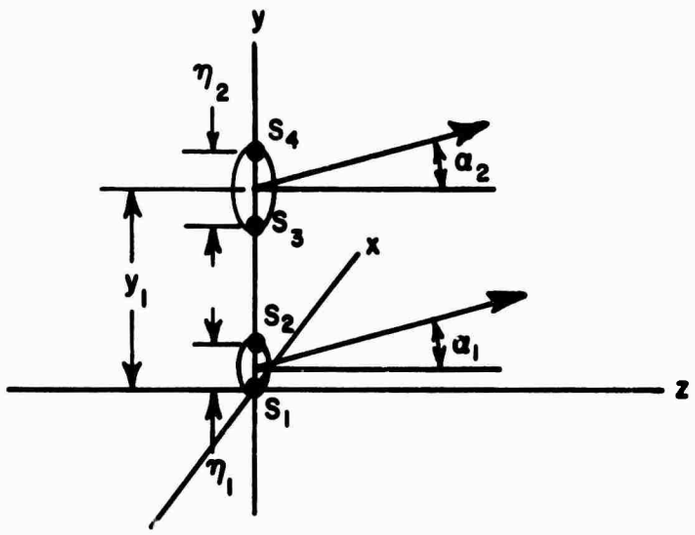

(a) B_α

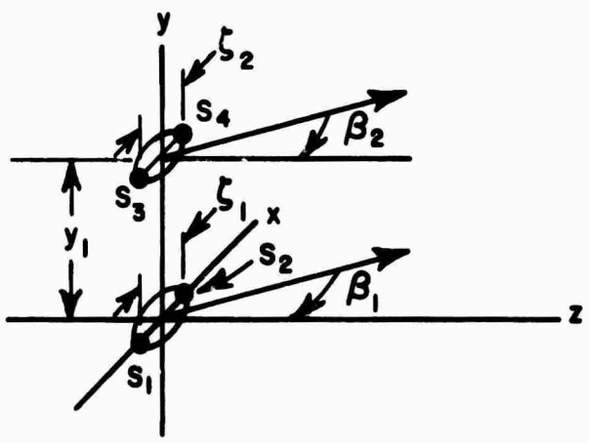

(b) B_β

Fig. 5. Geometry used to calculate small aperture arrival angle correlation functions.

(4a) $$\alpha_1 = \lim_{\eta_1 \to 0} \frac{[L(z,0,0) - L(z,0,\eta_1)]}{\eta_1}$$

$$= \lim_{\eta_1 \to 0} \frac{S_1 - S_2}{k\eta_1}$$

(4b) $$\alpha_2 = \lim_{\eta_2 \to 0} \frac{[L(z,0,y_1-\eta_2/2) - L(z,0,y_1 + \eta_2/2)]}{\eta_2}$$

$$= \lim_{\eta_2 \to 0} \frac{S_3 - S_4}{k\eta_2}$$

where

S_1 = phase at the point $(z,0,0)$

S_2 = phase at the point $(z,0,\eta_1)$

S_3 = phase at the point $(z,0,y_1-\eta_2/2)$

S_4 = phase at the point $(z,0,y_1+\eta_2/2)$.

These points are shown in Fig. 5a.

The elevation angle of arrival correlation is defined as

(5a) $$B_\alpha(y_1) = \langle\alpha(z,0,0)\ \alpha(z,0,y_1)\rangle.$$

To simplify we substitute Eq. (4a) and Eq. (4b) into Eq. (5a) giving

(5b) $$B_\alpha(y) = \lim_{\eta_1 \to 0} \frac{\langle (S_1 - S_2)(S_3 - S_4) \rangle}{k^2 \eta_1^2}$$

where $\eta_1 = \eta_2$.

Using the identity that

(5c) $$(S_1 - S_2)(S_3 - S_4) = 1/2[(S_1 - S_4)^2 + (S_2 - S_3)^2 - (S_1 - S_3)^2 - (S_2 - S_4)^2].$$

Equation (5b) can be written in terms of the phase structure function, $D_s(\rho)$.

(5d) $$B_\alpha(y_1) = \lim_{\eta_1 \to 0} \frac{1}{2k^2 \eta_1^2} [D_s(y_1+\eta_1) + D_s(y_1-\eta_1) - 2D_s(y_1)].$$

Expanding $D_s(y_1 \pm \eta_1)$ in a Taylor series we have

(5e) $$D_s(y_1 \pm \eta_1) = D_s(y_1) \pm \eta_1 D_s'(y_1) + 1/2 \eta_1^2 D_s''(y_1) + \cdots$$

which, when substituted into Eq. (5d), yields [5, (40.35)] written as Eq. (5f)

(5f) $$B_\alpha(y_1) = \frac{1}{2k^2} D_s''(y_1)$$

where $D_s(y)$ is the phase structure function and the primes denote derivatives with respect to the argument.

The azimuth angle of arrival, β, shown in Fig. (5b) is calculated in a similar manner. Using the points shown in Fig. (5b) we have

(6a) $$\beta_1 = \lim_{\zeta_1 \to 0} \frac{(S_1 - S_2)}{k\zeta_1}$$

(6b) $$\beta_2 = \lim_{\zeta_2 \to 0} \frac{(S_3 - S_4)}{k\zeta_2}$$

where

S_1 = phase at the point $(z, -\zeta_{1/2}, 0)$

S_2 = phase at the point $(z, +\zeta_{1/2}, 0)$

S_3 = phase at the point $(z, -\zeta_{2/2}, y_1)$

S_4 = phase at the point $(z, +\zeta_{2/2}, y_1)$

and with $\zeta_1 = \zeta_2$

(6c) $$B_\beta(y_1) = \lim_{\zeta_1 \to 0} \frac{1}{k^2\zeta_1^2} \langle (S_2 - S_1)(S_4 - S_3) \rangle .$$

Using the identity in Eq. (5c) we again have the correlation in terms of the phase structure function. The only difference is that

(6d) $$\langle (S_1 - S_4)^2 \rangle = D_s \left(\sqrt{\zeta_1^2 + y_1^2} \right).$$

Then Eq. (6c) becomes

(6e) $$B_\beta(y_1) = \lim_{\zeta_1 \to 0} \frac{1}{k^2\zeta_1^2} \left[D_s \left(\sqrt{y_1^2 + \zeta_1^2} \right) - D_s(y_1) \right].$$

Since the limit will force ζ to be arbitrarily small the square root in Eq. (6e) can be expanded in a power series.

(6f) $$\left(\sqrt{y_1^2 + \zeta_1^2} \right) = y_1 + \frac{\zeta_1^2}{2y_1} + \cdots \quad .$$

Using the Taylor's series expansion in Eq. (5e) we have

$$(6g) \qquad D_s\left(\sqrt{y_1^2 + \zeta_1^2}\right) = D_s(y_1) + \frac{\zeta_1^2}{2y_1} D_s'(y_1) + \cdots \quad .$$

When substituted into Eq. (6e) the resulting expression is [5,(40.38)], written as Eq. (6h)

$$(6h) \qquad B_\beta(y_1) = \frac{1}{2k^2} \frac{D_s'(y_1)}{y_1} \quad .$$

Comparing Eqs. (5f) and (6h) we see that the interpair displacement with respect to the pair separation determines the final form for $B_\alpha(y_1)$ and $B_\beta(y_1)$. To calculate $B_\alpha(y_1)$ the displacement was parallel to the separation. On the other hand, the displacement was transverse to the separation when $B_\beta(y_1)$ was calculated.

The dependence on the interpair displacement when the interpair direction is neither parallel or perpendicular to the interpoint direction has been found explicitly by Strobehn and Clifford.[7] For sample points oriented as in Fig. 6 we have

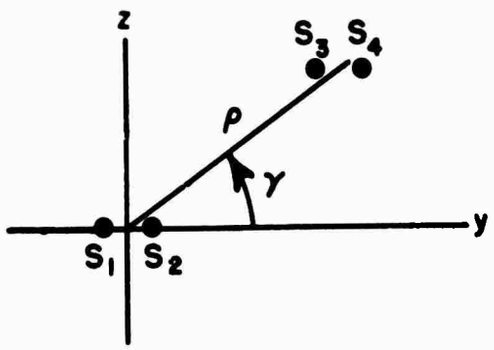

Fig. 6. Generalized geometry to calculate small aperture arrival angle correlation functions.

$$(7) \qquad B_\varepsilon(\rho) = \frac{1}{2k^2} D_S''(\rho) \cos^2\gamma + \frac{1}{2k^2} \frac{D_S'(\rho)}{\rho} \sin^2\gamma$$

where

ε = angle of arrival of interest

γ = angle between interpair displacement and pair separation.

For $\gamma = 0$ and $\pi/2$ we have the expressions for $B_\alpha(\rho)$ and $B_\beta(\rho)$ respectively.

The smallness criterion for the aperture size can now be considered. Recall that it was assumed that the aperture size had no effect on the angle of arrival. From Eqs. (5f) and (6h) we see that for $D_S(\rho) \alpha \rho^2$, the angle of arrival correlation is independent of ρ. It is well known that for the Kolmogorov refractive index fluctuation spectrum, $D_S(\rho)$ has this form for ρ less than the turbulence inner scale. Thus, these results apply to apertures smaller than the inner scale. For apertures larger than this, the large aperture method should be used.

In this section the basic equations for small aperture angle of arrival correlation functions have been derived. These expressions will be used in sections V and VI.

IV. LARGE APERTURE ANGLE OF ARRIVAL CALCULATIONS

In this section pertinent formulas for the large aperture angle of arrival mean square value are derived and discussed. The linear phase and constant amplitude assumptions made for the small aperture angle of arrival calculations begin to break down as the aperture becomes larger than the inner scale. The phase front becomes more distorted than can be accurately described with a linear wave tilt. Secondly, amplitude distortions become significant. These problems have been considered in part by various workers.

Two major approaches are used, both involving an extremum technique. The first approach to define the instantaneous arrival angle as the direction for which the instantaneous power is the maximum. The second is to fit expression for the instantaneous wavefront to a series of polynomial surfaces using a least squares fit.

One of the polynomials is a flat plane, so that the normal to the plane then is taken as the direction of the wave. Both approaches give the same basic expressions for the instantaneous angle of arrival direction. The derivations will now be outlined.

The first approach to be considered is that which uses the direction of maximum instantaneous power to define angle of arrival[10]. The technique is to split the mathematical expression for the electromagnetic phase into two parts, one representing a plane wave and the other representing the deviations from the plane wave. The direction of the plane wave normal is chosen to maximize the expression for the power. It is assumed that the deviations of the electromagnetic phase from the plane wave value are small and that amplitude fluctuations over the input aperture are neglegible. Thus, let the field arriving at the receiving aperture be

$$Ee^{i\phi(\bar{r})},$$

where $\bar{r} = (x,y)$ denotes the transverse position of the input aperture. The term $\phi(\bar{r})$ is equivalent to $S(x,y,z)$ in the previous section. Then the component of the field in the direction with transverse spatial frequency $\bar{\kappa}$ is

$$e(\bar{\kappa}) = \int d\bar{r}\, Ee^{i(\phi(r) - \bar{\kappa} \cdot \bar{r})} \tag{8}$$

and the power in the same direction is

$$P(\bar{\kappa}) = \frac{1}{Z_o}\left| \int d\bar{r}\, Ee^{i(\phi(\bar{r}) - \bar{\kappa} \cdot \bar{r})} \right|^2 . \tag{9}$$

Following Heidbredder,[10] we define $\Delta(\bar{r})$ the phase difference from a flat plane,

$$\Delta(\bar{r}) = \phi(\bar{r}) - \bar{\kappa} \cdot \bar{r}.$$

Our first object is to find an expression for the value of $\bar{\kappa}$ for which $P(\bar{\kappa})$ will be maximum. We assume that the phase difference $\Delta(\bar{r})$ from that optimum value will be small. Then, rewriting Eq. (9),

$$(10a) \qquad P(\bar{\kappa}) = \frac{1}{Z_0} \left| \int d\bar{r}\, E e^{i\Delta(\bar{r})} \right|^2$$

$$(10b) \qquad P(\bar{\kappa}) = \frac{1}{Z_0} \left\{ \int d\bar{r}\, E \cos\Delta(\bar{r}) \right\}^2 + \frac{1}{Z_0} \left\{ \int d\bar{r}\, E \sin\Delta(\bar{r}) \right\}^2$$

$$(10c) \qquad \doteq \frac{1}{Z_0} \left\{ \int d\bar{r}\, (1 - \frac{\Delta^2}{2})\, E \right\}^2 + \frac{1}{Z_0} \left\{ \int d\bar{r}\, \Delta E \right\}^2$$

where the r dependence of Δ is implied. Differentiating Eq. (10c) with respect to κ_x to find the optimum value we find

$$(11a) \qquad \frac{\partial P}{\partial \kappa_x} = 0 = 2 \int d\bar{r}_1\, (1 - \frac{\Delta^2}{2})\, E \int d\bar{r}_2\, \frac{\partial \Delta}{\partial \kappa_x} E$$

$$+ \int d\bar{r}_1\, \Delta E \int d\bar{r}_2\, \frac{\partial \Delta}{\partial \kappa_x} E$$

$$(11b) \qquad \doteq 2 \int d\bar{r}_1\, E \int d\bar{r}_2\, (\phi_2 - \bar{\kappa} \cdot \bar{r}_2)\, x_2\, E$$

$$- \int d\bar{r}\, E \int d\bar{r}_2\, E x_2 .$$

The aperture is assumed to be symmetric so that the integrals over odd powers of x and y are zero. Thus the integral in the second term and the integral over $x_2 y_2$ in the first term vanish. Solving for κ_x then gives

$$(12) \qquad \kappa_x = \frac{\int d\bar{r}\, \phi(\bar{r})\, x\, E}{\int d\bar{r}\, x^2\, E} \quad .$$

The mean value of κ_x is taken to be zero. This is based on the assumption that the atmospheric turbulence is isotropic so that the mean value of $\phi(\bar{r})$ is zero, i.e., fluctuations of phase are equally likely.

The variance of κ_x and the associated component of the angle of arrival, α_x

$$\alpha_x = \frac{\kappa_x}{k} \tag{13}$$

are given by

$$\langle \alpha_x^2 \rangle = \frac{\langle \kappa_x^2 \rangle}{k^2} = \frac{\iint d\bar{r}_1\, d\bar{r}_2\, E_1\, E_2 \langle \phi(\bar{r}_1)\, \phi(\bar{r}_2) \rangle\, x_1 x_2}{k^2 \left| \int d\bar{r}\, x^2\, E \right|^2} \tag{14}$$

Identifying the phase correlation function

$$B_s(\overline{r_2 - r_1}) = \langle \phi(r_1)\, \phi(r_2) \rangle$$

relating it to the phase structure function

$$B_s(\overline{r_2 - r_1}) = \frac{1}{2} \left[D_s(\infty) - D_s(\overline{r_2 - r_1}) \right] \tag{15}$$

and again using the fact that the aperture is symmetric gives

$$\langle \alpha_x^2 \rangle = - \frac{\iint d\bar{r}_1\, d\bar{r}_2\, E_1\, E_2\, D_s(\overline{r_s - r_1})\, x_1\, x_2}{2k^2 \left| \int d\bar{r}\, x^2\, E \right|^2} \tag{16}$$

Equation (16) is generally evaluated for circular apertures. To obtain the appropriate expression for that case first define

$$r_1 = |\bar{r}_1| \qquad r_2 = |\bar{r}_2|$$

$$x_1 = r_1 \cos\theta_1 \qquad x_2 = r_2 \cos\theta_2$$

so that the denominator of Eq. (16) is (taking the amplitude E to be constant),

$$(17) \qquad 2k^2 \left| \int_0^R \int_0^{2\pi} dr_1\, d\theta\, r_1^3 \cos^2\theta\, E \right|^2 = 2k^2 \left(\pi \frac{R^4}{4}\right)^2 E^2.$$

The expression for the arrival angle variance is then

$$(18) \langle \alpha_x^2 \rangle = - \frac{\int_0^R \int_0^{2\pi} r_1^2\, dr_1\, d\theta \int_0^R \int_0^{2\pi} r_2^2 dr_2 d\theta_2 E_1 E_2 \cos(\theta_1-\theta_2) D_s\left(\sqrt{r_1^2+r_2^2-2r_1 r_2 \cos(\theta_2-\theta_1)}\right)}{2k^2\ (\pi R^4/4)^2\ E^2}.$$

After further defining

$$\gamma = \theta_2 - \theta_1$$

$$\beta = 1/2(\theta_2+\theta_1)$$

and performing the β integral, the result is,

$$(19) \qquad \langle \alpha_x^2 \rangle = - \frac{\int_0^R dr_1 r_1^2 \int_0^R dr_2\, r_2^2 \int_0^{\pi} d\gamma \cos\gamma\, D_s\left(\sqrt{r_1^2+r_2^2-2r_1 r_2 \cos\gamma}\right)}{\pi\, k^2 (R^4/4)^2}.$$

Equation (19) will be used in the next section for numerical evaluations. Heidbreder evaluates Eq. (10) with various symmetric aperture weighting functions $W(r_1)W(r_2)$ multiplying the phase structure function finding relatively small changes for gaussian weighting functions with half-widths the order of the radius. He also finds some small correlation between the plane wave fluctuations of the phase front and the residual phase for a one dimensional aperture (infinitesimal in the other dimension).

The second approach, due to Fried,[9] in which the expression for the instantaneous wavefront is fitted to a series of polynomials will now be considered. The polynomials are similar to the Zernike polynomials, orthogonal over a circular area. The first six are

$$F_1(\bar{r}) = \frac{1}{\sqrt{\pi R^2}} \quad , \qquad F_4(\bar{r}) = \frac{(x^2 - y^2)}{\sqrt{\pi R^{6/12}}}$$

$$F_2(\bar{r}) = \frac{x}{\sqrt{\pi R^{4/4}}} \quad , \qquad F_5(\bar{r}) = \frac{(x^2 - y^2)}{\sqrt{\pi R^{6/6}}} \tag{20}$$

$$F_3(\bar{r}) = \frac{y}{\sqrt{\pi R^{4/4}}} \quad , \qquad F_6(\bar{r}) = \frac{xy}{\sqrt{\pi R^{6/24}}}$$

they are orthonormal so that

$$\int d\bar{r}\, W(\bar{r})\, F_n(\bar{r})\, F_m(\bar{r}) = \delta_{mn} \tag{21}$$

where

$$W(\bar{r}) = \begin{cases} 1 & \bar{r} \leq R \\ 0 & \bar{r} > R \end{cases} \quad . \tag{22}$$

The wavefront $\phi(\bar{r})$ is then expressed as an infinite series of these polynomials:

$$\phi(\bar{r}) = \sum_{n=1}^{\infty} a_n F_n(\bar{r}).$$

The second and third polynomials represent the flat of the wavefront. Thus the spatial frequency and arrival angle associated with the flat componant are given by

$$\bar{\alpha} = \frac{\bar{\kappa}}{k} = \overline{\text{grad}} \{a_2 F_2(\bar{r}) + a_3 F_3(\bar{r})\} \tag{23a}$$

$$= \frac{1}{\sqrt{\pi R^4/4}} \{a_2 \hat{x} + a_3 \hat{y}\}$$

($\hat{x}$ and $\hat{y}$ are unit vectors.) Further, the variance of the angle of arrival in the x direction is

$$\langle \alpha_x^2 \rangle = \frac{1}{\pi R^4/4} \langle a_2^2 \rangle \quad . \tag{24}$$

The polynomial series is fitted to the wavefront at any instant by choosing the coefficients so as to minimize the mean square deviation between the series and the wavefront proper:

$$\frac{d}{da_2} \int d\bar{r}\, W(\bar{r}) \left[\phi(\bar{r}) - \sum_{n=1}^{\infty} a_n F_n(\bar{r})\right]^2 = 0. \tag{25}$$

Squaring the term in the brackets, performing the indicated differentiation, and solving for a_2 gives

$$a_2 = \int d\bar{r}\, W(\bar{r})\, \phi(\bar{r})\, F_\infty(\bar{r}). \tag{26}$$

Equation (26) can be shown to be comparable with the expression by Heidbreder. To do that, use the expression for $F_2(\bar{r})$ in Eq. (20) to give a_2 in Eq. (26) and substitute into Eq. (24). After using Eq. (15) to simplify, the result is

$$(27) \qquad \langle \alpha_x^2 \rangle = \frac{1}{2k^2(\pi R^4/4)^2} \iint d\bar{r}_1 \, d\bar{r}_2 \, W(\bar{r}_1) \, W(\bar{r}_2) \, x_1 x_2 \, D_s(\overline{r_2 - r_1})$$

which coincides very nicely with Eq. (18).

Fried and Heidbreder both evaluate the angle of arrival variance assuming that the wave structure function is approximated by the phase structure function, i.e., the range is sufficiently short that amplitude effects are negligible:

$$(28) \qquad D_W(r) = D_S(r) = 6.88\left(\frac{r}{r_o}\right)^{5/3}$$

where r_o is Fried's transverse coherence length given by

$$(29) \qquad r_o = (6.88/2.91 \, k^2 L C_N^2)^{3/5} \quad .$$

The result is

$$(30a) \qquad \langle \alpha_x^2 \rangle = 7.064/k^2 \, r_o^{5/3} \, D^{1/3}$$

$$(30b) \qquad = 1.026 \times 6.88/k^2 \, r_o^{5/3} \, D^{1/3}.$$

Equation (30b) agrees closely with the approximate expression derived by Hufnagel[8] (Eq. (3e)).

To account for amplitude effects the phase structure function can be replaced with the wave structure function and the polynomial series now has complex coefficients.[9] One drawback as explained by Fried is that the results are difficult to interpret.

Concluding, we see that the angle of arrival for a large aperture depends on the phase structure function also. Thus, these results are as general as the approximations used to calculate the phase structure function. A specific phase structure function more general than Eq. (28) will now be used to calculate extended numeric results.

V. NUMERIC CALCULATIONS OF ANGLE OF ARRIVAL

In this section the general expressions given previously for arrival angle mean square and correlation functions are evaluated. The effects of such parameters as outer and inner scale, range and type of wave are demonstrated for both large and small aperture cases. The range of parameters covered is such as to give a reasonably complete set of curves for comparison with experiments 10.6μ performed at the RADC Laser Propagation Range.

To proceed with the evaluation, we note that the angle of arrival statistical functions in Eqs. (2c), (5f), and (6h) are all in terms of the phase structure function. To evaluate these expressions an integral form of $D_S(\rho)$ is used,[5]

$$(31) \qquad D_S(\rho) = 4\pi^2 k^2 L \int_0^\infty [1 - J_0(\kappa\rho)] \left[1 + \frac{k}{\kappa^2 L} \sin \frac{\kappa^2 L}{k}\right]^2 \cdot \Phi_N(\kappa)\, \kappa\, d\kappa$$

where $k = \frac{2\pi}{\lambda}$

ρ = separation

L = propagation range

$\Phi_N(\kappa)$ = three dimensional refractive index fluctuation spectrum.

For a spherical wave, a similar expression was derived by Carlson and Ishimaru.[16]

$$(32) \qquad D_s(\rho) = 8\pi^2 k^2 \int_0^\infty [1 - J_0(\kappa\rho)] \int_0^L \left\{ \frac{L}{\eta} \cos \left(\frac{L(L-\eta)\kappa^2}{2k\eta} \right) \right\}^2 \Phi_N \left(\frac{\kappa L}{\eta} \right) d\eta \, \kappa d\kappa .$$

Both of these expressions are the result of using the Rytov approximation and are valid where the Rytov approximation is valid. This validity will be discussed later.

Both expressions (31) and (32), use the refractive index fluctuation spectrum $\Phi_N(\kappa)$. Several models for Φ_N have been proposed and these are discussed in Appendix A. For the calculations in this report, the model used is

$$(33) \qquad \Phi_N(\kappa) = .033 \, C_N^2 \, \frac{e^{-\kappa^2/\kappa_m^2}}{(\kappa^2 + \kappa_0^2)^{11/6}}$$

where $\kappa_m = 5.92/\ell_0$

ℓ_0 = inner scale of the turbulence

$\kappa_0 = 1/L_0$

L_0 = outer scale of the turbulence.

Using Eq. (31) in the expressions derived earlier in Eqs. (2c), (5f), and (6h) we have for the small aperture angle of arrival expressions

$$(34) \qquad \langle \alpha^2 \rangle = \pi^2 L \int_0^\infty \left[1 + \frac{k}{\kappa^2 L} \sin \frac{\kappa^2 L}{k} \right] \kappa^3 \, \Phi_N(\kappa) \, d\kappa$$

$$(35) \qquad B_\beta(\rho) = 2\pi^2 L \int_0^\infty \left[1 + \frac{k}{\kappa^2 L} \sin \frac{\kappa^2 L}{k}\right] \frac{J_1(\kappa\rho)}{\kappa\rho} \kappa^3 \Phi_N(\kappa)\, d\kappa$$

$$(36) \qquad B_\alpha(\rho) = 2\pi^2 L \int_0^\infty \left[1 + \frac{k}{\kappa^2 L} \sin \frac{\kappa^2 L}{k}\right] J_0(\kappa\rho)\, \kappa^3 \Phi_N(\kappa)\, d\kappa - B_\beta(\rho).$$

Similar expressions were also obtained by Strobehn.[17] The corresponding equations for the spherical wave case can be found by making the substitution

$$(37) \qquad L\left[1 + \frac{k}{\kappa^2 L} \sin \frac{\kappa^2 L}{k}\right] \Phi_N(\kappa) \rightarrow 2 \int_0^L \left[\frac{L}{\eta} \cos\left(\frac{L(L-\eta)\kappa^2}{2k\eta}\right)\right]^2 \cdot \Phi_N\left(\frac{\kappa L}{\eta}\right) d\eta$$

in Eqs. (34)-(36). These expressions are suitable for numeric evaluation since $\Phi_N(\kappa)$ approaches zero rapidly for a finite value of κ so that the upper limit of the integrals can be made finite.

As noted in Appendix B, when the outer scale, L_0 becomes infinite, Eq. (33) reduces to the Kolmogorov spectrum with inner scale, ℓ_0,[5] and Eqs. (32) and (34)-(36) can be integrated analytically. Thus, defining

$$D = \frac{\kappa_m^2 L}{k} \quad \text{and} \quad g = \frac{\kappa_m^2 \rho^2}{4},$$

we have

(38) $$B_\beta(\rho) = 1.028\, L\, C_N^2\, \kappa_m^{1/3} \left\{ \frac{5}{6}\, {}_1F_1\left(\frac{1}{6},2,-g\right) + D^{-1/6} \left[\cos\frac{\pi}{12}\, \mathrm{Re}\left\{ {}_1F_1\left(-\frac{5}{6},2,\frac{ig}{D}\right)\right\} + \sin\frac{\pi}{12}\, \mathrm{Im}\left\{ {}_1F_1\left(-\frac{5}{6},2,\frac{ig}{D}\right)\right\}\right]\right\}$$

(39) $$B_\alpha(\rho) = B_\beta(\rho) - .226\, L\, C_N^2\, \kappa_m^{7/3} \left\{ \frac{1}{6}\, {}_1F_1\left(\frac{7}{6},3,-g\right) + D^{-7/6} \left[\sin\frac{\pi}{12}\, \mathrm{Re}\left\{ {}_1F_1\left(\frac{1}{6},3,\frac{ig}{D}\right)\right\} - \cos\frac{\pi}{12}\, \mathrm{Im}\left\{ {}_1F_1\left(\frac{1}{6},3,\frac{ig}{D}\right)\right\}\right]\right\}$$

(40) $$\langle\alpha^2\rangle = \langle\beta^2\rangle = L\, C_N^2\, \kappa_m^{1/3}\, (.904 + 1.088\, D^{-1/6} \cos\frac{\pi}{12}).$$

For large ρ, the asymptotic forms are

(41) $$B_\beta(\rho) \approx 2.43\, L\, C_N^2\, \rho^{-1/3}$$

(42) $$B_\alpha(\rho) \approx 1.62\, L\, C_N^2\, \rho^{-1/3}.$$

The small aperture angle of arrival mean square and correlation function were calculated for many cases. These will now be presented. Equations (38), (39), and (40) were evaluated for several typical values of range and inner scale. The results are shown in Figs. 7-34. The parameters used were chosen to agree with those that might be present at the RADC Laser Propagation Range. For example the ranges of 304.8 m, 914.4 m and 1524 m correspond respectively to 1000 ft, 3000 ft and 5000 ft, all ranges used at the RADC Range.

First the mean square angle of arrival is considered. Figures 7 and 8 show it as a function of range, first for two inner scales and infinite outer scale as given in Eq. (40), and second for three different outer scales taking the inner scale as 1 mm and numerically integrating Eqs. (33) and (34). For simplicity the mean square is normalized to the refractive index structure parameter, C_N^2. It is noted that the mean square increases as the outer scale increases and as the inner scale decreases. In either case the range of turbulent spatial frequencies interacting with the light beam has increased, thus increasing the effect. Of the two scales the inner scale has the larger effect on the arrival angle flucuations, because, while the smaller scale eddies are less prevalent, they scatter light at the greatest angles.

Typical angle of arrival correlation curves are shown in Figs. 9, 10, and 11, evaluated from Eqs. (34), (35), and (36). They show the effect of inner scale on the correlation functions. Figures 9 and 10 show the autocorrelation functions $B_\alpha(\rho)/\langle\alpha^2\rangle$ and $B_\beta(\rho)/\langle\alpha^2\rangle$ for a range of 304.8 m, infinite outer scale and inner scales of 1 cm and 1 mm. Figure 11 shows the left hand portion of Fig. 10 in detail to display the fine structure of the initial roll-offs. The rapid roll-offs of the autocorrelations, as the separation is increased slightly from zero, is evident. However, as the separation exceeds the inner scale, the curves level off. The roll-off and break point are strongly dependent on the inner scale.

The inner scale dependence can be explained. As noted earlier for $\rho < \ell_0$, the phase structure function obeys a square power law and the correlations $B_\beta(\rho)$ and $B_\alpha(\rho)$ are equal to the mean square angle of arrival. From a physical standpoint we note that the inner scale is a characteristic dimension of the smallest blob in a turbulence cell. Thus, we expect the angle of arrival correlation for $\rho < \ell_0$ to be nearly the same as the mean square value. It is very likely, that the two regions considered on the wavefront were perturbed by the same blob or a closely correlated blob. As the separation is increased and approaches the inner scale the number of blobs increases rapidly in comparison to the increase in separation. However, as the separation becomes sufficiently large the total number of blobs masks the increase in blobs. Thus, the roll-off of the correlation slows down and levels off.

The inner scale dependence can be derived from the expressions used earlier. Since we are dealing with an inner scale phenomenon the outer scale can be ignored and the analytic expressions are used. Thus, for $\rho << \ell_0$ we have

$$\frac{B_\beta(\rho)}{\langle\beta^2\rangle} = 1 - .0206 \left(\frac{\rho}{\ell_0}\right)^{2} \tag{43}$$

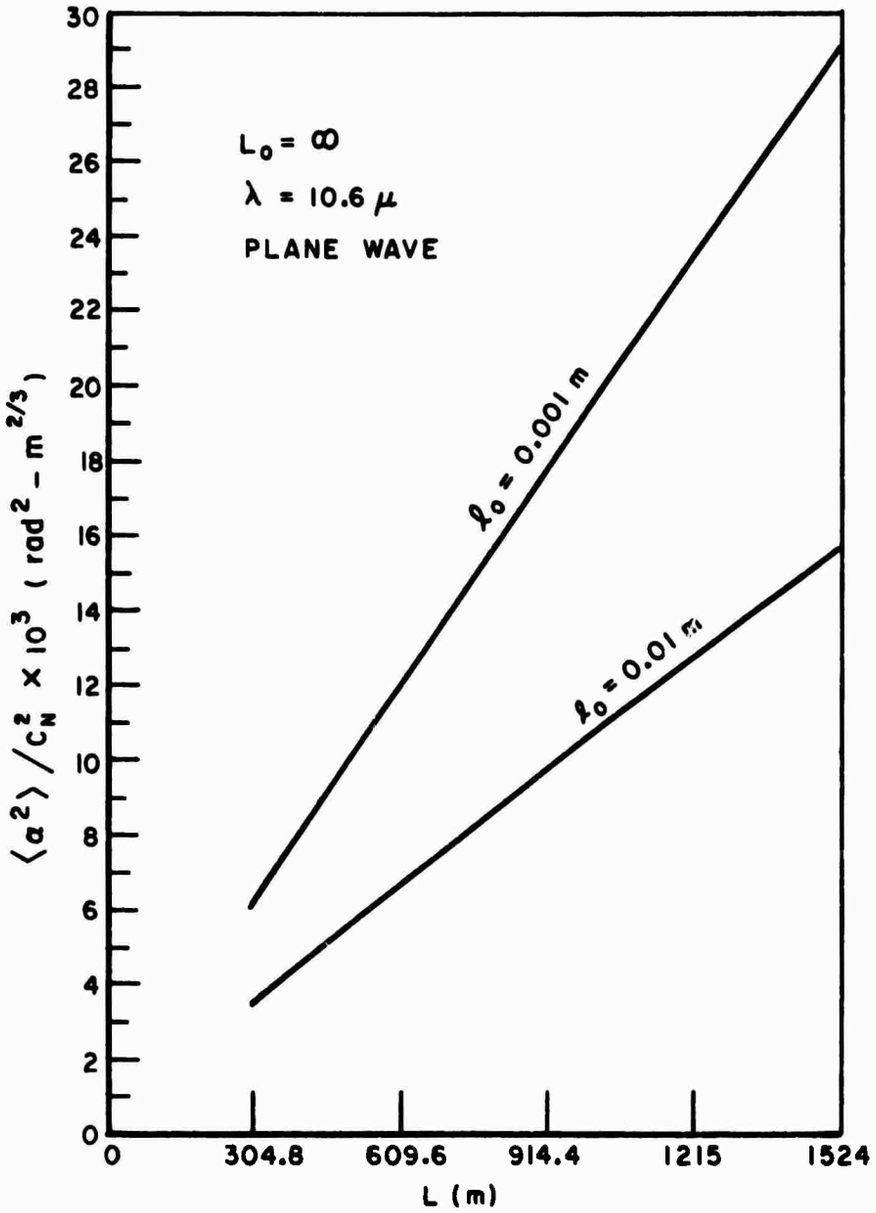

Fig. 7. Small aperture mean square angle of arrival versus range for infinite outer scale and two inner scales.

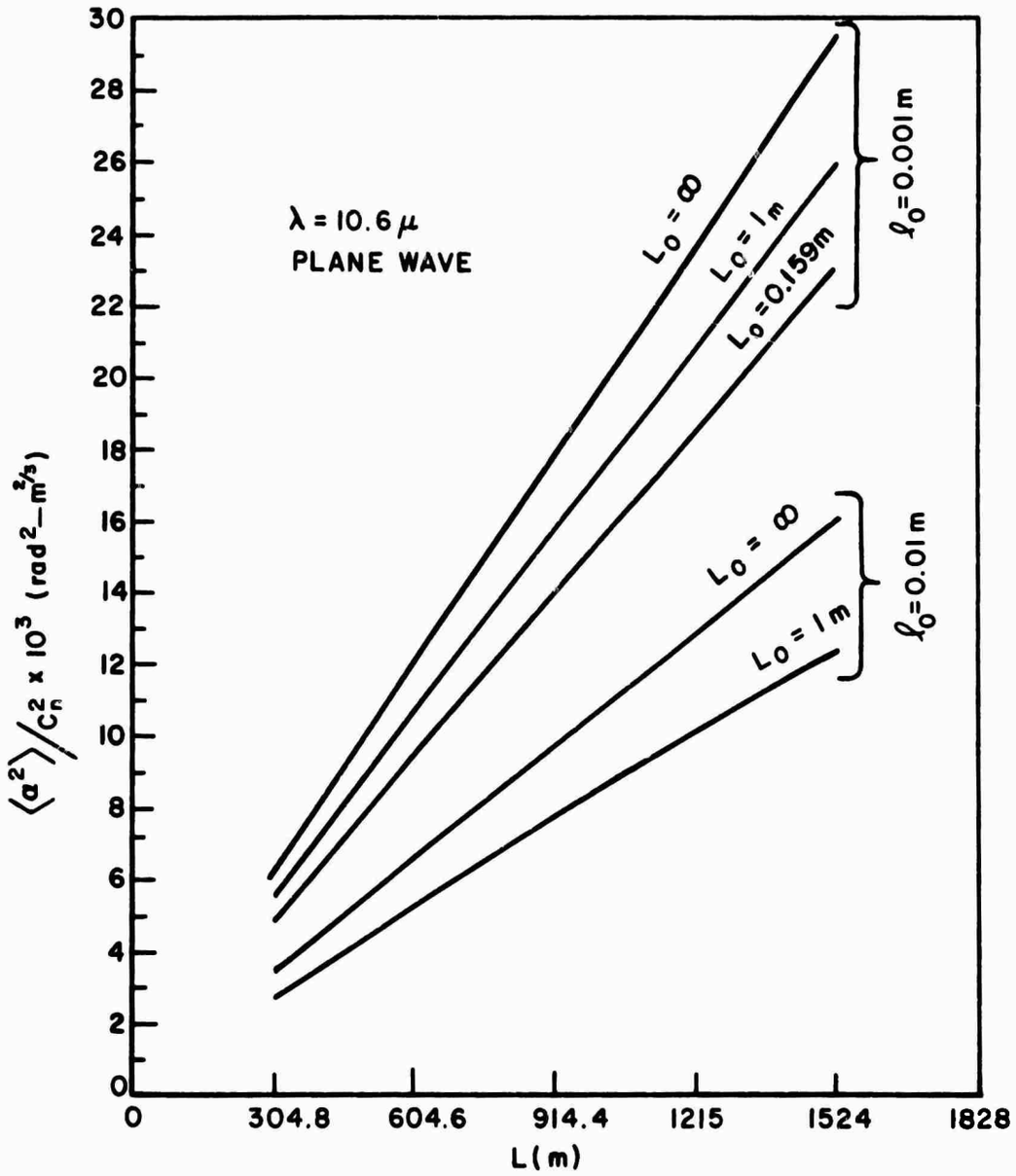

Fig. 8. Small aperture mean square angle of arrival versus range for two inner scales and three outer scales.

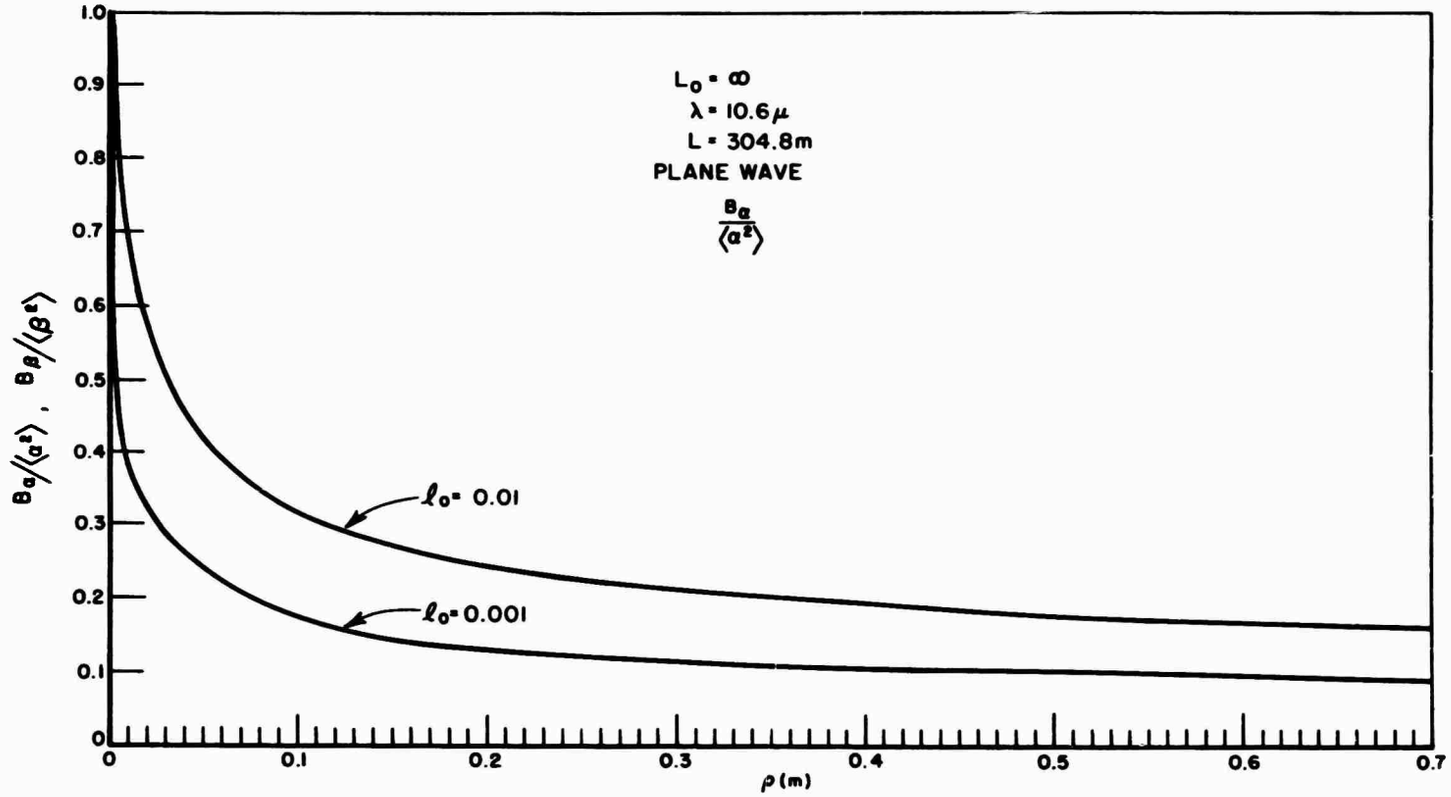

Fig. 9. Small aperture elevation angle of arrival autocorrelation function for two inner scales.

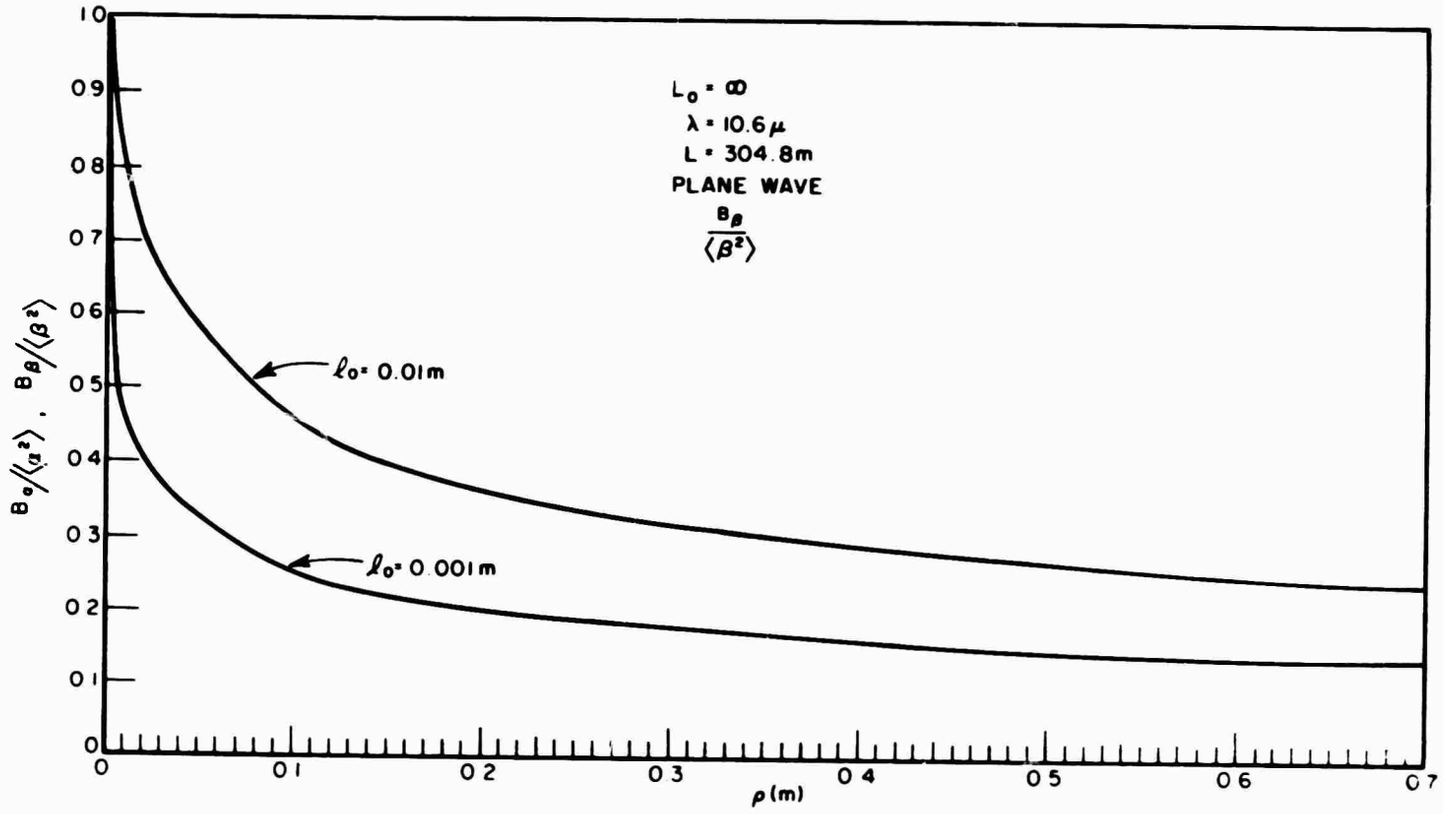

Fig. 10. Small aperture azimuth angle of arrival autocorrelation function for two inner scales.

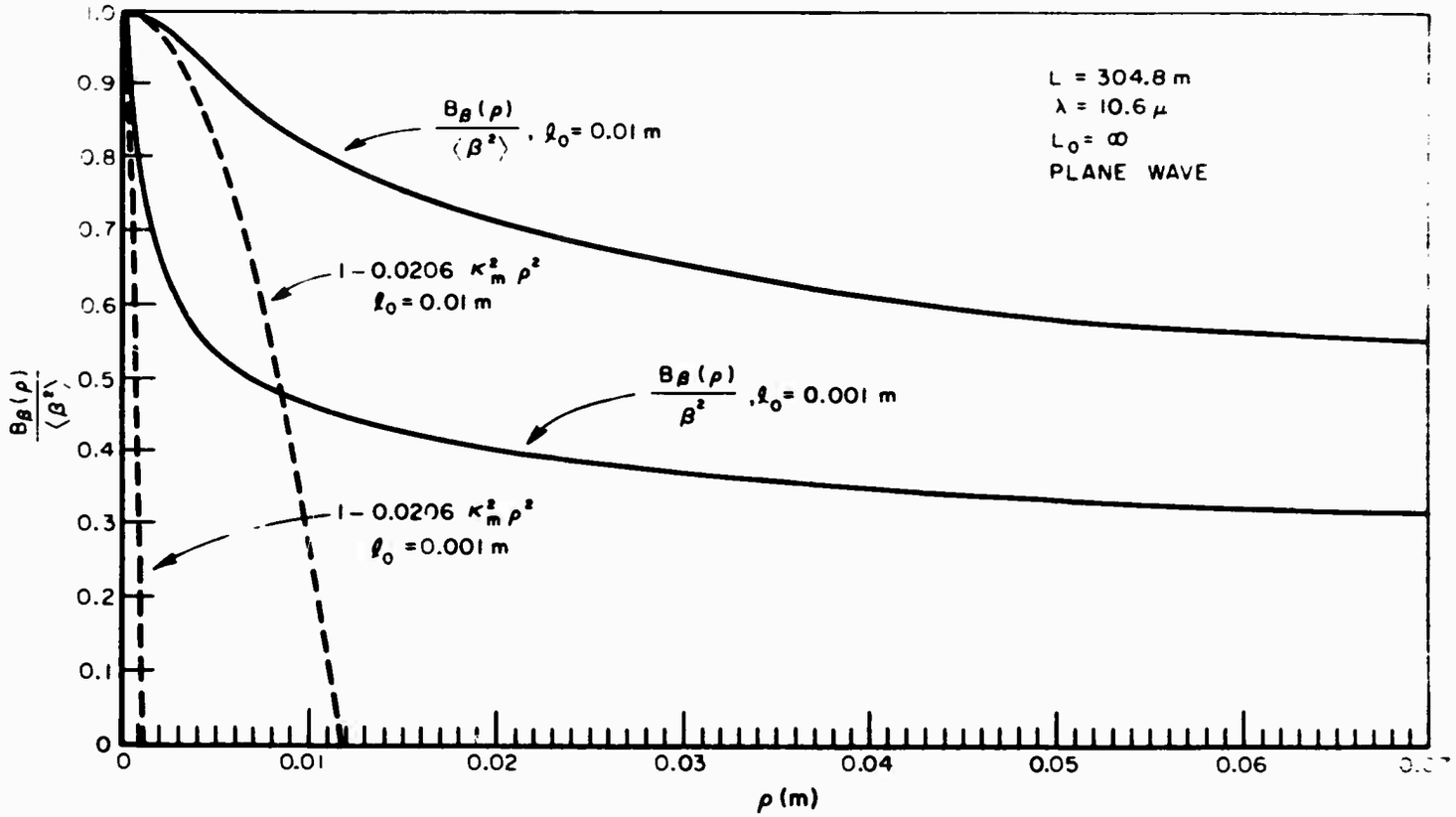

Fig. 11. Comparison of exact and approximate equations for the small aperture azimuth angle of arrival autocorrelation function.

within a correction of $D^{-1/6} \cos \pi/12$. For $\rho << \ell_0$ we see that $\kappa_m \rho$ will be less than one and from Eq. (43), $B_\beta(\rho) = \langle \beta^2 \rangle$ as expected. A comparison of the exact result and the approximate result is shown in Figs. 11 and 12. Figure 11 shows both cases of ℓ_0 = 1 mm and 1 cm and Fig. 12 is a magnified view of the case of ℓ_0 = 1 cm. The structure function, $D_N(\rho)/C_N^2$, is also shown in Fig. 12. We see that the approximation given in Eq. (43) breaks down around the point where $D_N(\rho)$ changes from a r^2 dependence to $r^{2/3}$ dependence as expected.

The information in Figs. 9, 10, and 11 is repeated in Figs. 13-16, along with other curves to show the effect of varying the range. Instead of plotting the curves on linear scale which has a rapid variation near zero separation, the curves are plotted on log-log paper. Also, instead of plotting the autocorrelation which suppresses the range information, the correlation function is plotted, normalized for convenience to the turbulent structure parameter. The fact that the curves are identical except for a vertical displacement indicates that the range information is primarily in the mean square for infinite outer scale.

The effects of the outer scale obtained from computer evaluation of Eqs. (33)-(36) are shown in Figs. 17-20. The azimuth and elevation angle correlation are shown in Figs. 17 and 18 for a range of 304.8 m, inner scale of 1 mm and three values of the outer scale. The information is repeated in Figs. 19 and 20 as log-log plots of the two arrival angle correlation functions normalized to the turbulence structure parameter, C_N^2.

The effect of the outer scale is shown quite dramatically. The elevation angle of arrival, $B_\alpha(\rho)/\langle \alpha^2 \rangle$ in Fig. 17 shows a slightly negative correlation for $\rho = L_0$. This negative correlation is sufficiently large that it is not believed to be an artifact of the computation. Further showing the effect of outer scale, the azimuth angle of arrival correlation $B_\beta(\rho)/\langle \alpha^2 \rangle$ shown in Fig. 18 falls below 5% of the mean value for $\rho = L_0$.

The effects of range with a finite outer scale are shown in Figs. 21 and 22 where we see the normalized correlation functions plotted for an outer scale of 1 m, and inner scale of 1 mm and ranges of 304.8 m ft, 914.4 m ft and 1524 m ft. Figures 23 and 24 contain the same information except with an inner scale of 1 cm. It is noted that in these cases the outer scale dependence is almost entirely determined by the variation of the mean square arrival angle caused by the outer scale. Thus, the correlation function is almost directly proportional to range.

The preceeding graphs have all been for a plane wave. The equivalent graphs are also presented for a spherical wave in Figs. 25-34. Thus Figs. 25 and 26 give the mean square arrival angle for two outer scales for 1 mm and 1 cm inner scales respectively. Figures 27 and 28 give the normalized arrival angle correlation functions for three ranges for an infinite outer scale and inner scale of 1 mm.

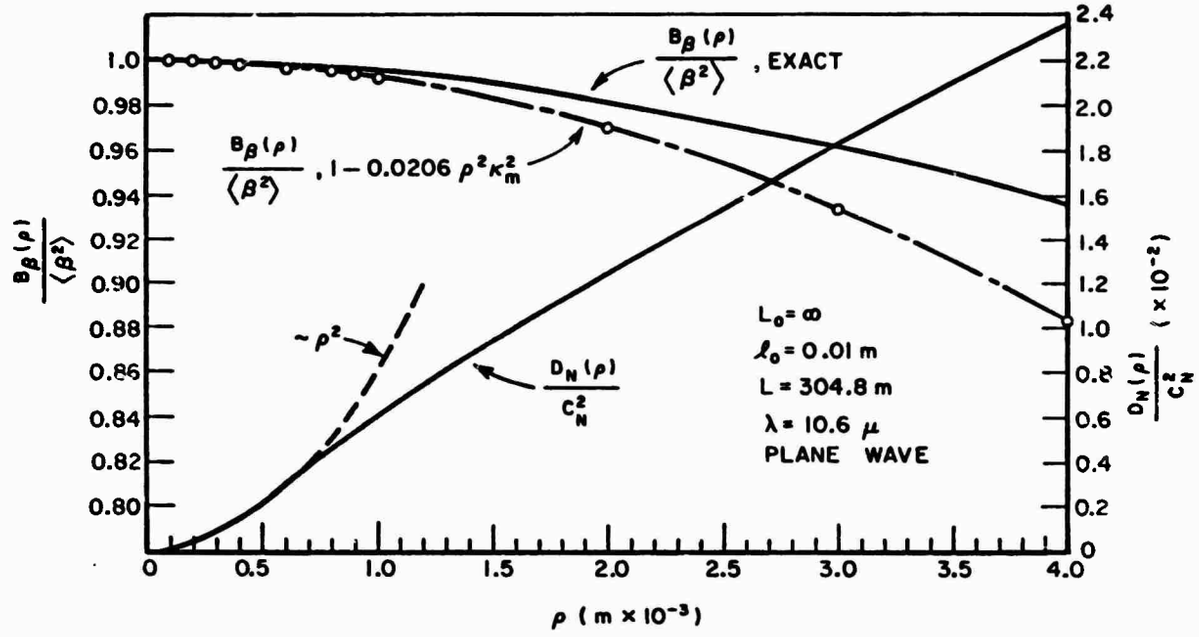

Fig. 12. Magnified comparison of exact and approximate equations for the small aperture azimuth angle of arrival auto-correlation function and the refractive index fluctuation structure function.

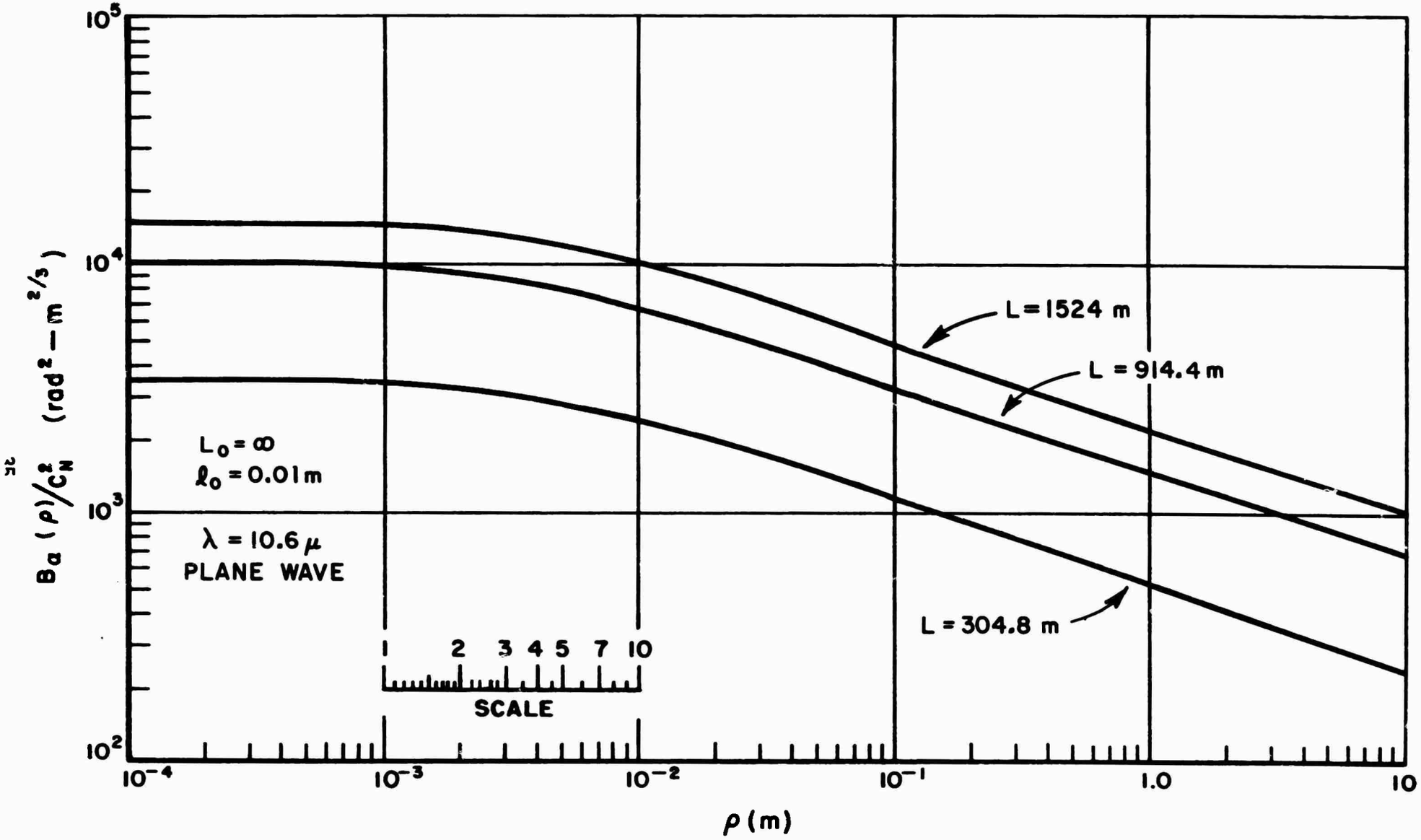

Fig. 13. Small aperture elevation angle of arrival correlation versus separation for plane wave input, $L_0 = \infty$, $\ell_0 = 0.01$ m.

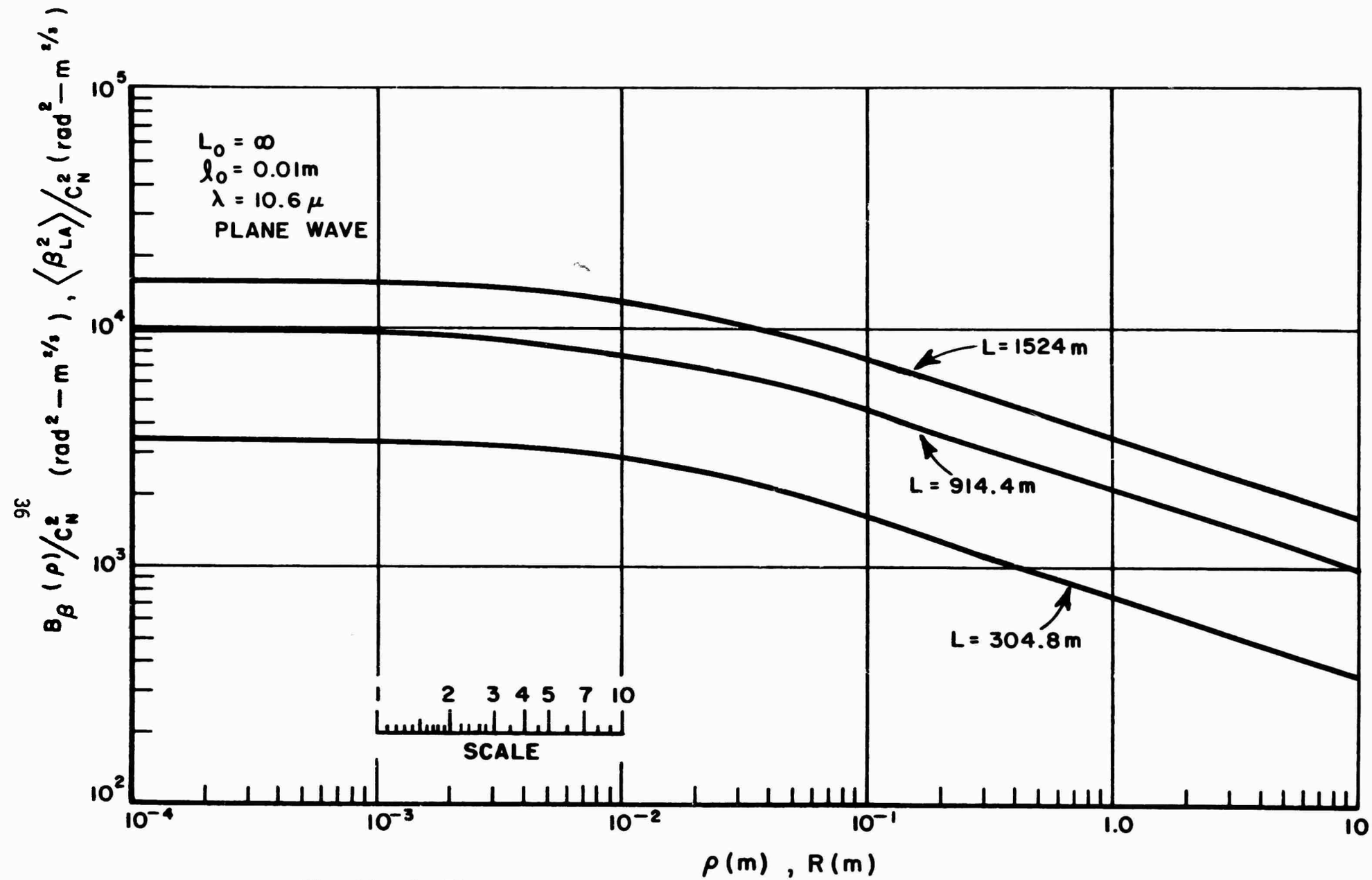

Fig. 14. Small aperture azimuth angle of arrival correlation versus separation and large aperture mean square angle of arrival versus aperture radius for plane wave input, $L_0 = \infty$, $\ell_0 = 0.01$ m.

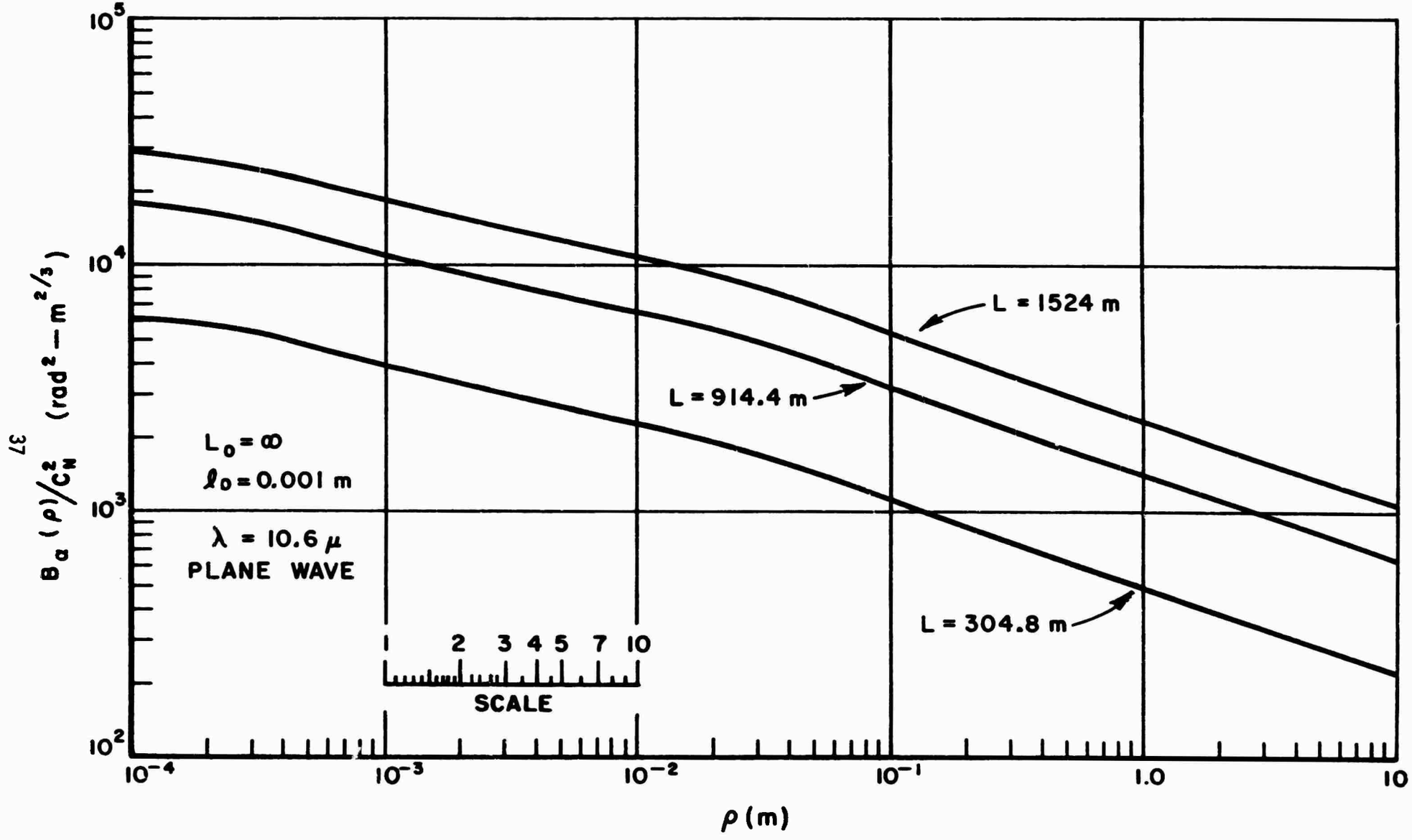

Fig. 15. Small aperture elevation angle of arrival correlation versus separation for plane wave input, $L_0 = \infty$, $\ell_0 = 0.001$ m.

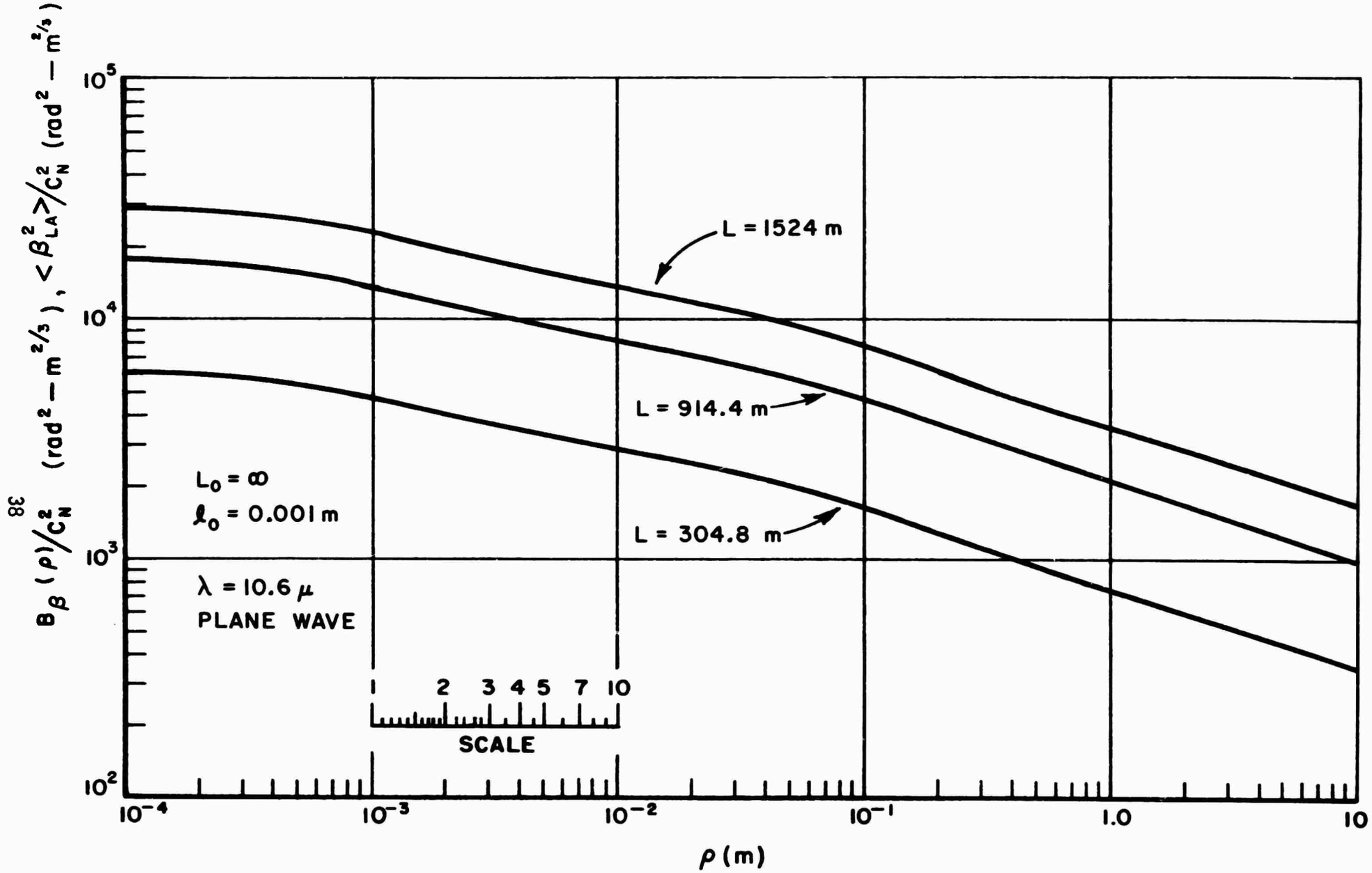

Fig. 16. Small aperture azimuth angle of arrival correlation versus separation and large aperture mean square angle of arrival versus aperture radius for plane wave input, $L_0 = \infty$, $\ell_0 = 0.001$ m.

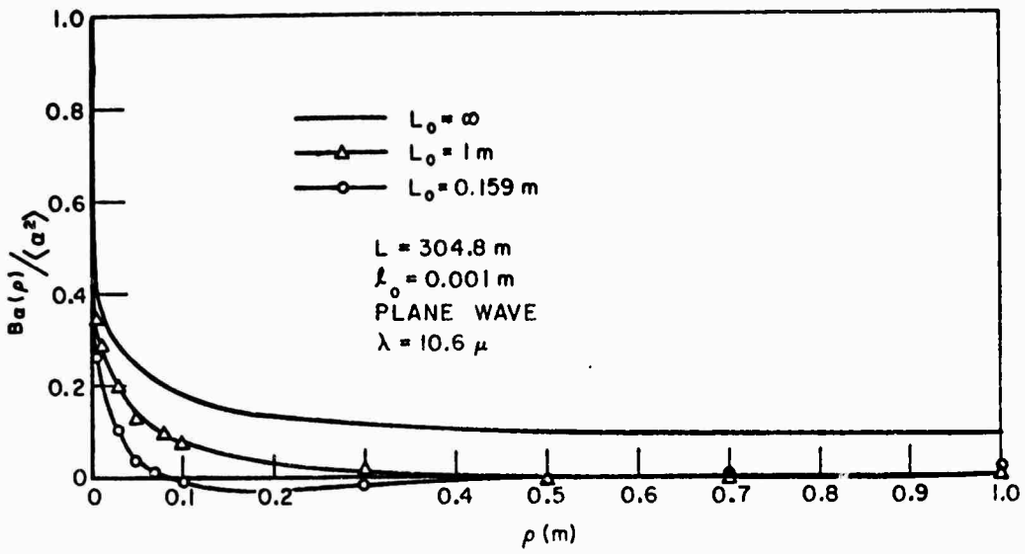

Fig. 17. Small aperture elevation angle of arrival autocorrelation versus separation for plane wave input and three outer scales.

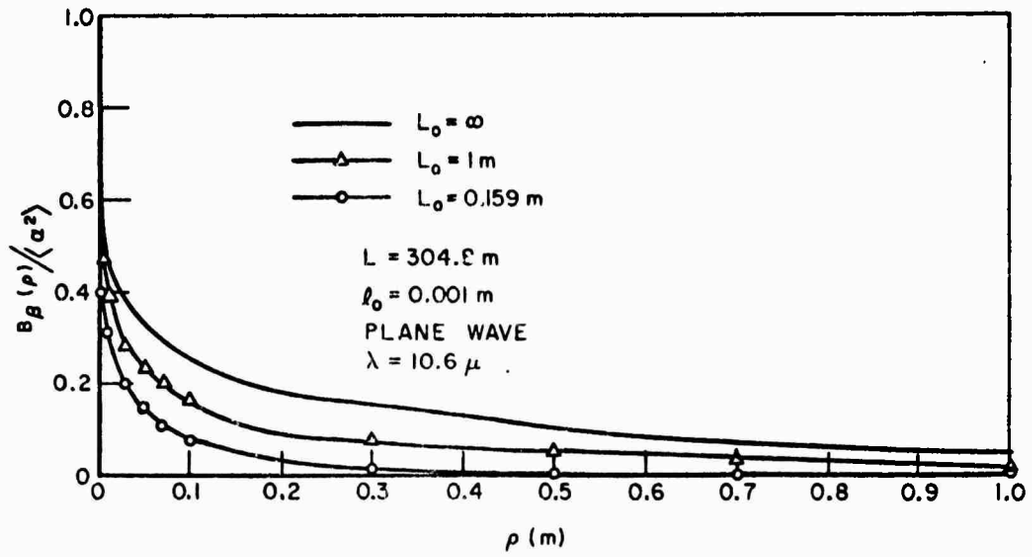

Fig. 18. Small aperture azimuth angle of arrival autocorrelation versus separation for plane wave input and three outer scales.

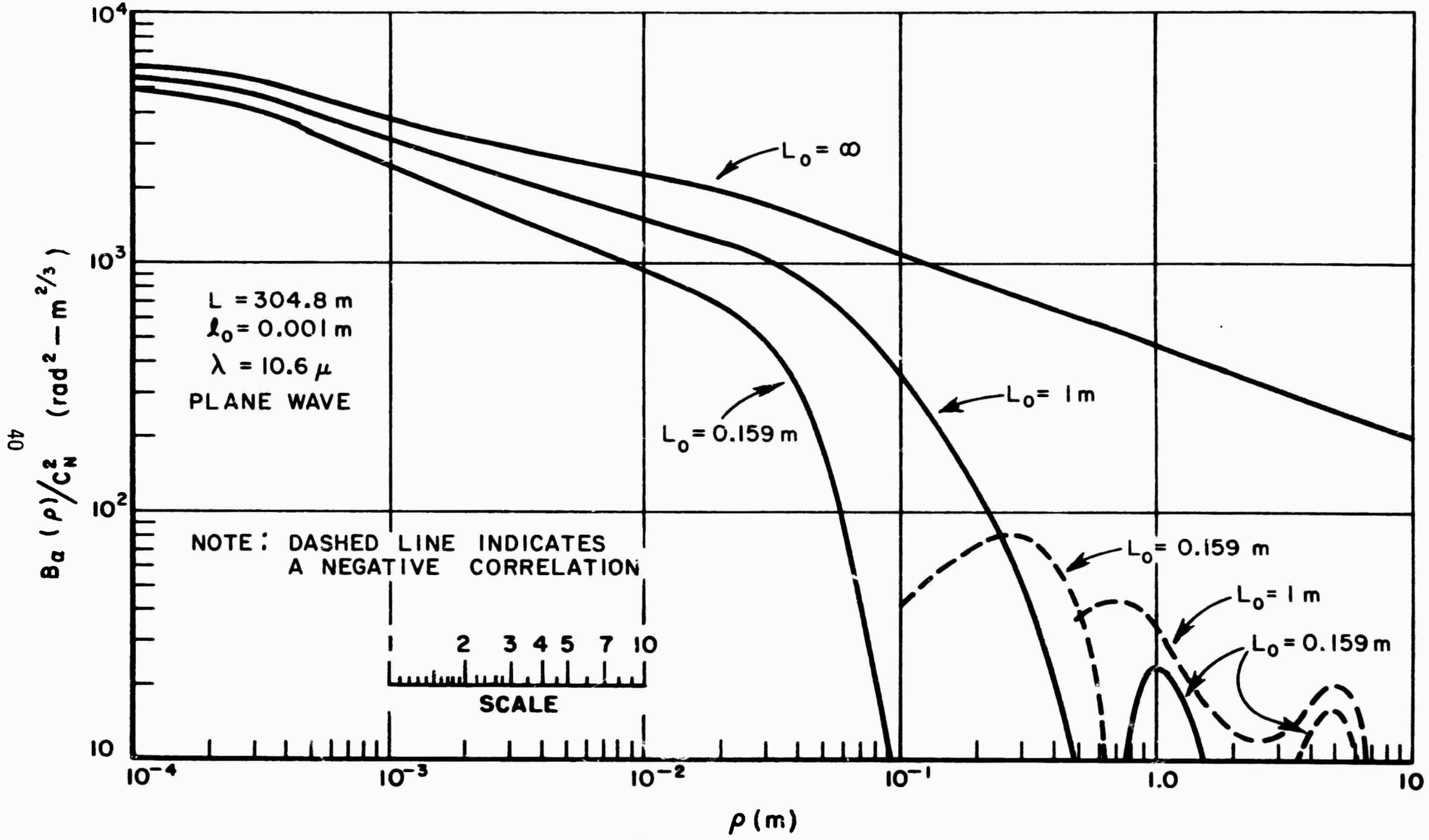

Fig. 19. Small aperture elevation angle of arrival correlation versus separation for plane wave input and three outer scales.

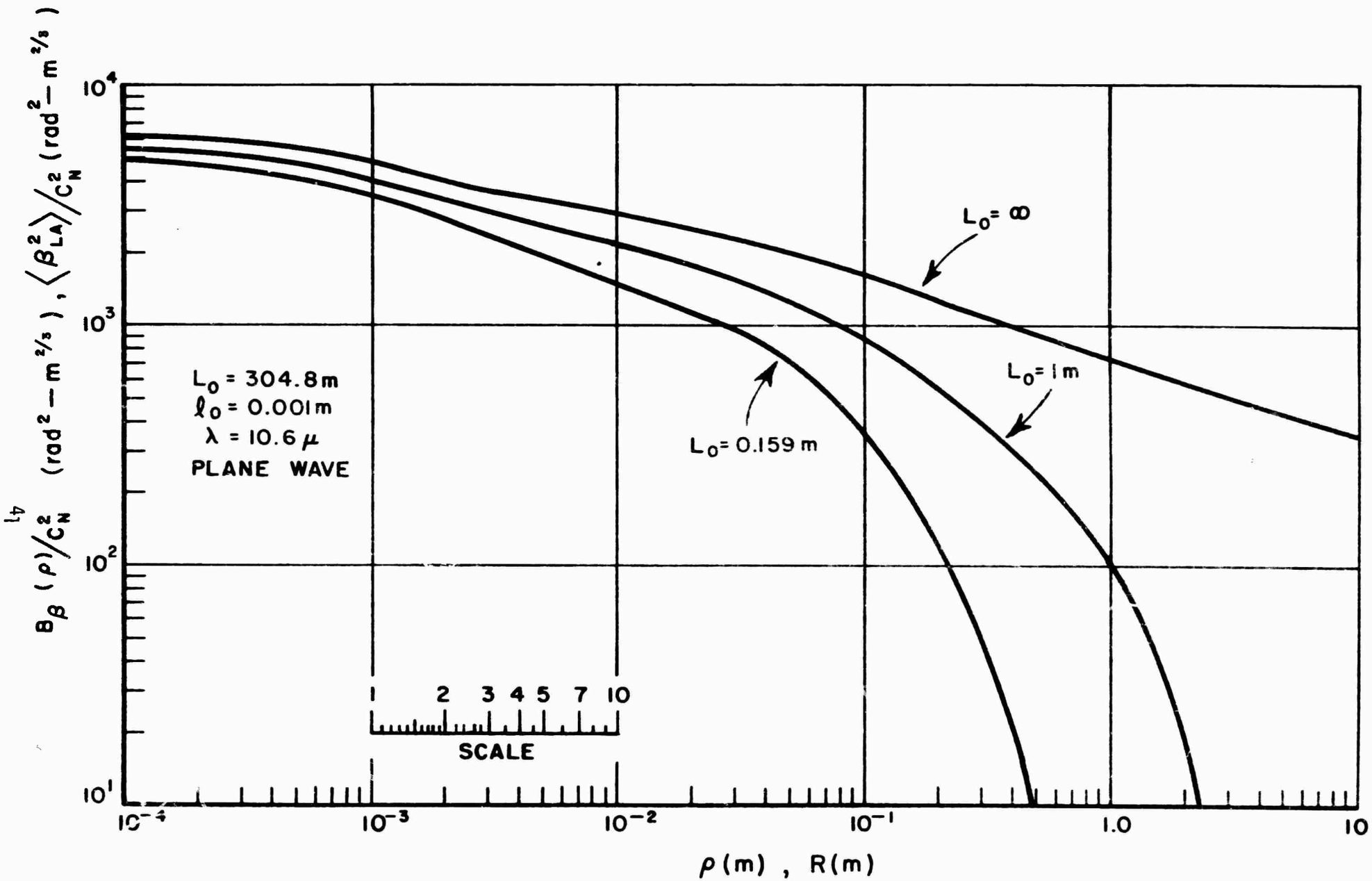

Fig. 20. Small aperture azimuth angle of arrival correlation versus separation and large aperture mean square angle of arrival versus aperture radius for plane wave input and three outer scales.

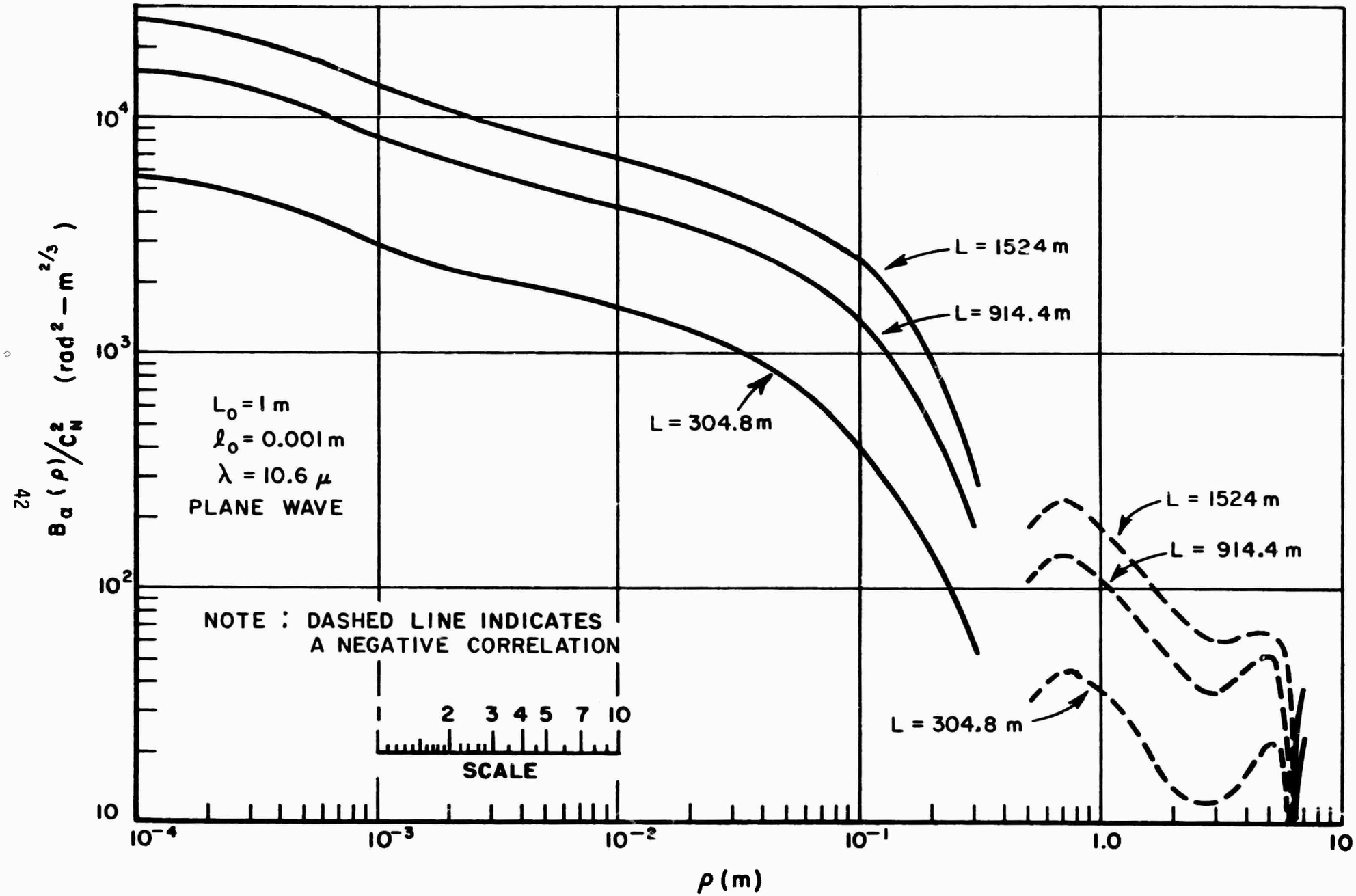

Fig. 21. Small aperture elevation angle of arrival correlation versus separation for plane wave input L_0 = 1 m, ℓ_0 = .001 m.

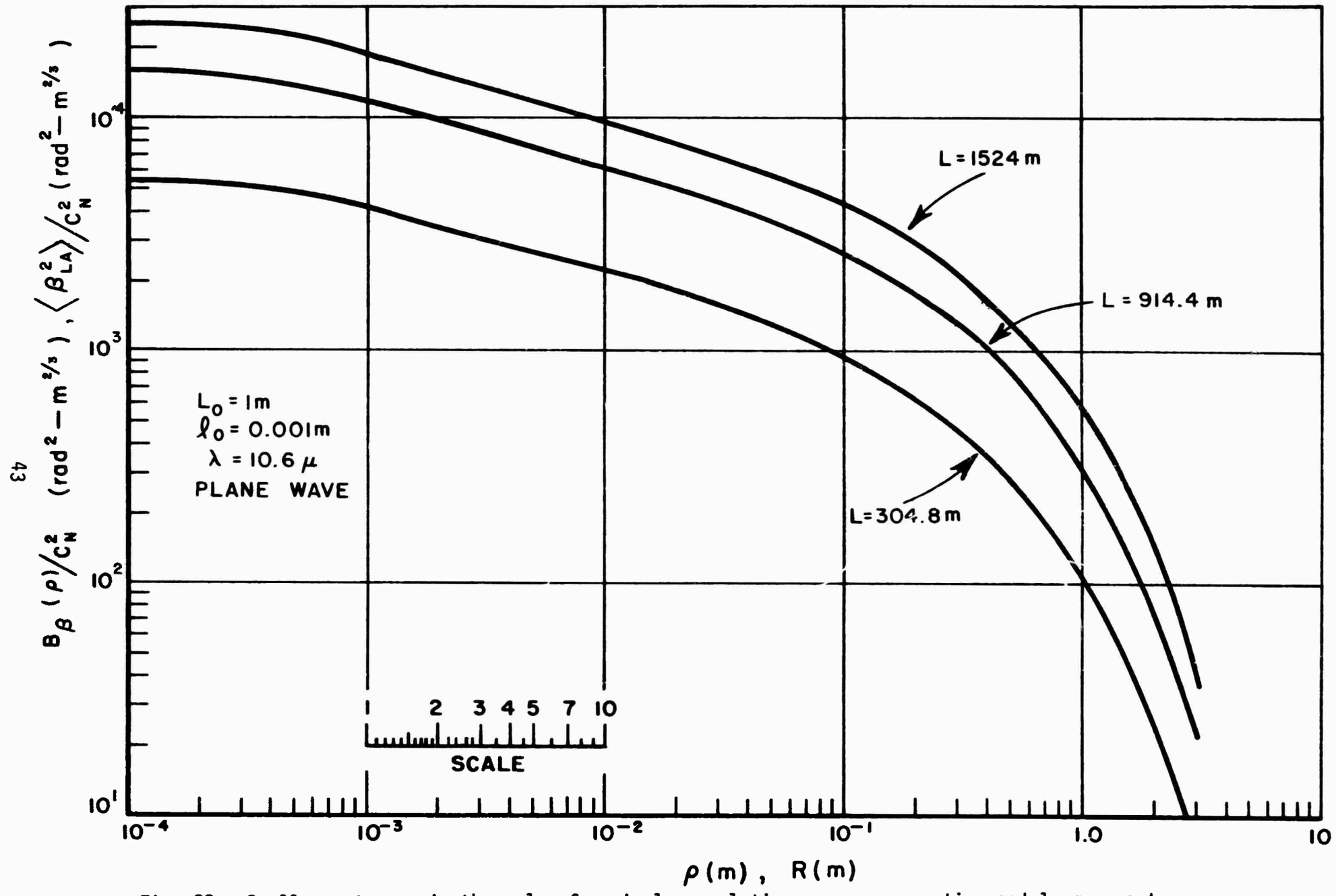

Fig. 22. Small aperture azimuth angle of arrival correlation versus separation and large aperture mean square angle of arrival versus aperture radius for plane wave input, L_0 = 1 m, ℓ_0 = 0.001 m.

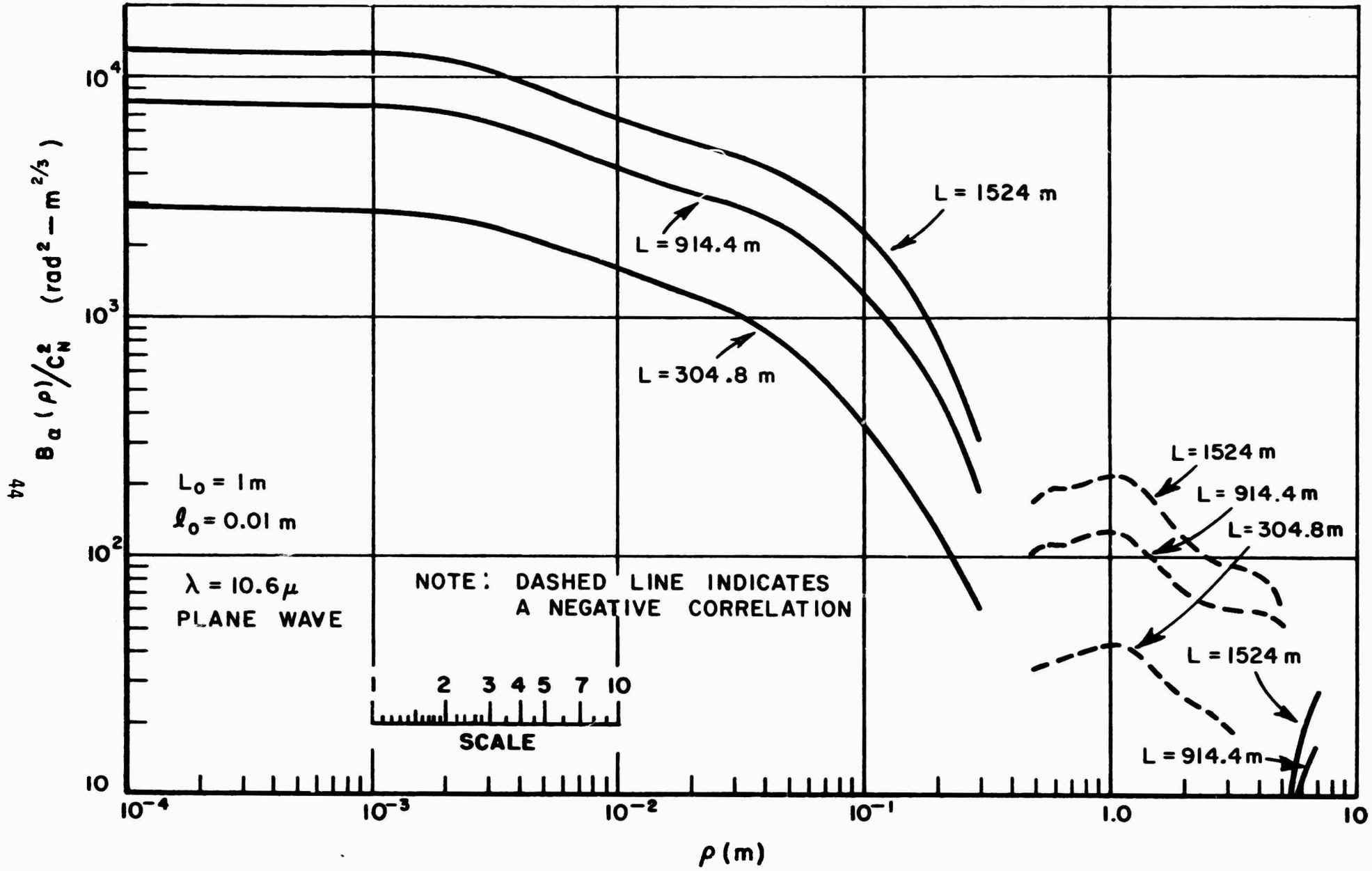

Fig. 23. Small aperture elevation angle of arrival correlation versus separation for plane wave input, L_0 = 1 m, ℓ_0 = 0.01 m.

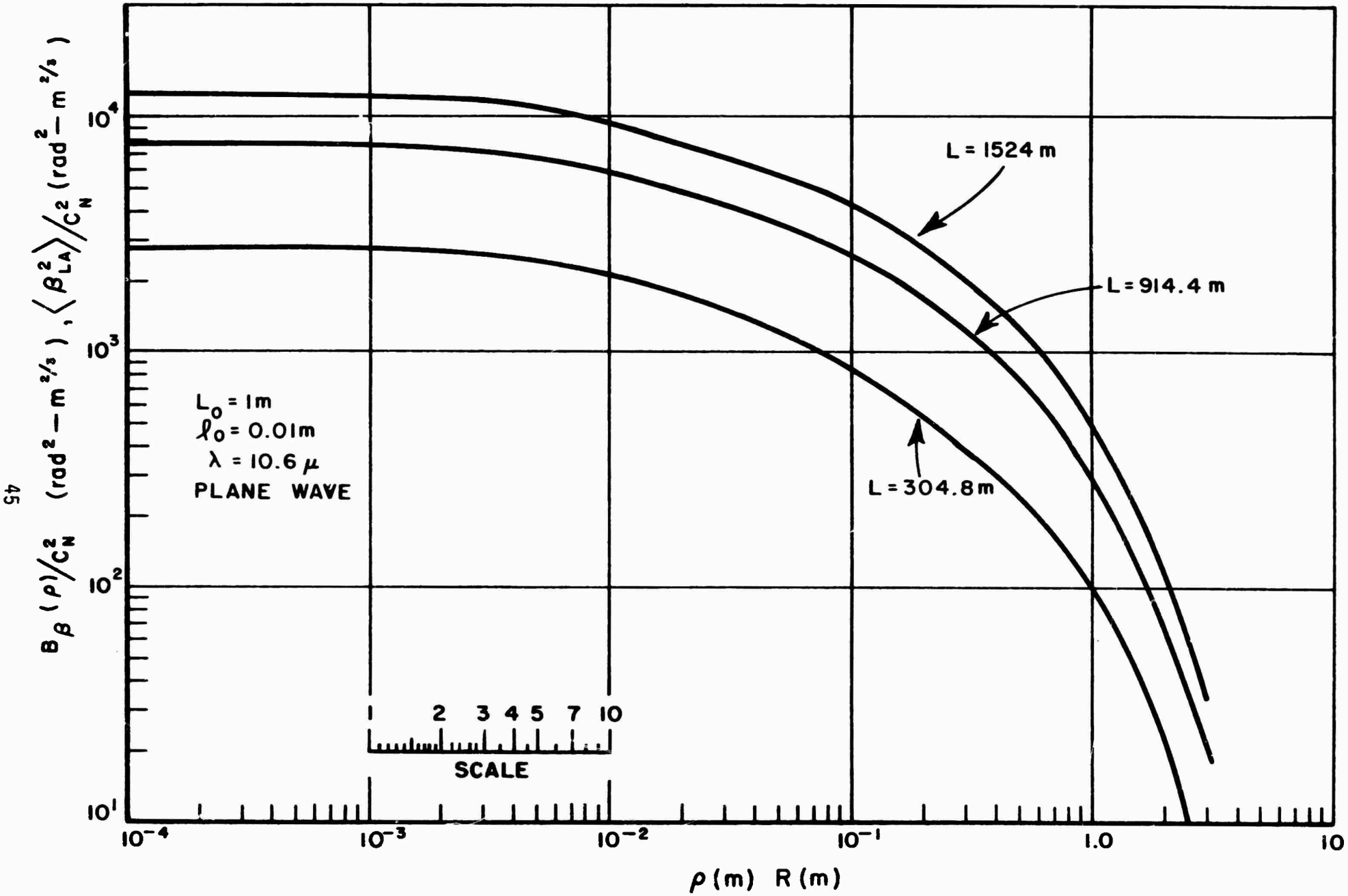

Fig. 24. Small aperture azimuth angle of arrival correlation versus separation and large aperture mean square angle of arrival versus aperture radius for plane wave input, L_0 = 1 m, ℓ_0 = 0.01 m.

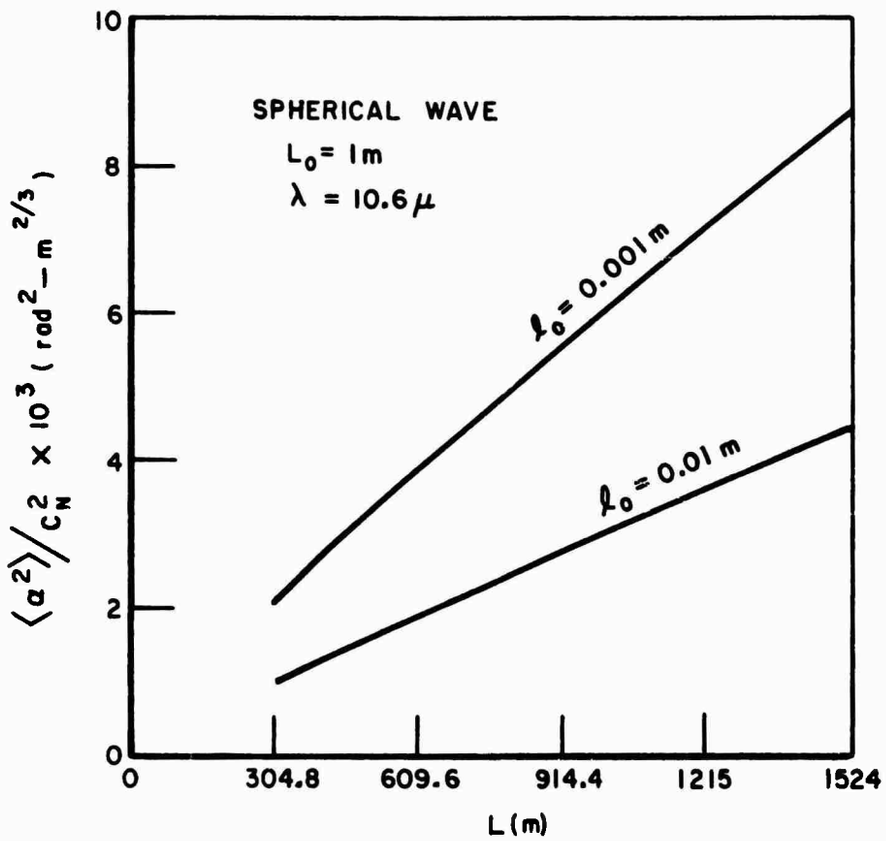

Fig. 25. Small aperture mean square angle of arrival for spherical wave input, finite outer scale and two inner scales.

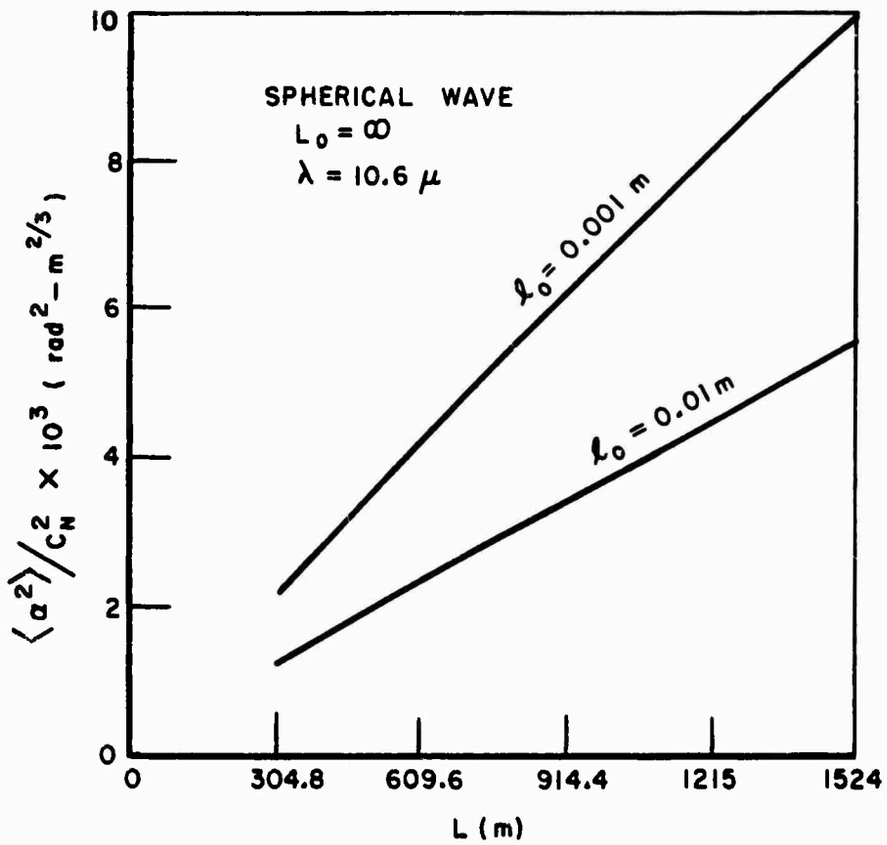

Fig. 26. Small aperture mean square angle of arrival for spherical wave input, infinite outer scale, and two inner scales.

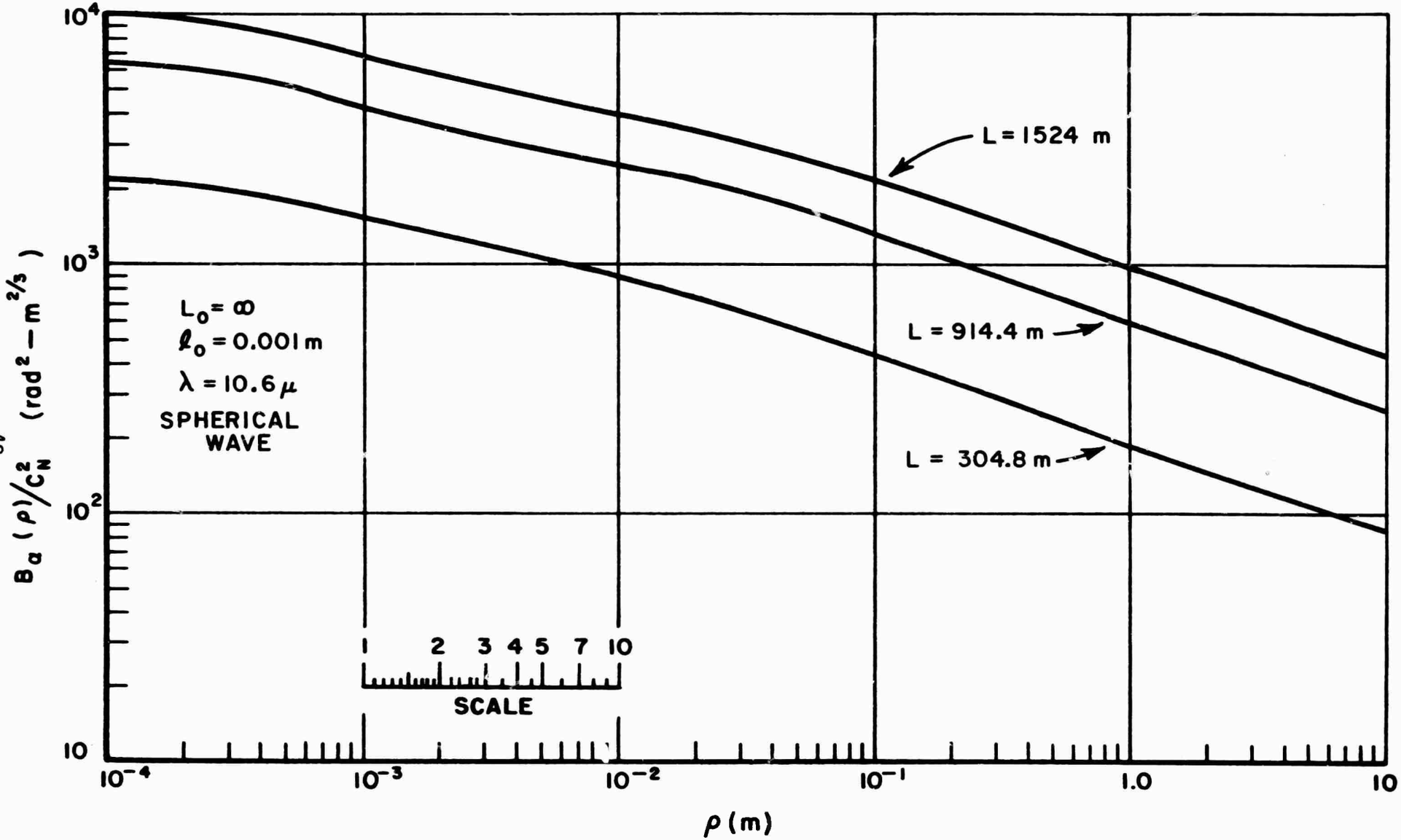

Fig. 27. Small aperture elevation angle of arrival correlation versus separation for spherical wave input, $L_0 = \infty$, $\ell_0 = 0.001$ m.

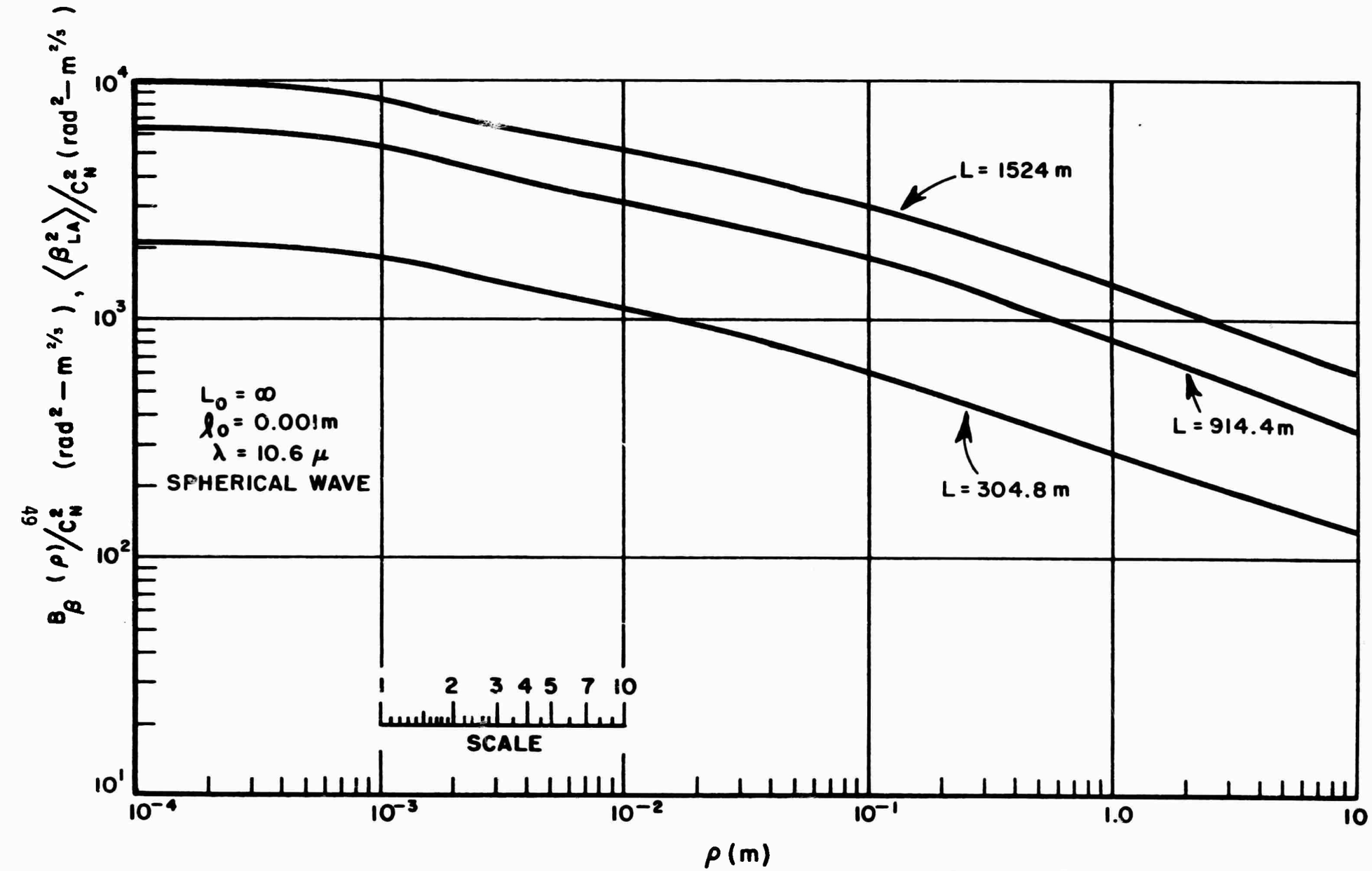

Fig. 28. Small aperture azimuth angle of arrival correlation and large aperture mean square angle of arrival versus aperture radius for spherical wave input, $L_0 = \infty$, $\ell_0 = 0.001$ m.

Figures 29 and 30 give the same data except that the inner scale is 1 cm. Figures 31 and 32 give the normalized arrival angle correlations for a 1 m outer scale and 1 mm inner scale for the three different ranges and Figs. 33 and 34 hold for 1 m outer scale, 1 cm inner scale and the three different ranges. These were all computed the same as the plane wave data, except with Eq. (32) replacing (31).

The accuracy of the computer evaluations of Eqs. (33)-(36) was checked by evaluating them for the case where $L_0 = \infty$ and comparing with the closed form analytic expressions in Eqs. (38)-(40). Several orders of Gaussian quadrature integration were tried and compared to the closed form results as shown in Fig. 35. We see that the 96-point Gaussian quadrature integration used in the previous calculations provides good agreement.

Extensive results are also available for the large aperture arrival angle variance. Figures 36 and 37 are plots of mean square arrival angle normalized to turbulence structure parameter, C_N^2, plotted as a function of aperture radius. The numbers were obtained by numerically integrating Eq. (19) with the expression in Eq. (33) used for $\Phi_N(\kappa)$. In Fig. 36 curves are shown for plane waves for an inner scale of 1 mm, a range of 304.8 m ft and three values of outer scale. Figure 37 shows the effect of range for an outer scale of 1 m and an inner scale of 1 mm. These curves show changes with outer scale and range similar to the small aperture arrival angle correlation functions.

Verifying the accuracy for these results is much more difficult and time consuming since four numeric integrations are used. However, increasing the order of integrations used yielded results which differed in the third and higher order digits. Thus, these results are believed to be accurate to 3 digits. Higher accuracy can be obtained by increasing the Gaussian integration orders.

Further data is also available on large aperture mean square arrival angle, because, to a very good degree of approximation, the large aperture mean square arrival angle taken as a function of aperture radius, is equal to the small aperture azimuth arrival angle correlation function, $B_\beta(\rho)$ taken as a function of point separation, ρ. This synonymity is discussed in detail in the next section. However the results are used here to indicate the further data on large aperture arrival angle mean square available. Thus the even numbered figures between Fig. 14 and Fig. 24 can all be retitled to give large aperture mean square angle of arrival versus radius for the particular case for plane waves, and the even numbered figures between Fig. 27 and Fig. 34 can all be retitled to give the mean square arrival angle versus radius for the particular cases for spherical waves. Thus data is available for a large number of cases for the large aperture situation also. The discussion of the curves parallels that for the small aperture case.

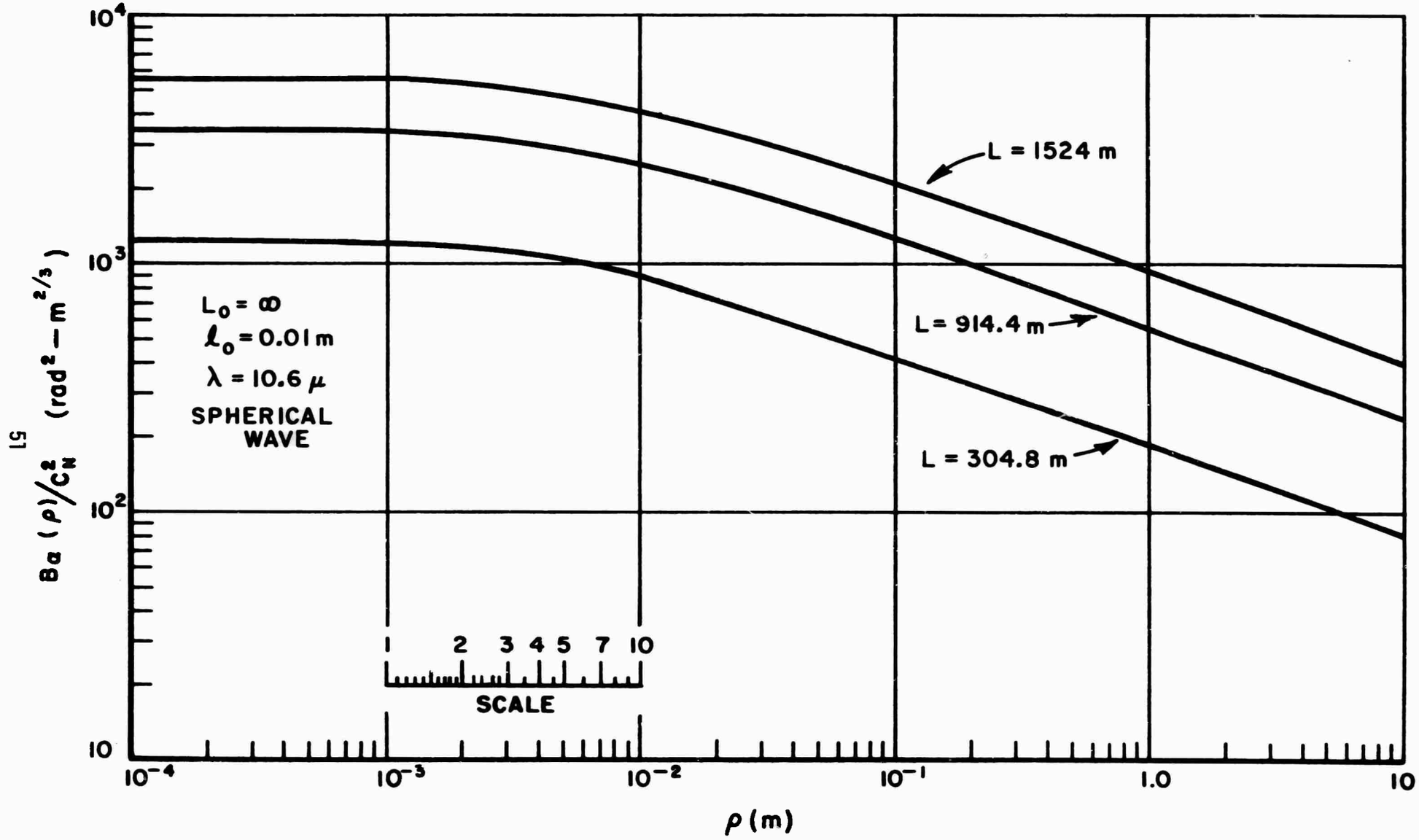

Fig. 29. Small aperture elevation angle of arrival correlation versus separation for spherical wave input, $L_o = \infty$, $\ell_o = 0.01$ m.

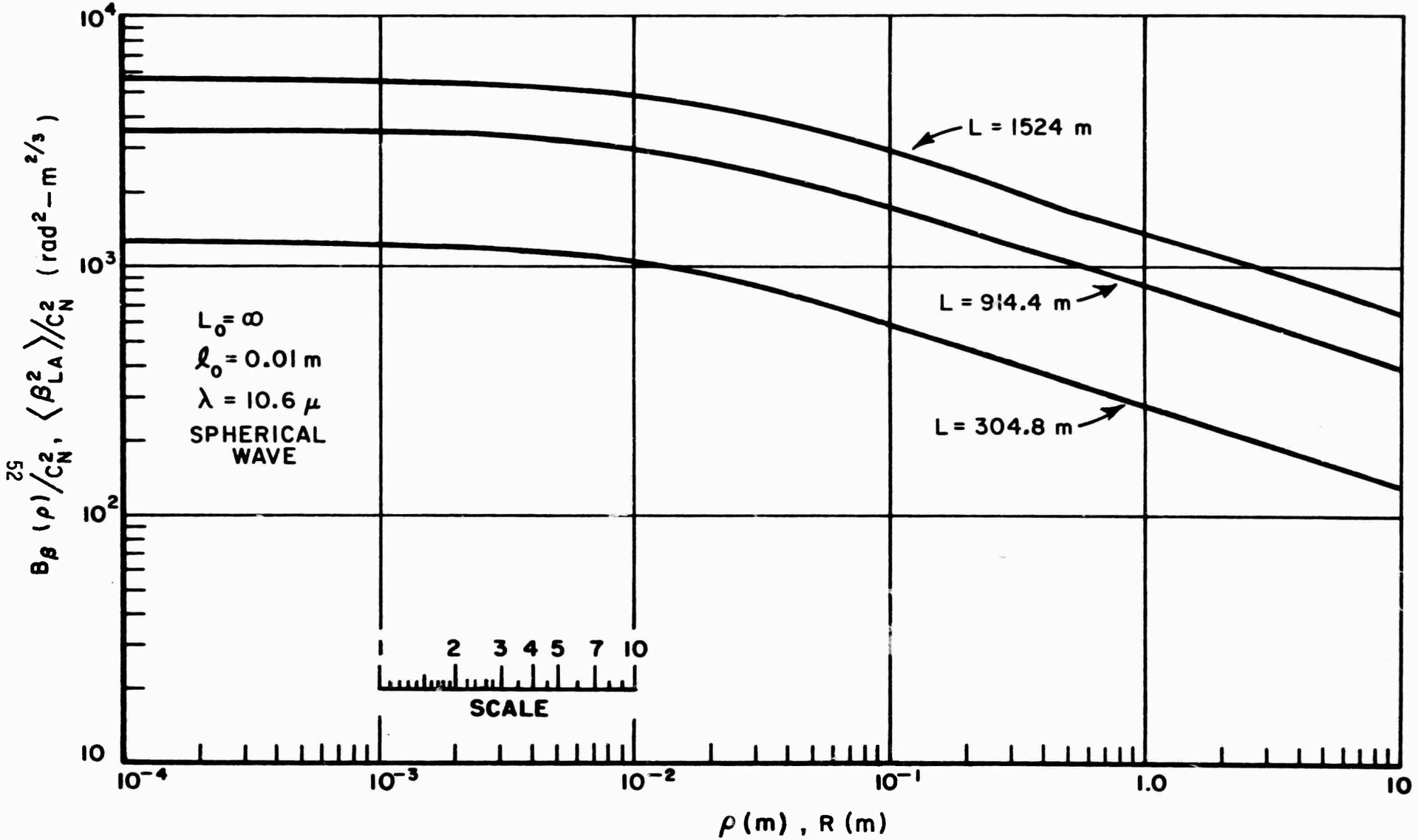

Fig. 30. Small aperture azimuth angle of arrival correlation and large aperture mean square angle of arrival versus aperture radius for spherical wave input, $L_0 = \infty$, $\ell_0 = 0.01$ m.

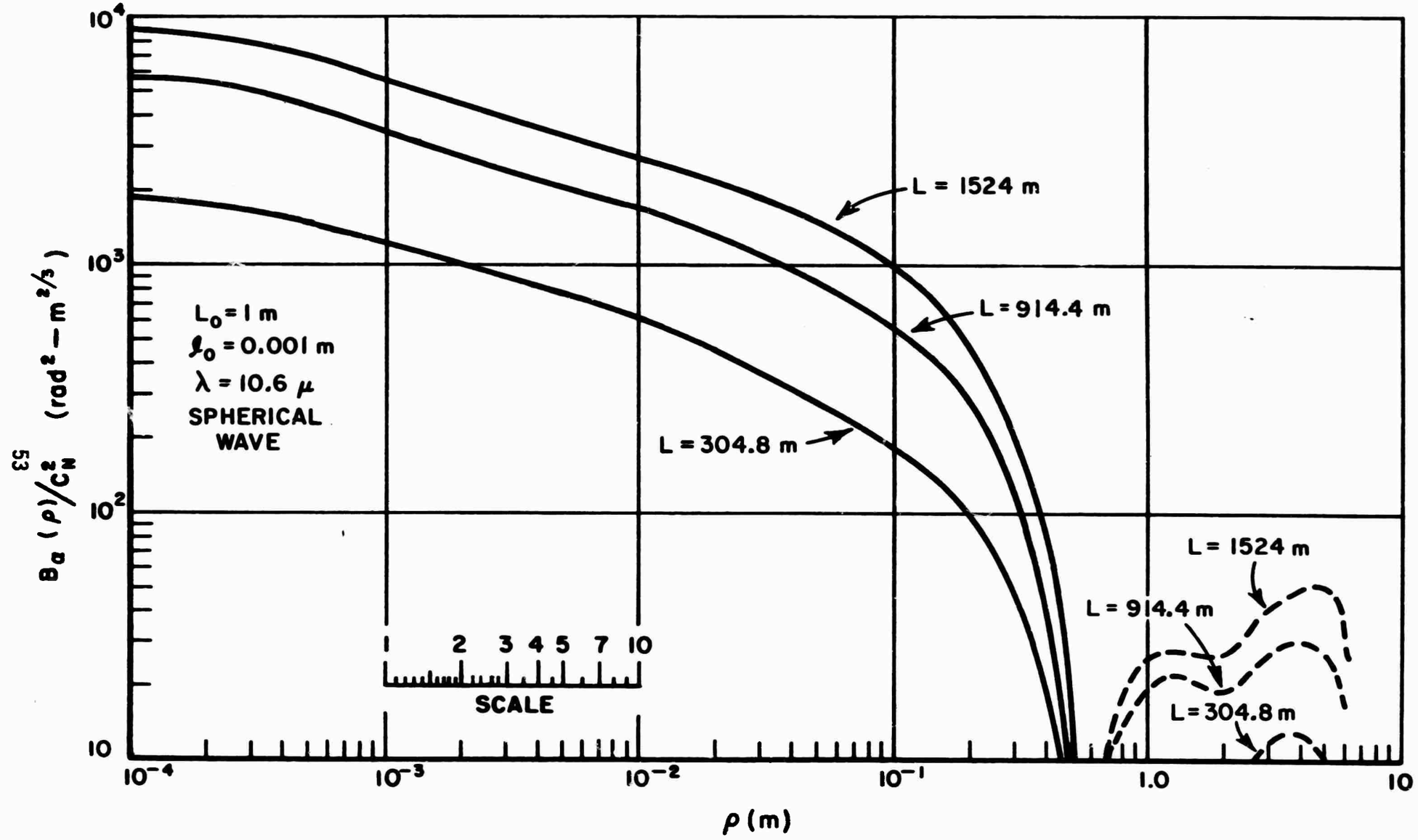

Fig. 31. Small aperture elevation angle of arrival correlation versus separation for spherical wave input, L_o = 1 m, ℓ_o = 0.001 m.

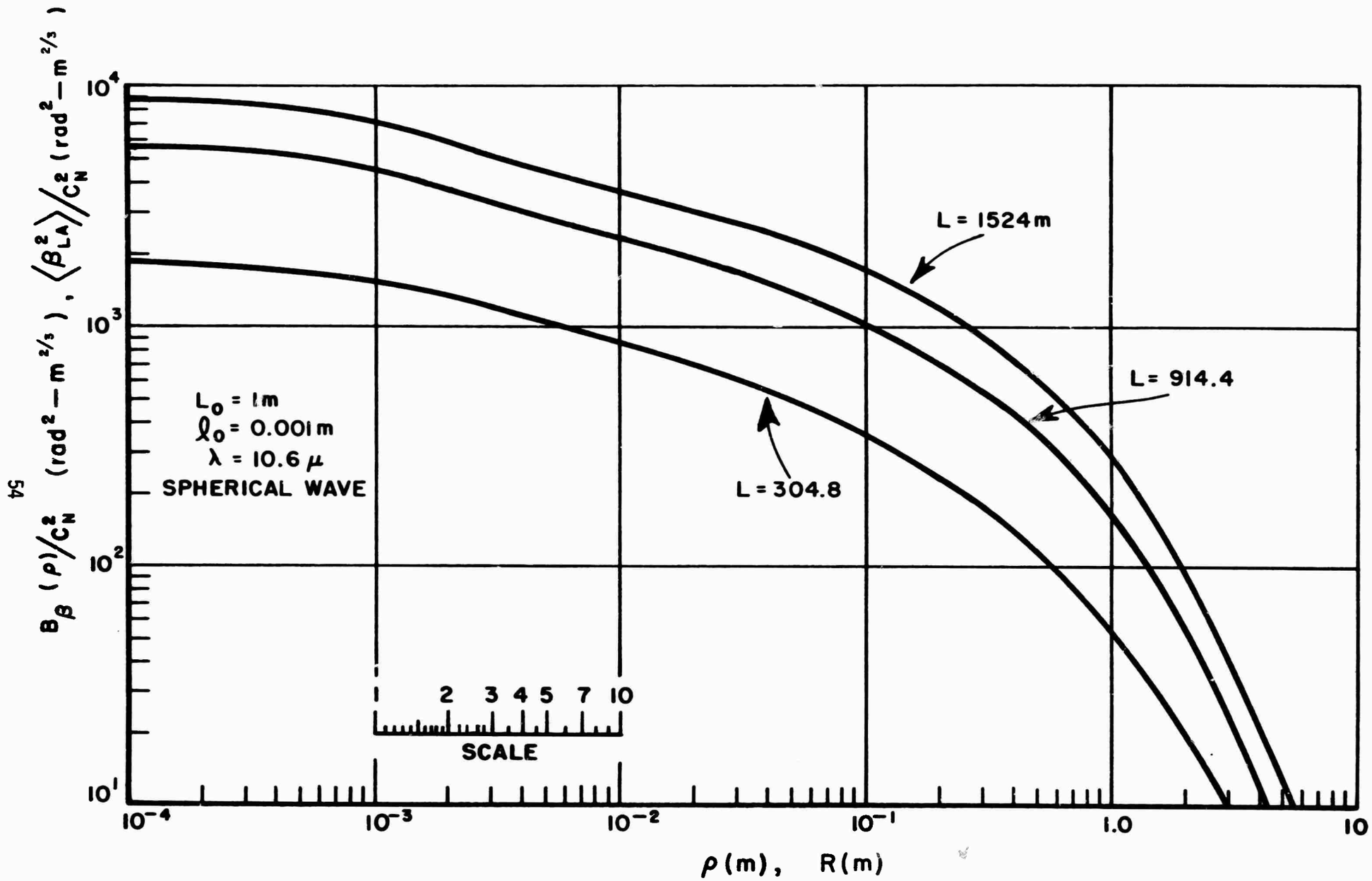

Fig. 32. Small aperture azimuth angle of arrival correlation versus separation and large aperture mean square angle of arrival versus aperture radius for spherical wave input, L_0 = 1 m, ℓ_0 = 0.001 m.

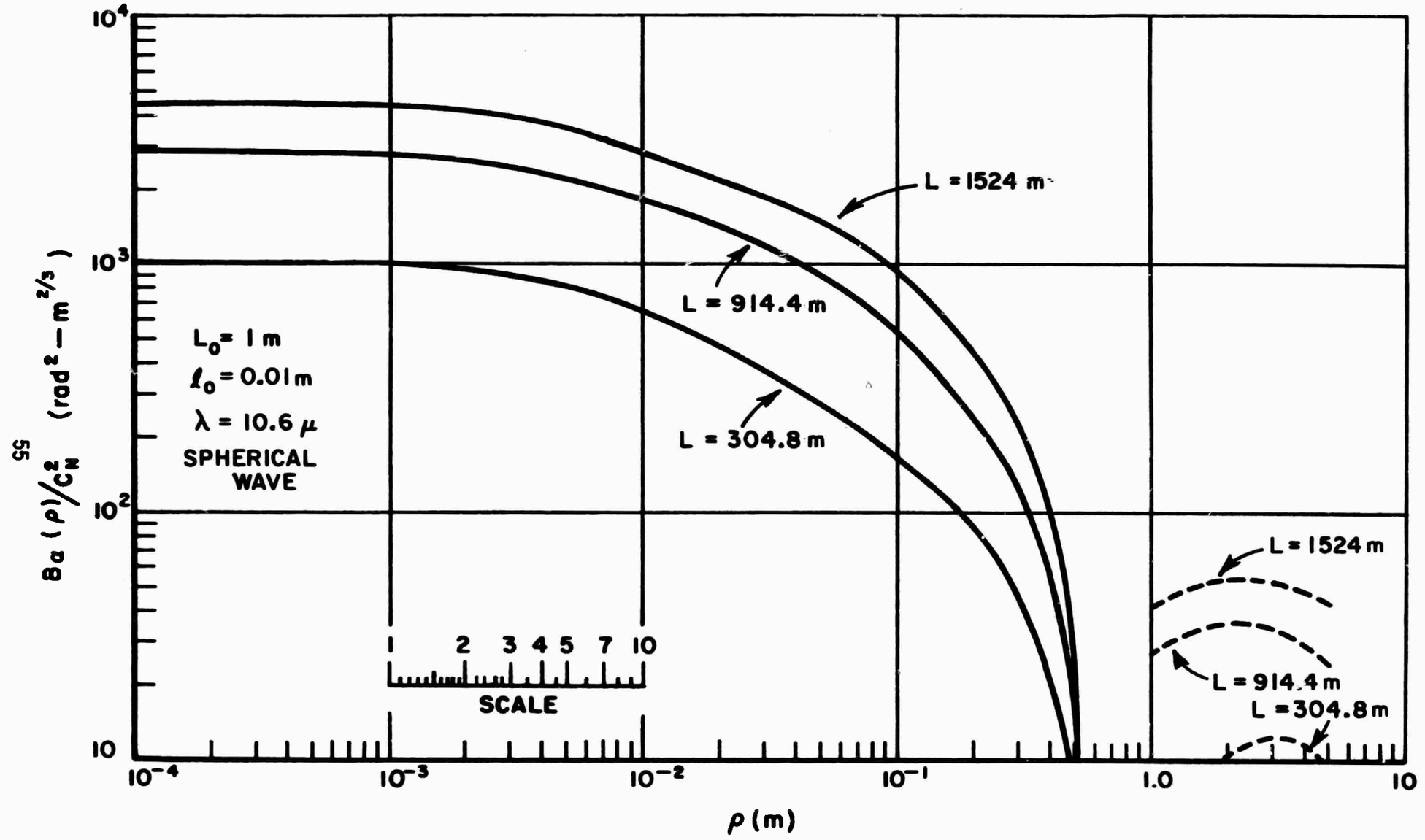

Fig. 33. Small aperture elevation angle of arrival correlation versus separation for spherical wave input, L_0 = 1 m, ℓ_0 = 0.01 m.

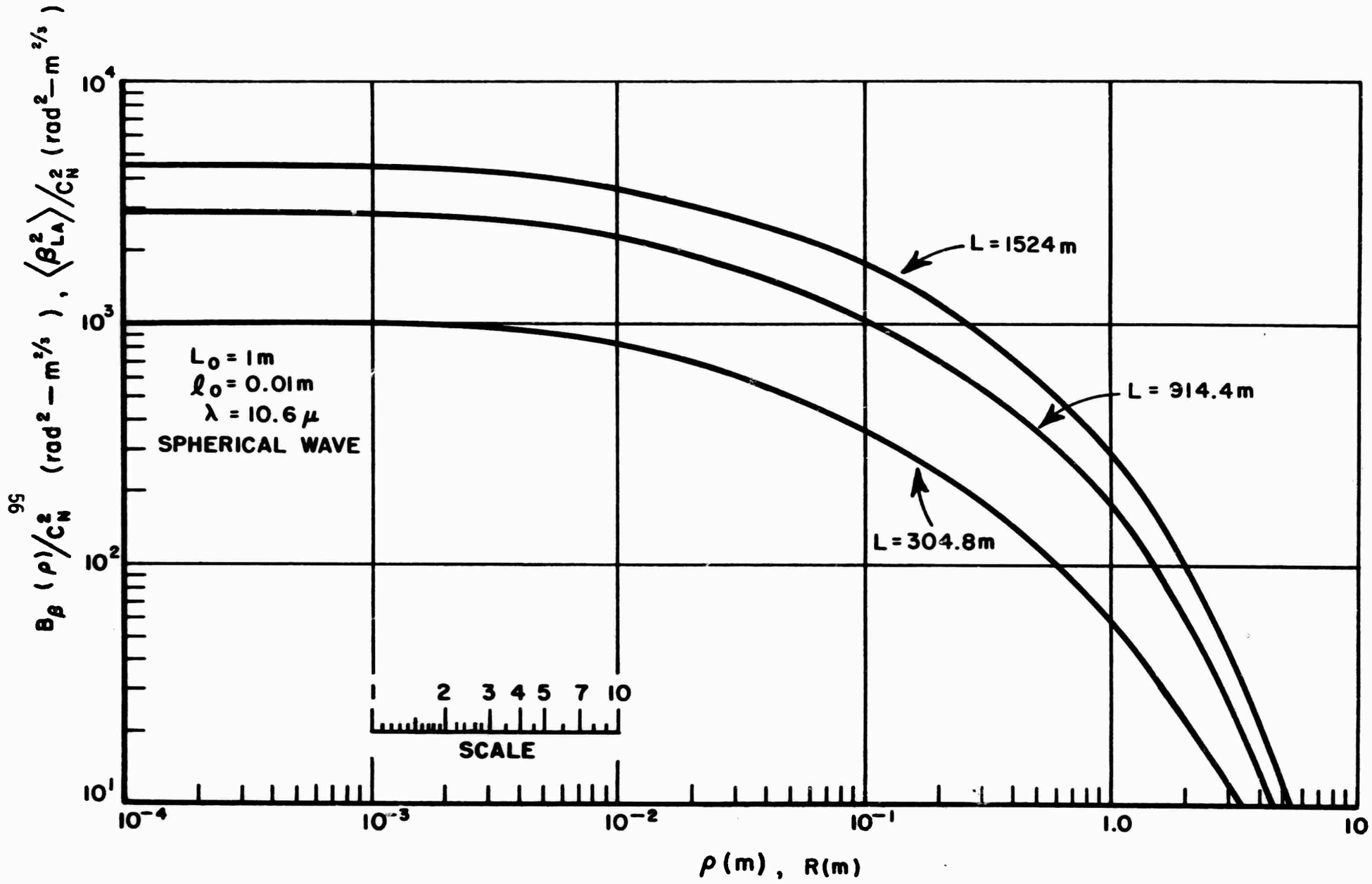

Fig. 34. Small aperture azimuth angle of arrival correlation versus separation and large aperture mean square angle of arrival versus aperture radius for spherical wave input, L_0 = 1 m, ℓ_0 = 0.01 m.

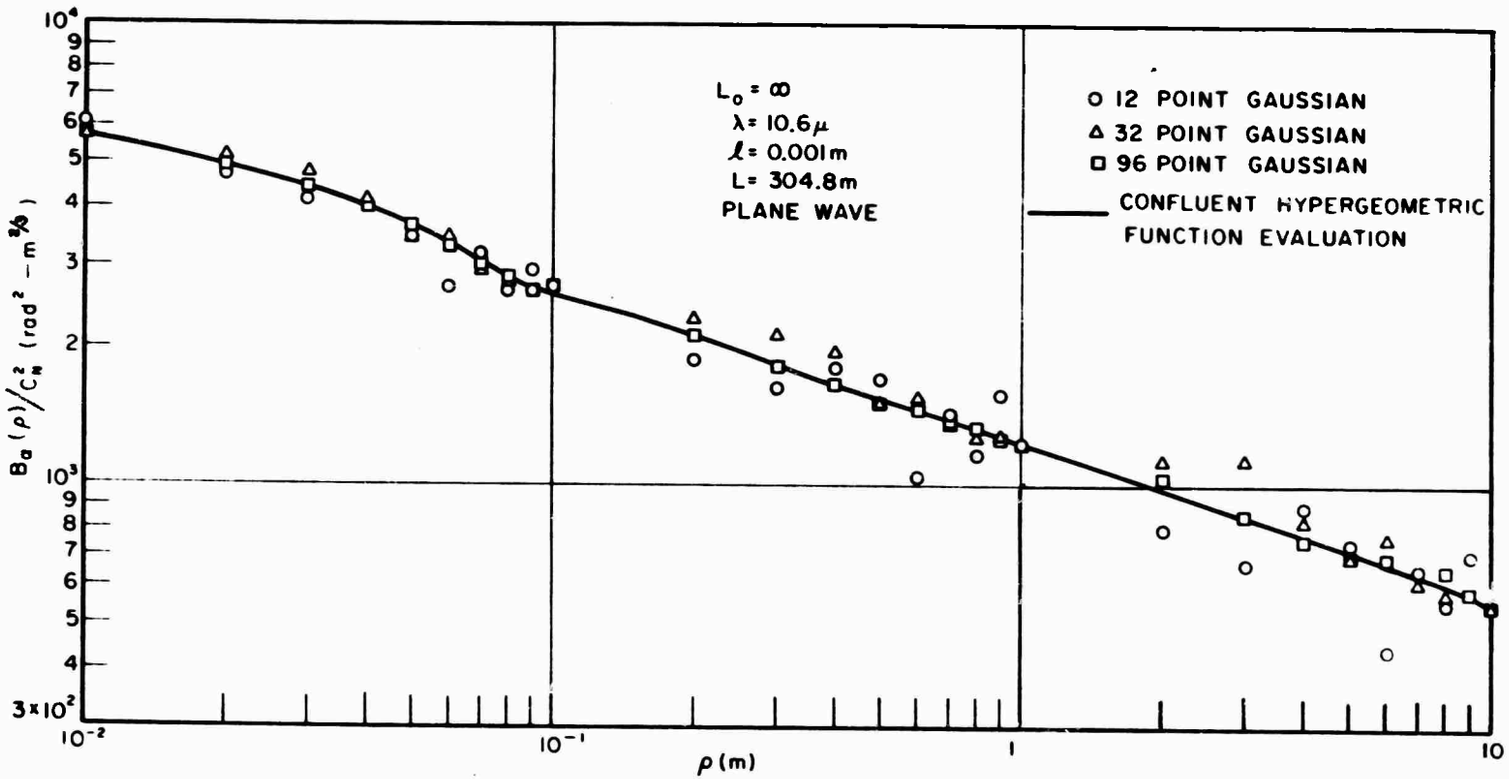

Fig. 35. Comparison of numerical techniques used to calculate small aperture angle of arrival correlation functions.

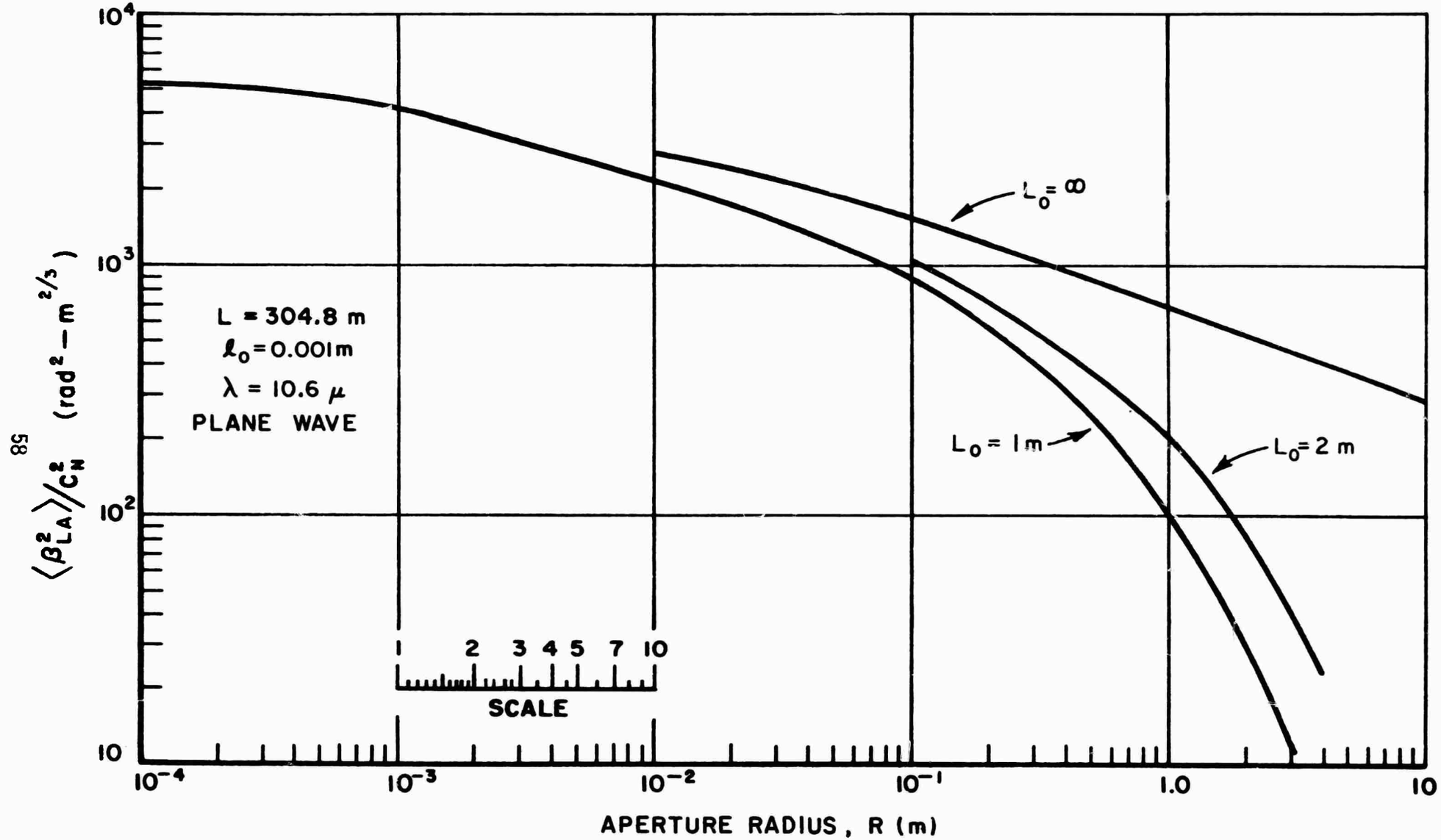

Fig. 36. Large aperture mean square angle of arrival versus aperture radius for three outer scales.

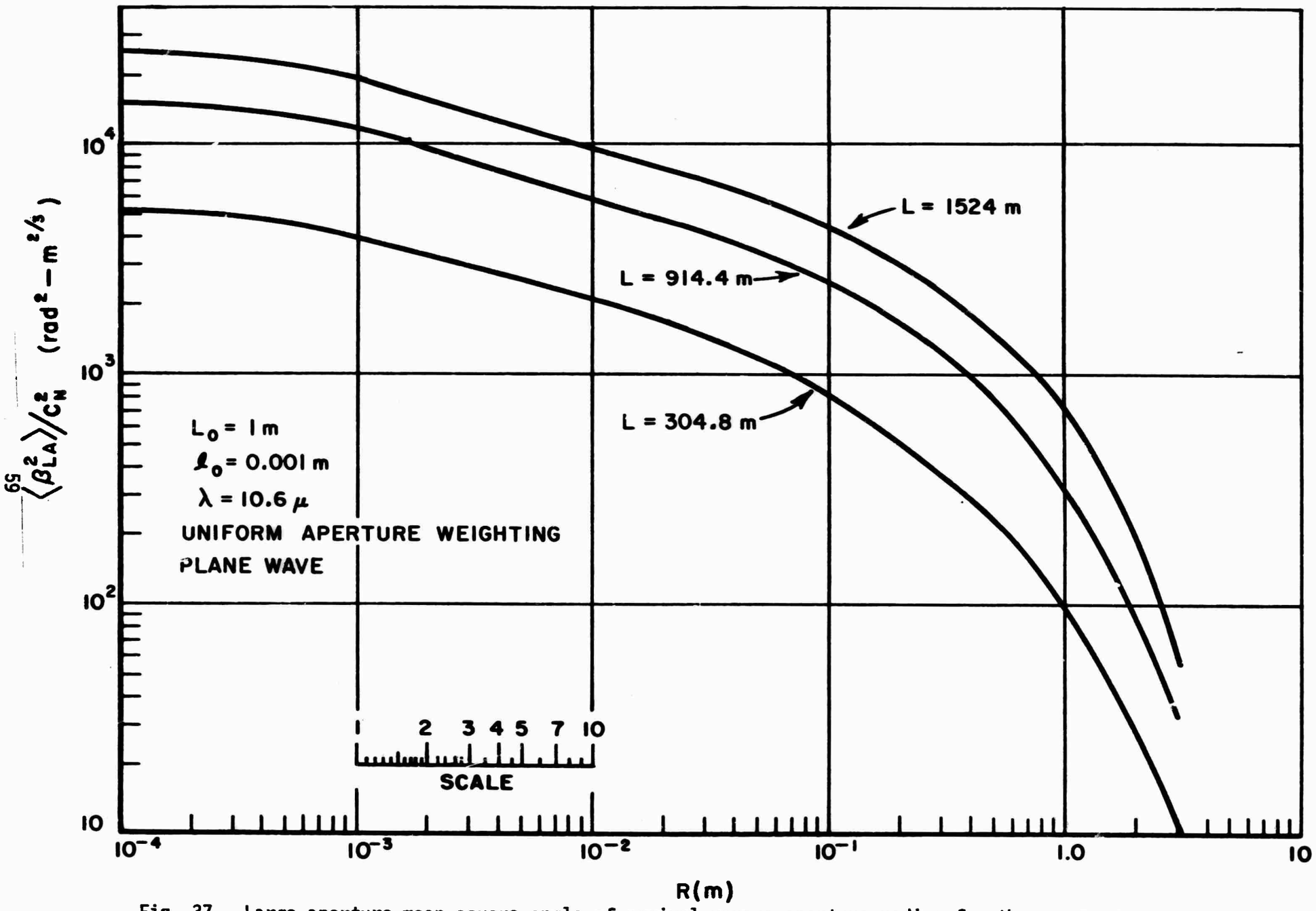

Fig. 37. Large aperture mean square angle of arrival versus aperture radius for three ranges.

This concludes the presentation of data. Large and small aperture angle of arrival data predicting experimental results have been calculated for a range of typical cases. The effects of range, inner and outer scales, separation and aperture size have all been demonstrated.

Since all of the equations derived in this report are functions of $D_S(\rho)$, the validity of these results depends on the validity of the Rytov approximation. This topic will now be briefly considered. The question has been the subject of many discussions[18-26] and the criterion which seems appropriate at this time to the calculations in this report is $D_S(\rho) << \pi$. This result was reached by Tatarski from calculations of the second order term of $D_S(\rho)$.[18] A similar result was also reached by DeWolf.[19] To quantify this result we consider ρ much greater than ℓ_0 and set [5,(47.37)]

$$D_S(\rho) = 2.92\, C_N^2\, k^2\, \rho^{5/3}\, L << \pi. \tag{44}$$

For convenience, replace the "much less than π" with $\pi/10$. Thus, we can write Eq. (44) as

$$\rho = \left(\frac{\pi}{29.2k^2}\right)^{3/5} (C_N^2\, L)^{-3/5}. \tag{45}$$

This is shown plotted in Fig. 38.

In Fig. 38 several range, $C_N^2 L$, combinations are shown. We see that for the longest range used earlier, 1524 m and for strong turbulence $C_N^2 = 10^{-14}\ m^{-2/3}$, the maximum permissible separation, ρ, is approximately 9.2 cm. This means that the angle of arrival two-point correlation is valid for $\rho < 9.2$ cm and the large aperture results are valid for $R < 9.2$ cm. As the range and turbulence levels decrease we note that the restrictions are relaxed.

It should also be noted that the form used for $D_S(\rho)$ does not include saturation effects due to the outer scale. Since the validity criterion was derived independently of the exact form of the refractive index fluctuations saturation effects may extend the region of validity. Furthermore, it has been suggested the region of validity may be larger than calculated.[5],[27] Measurements by Bouricius and Clifford at .632μ[27] suggest this result and indicate that more study is required.

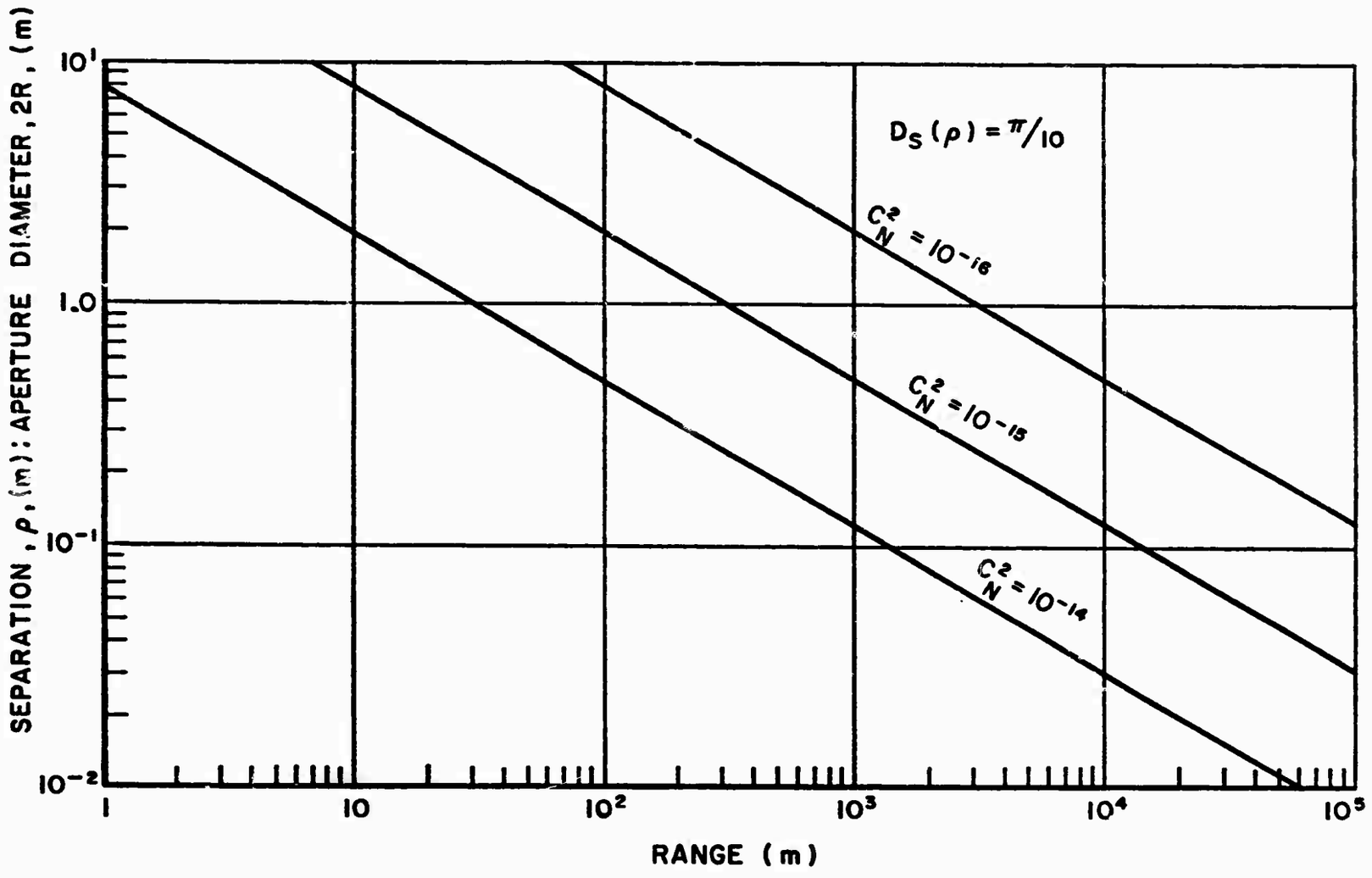

Fig. 38. Areas of validity for Rytov approximation.

To summarize the work presented in this section, data were presented predicting results of various angle of arrival experiments for various conditions. First the formulae to be used for the phase structure function and refractive index turbulence spectra were presented. Then expressions given in previous sections for small aperture arrival correlation functions were evaluated, and plotted. For infinite outer scale the expressions could be written as closed form expressions, for finite outer scale they had to be evaluated numerically. Both elevation and azimuth angle correlation functions, respectively $B_\alpha(\rho)$ and $B_\beta(\rho)$, were calculated and graphed for plane waves for ranges 304.8 m, 914.4 m and 1524 m, outer scales of infinity, 1 m and 0.159 m, and inner scales of 0.001 m and 0.01 m. This data was then repeated for spherical waves. The large aperture mean square arrival angle was also evaluated from a previously presented formula. Only a few cases were evaluated because of a synonymity which allowed the small aperture azimuth arrival angle correlation curves as a function of separation, ρ, to be relabled with large aperture mean square arrival angle as a function of aperture radius, R, thus allowing many of the results to serve double duty. The section was concluded with a discussion of the Rytov approximation on which the phase structure function was based.

VI. ANGLE OF ARRIVAL SYNONYMITY

This section deals explicitly with a relationship between the angle of arrival variance for large aperture receiver as a function of aperture radius, R, and the small aperture azimuth correlation function, $B_\beta(\rho)$ taken as a function of ρ. The particular relationship is that they are synonymous over a sizable range of values of the argument. These two situations are shown in Fig. 39 to facilitate the comparison between the two. Figure 39a shows a standard large aperture arrival angle measurement situation. An atmospherically degraded beam from a point source is focussed to a degraded spot. The information about angle of arrival is obtained from the transverse motion of the spot, the arrival angle being proportional to the spot displacement. Figure 39b shows a possible situation for the measurement of small aperture arrival angle correlation function. The angles of arrival at two pinholes are determined independently by monitoring the two pinhole diffraction patterns, the motion of the center of each pattern being proportional to the individual arrival angle. In the case at hand, only the x component of motion is of interest. The pinholes are sufficiently small that the amplitude is constant over the hole. Then the quantity of interest is the correlation of arrival angles between these two pinholes, the correlation being a function of ρ, the separation of the pinholes. In the case of interest the pinholes are separated in the direction perpendicular to the direction in which the spot motion is being monitored, (the x direction in Fig. 39).

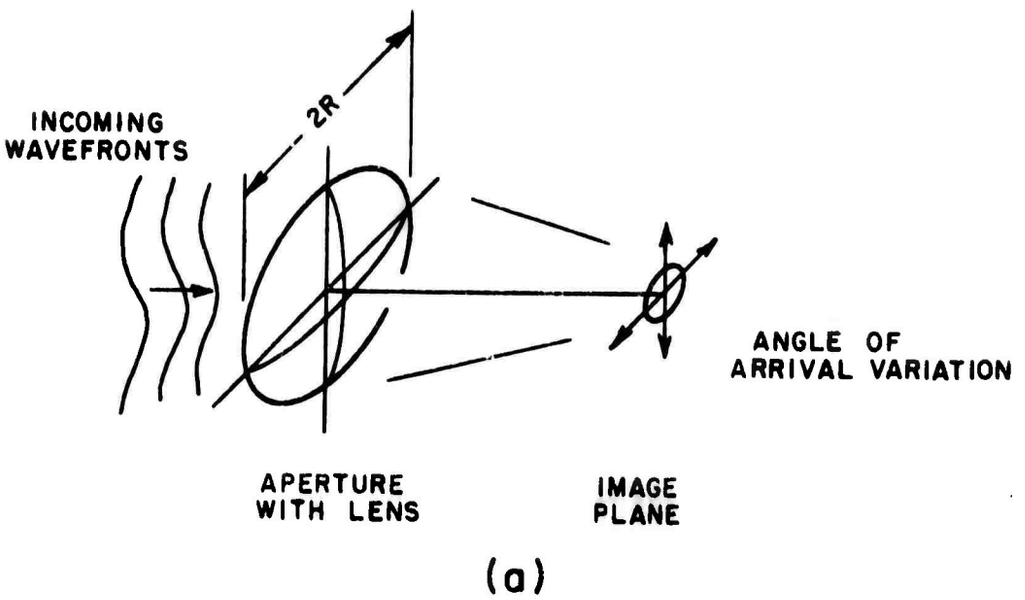

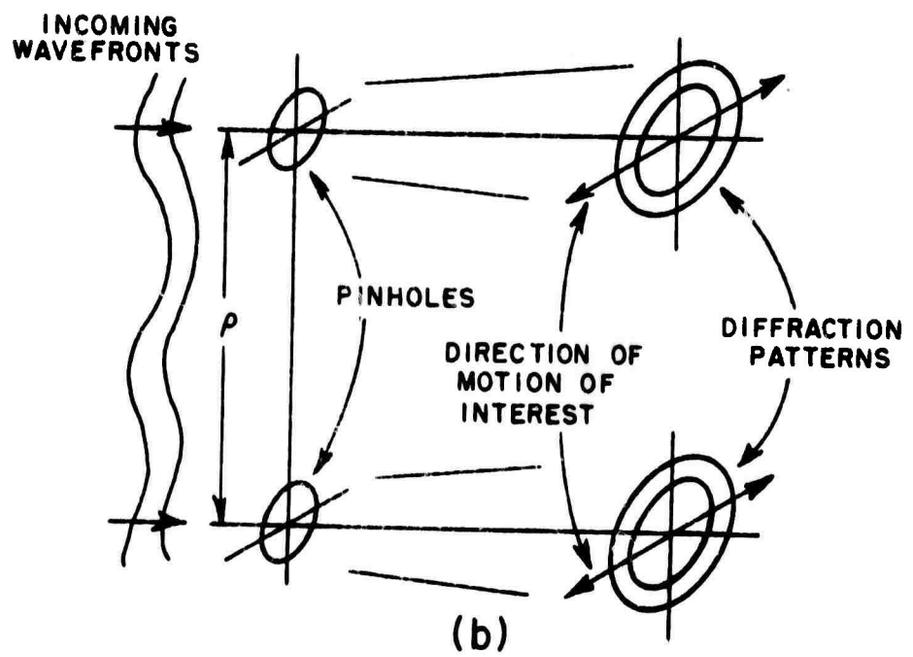

Fig. 39. Comparison of the definitions of the large aperture mean square angle of arrival and the small aperture angle of arrival correlation.

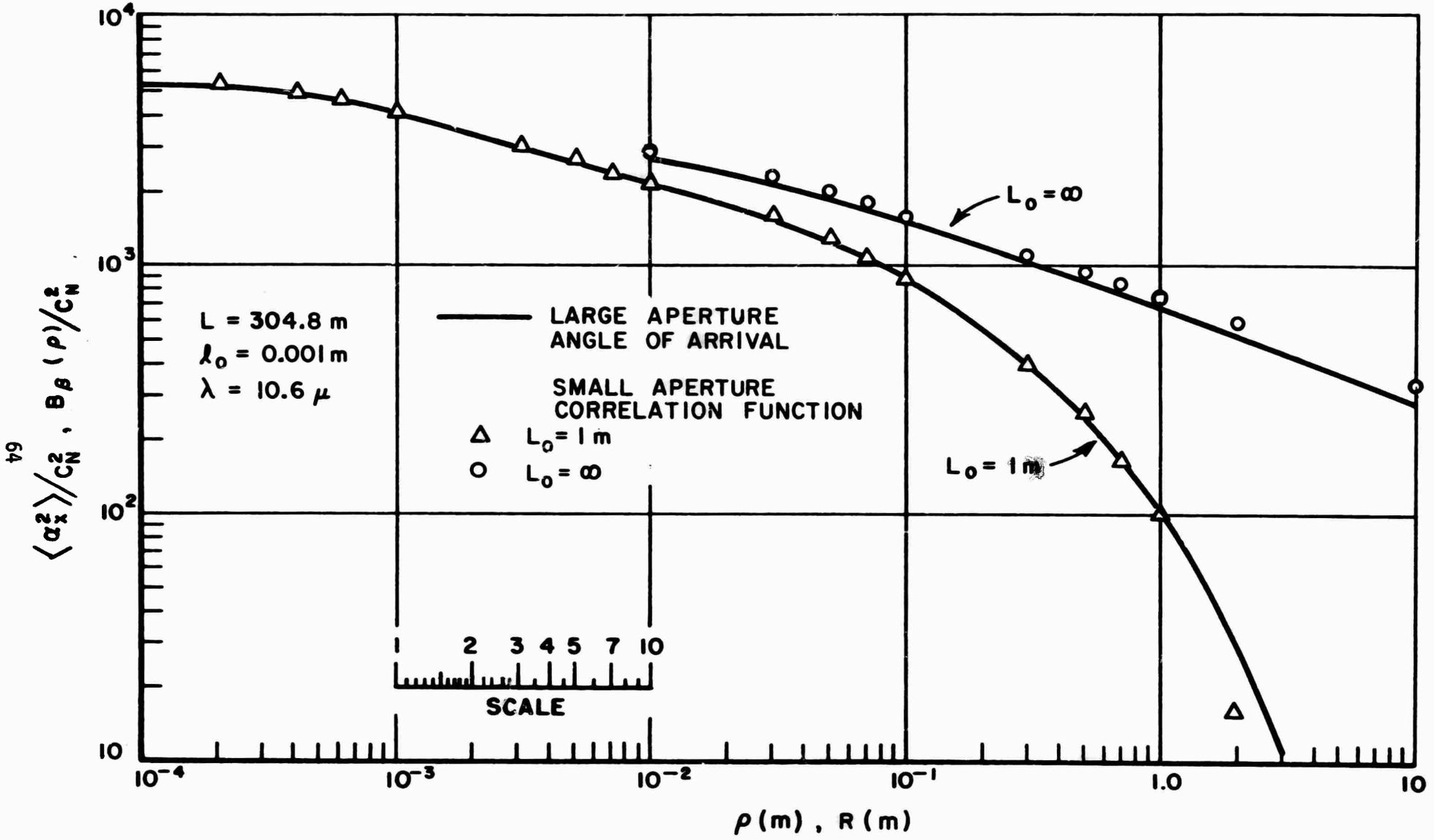

Fig. 40. Comparison of the large aperture mean square angle of arrival and the small aperture azimuth angle of arrival correlation function.

Comparing Eqs. (46) and (47) we see that both expressions can be written in the form

$$(48) \qquad 4\pi^2 L \int T(\kappa)\, F(\kappa)\, \Phi_N(\kappa)\, \kappa^3\, d\kappa$$

where $T(\kappa)$ is the filter function peculiar to the particular operation, $F(\kappa)$ identifies the type of wave, and $\Phi_N(\kappa)$ is the refractive index turbulence spectrum. Denoting the particular small and large aperture filter functions by $SA(\kappa\rho)$ and $LA(\kappa R)$ respectively, we have

$$(49) \qquad SA(\kappa\rho) = J_1(\kappa\rho)/\kappa\rho$$

$$(50) \qquad LA(\kappa R) = -(16/\pi R^8 \kappa^2) \int_0^R r^2\, dr \int_0^R \rho^2\, d\rho \int_0^\pi \cos\gamma\, [1 - J_0(\kappa\sqrt{r^2+\rho^2-2r\rho\cos\gamma})]\, d\gamma .$$

Equations (49) and (50) describe the manner in which the receiving aperture interprets the angle of arrival. Graphs of these functions are shown in Fig. 41. For convenience in comparison we shall take them both to be functions of the same variable to be called R. We see in this figure that the two filter functions are synonymous over a wide range of κR.

The synonymity is limited with respect to the range of the variable R over which it applies. This occurs because of the relative size of the filter function and the other functions, $F(\kappa), \Phi_N(\kappa)\, \kappa^3$ in the frequency integral. If the other functions are of significant size only when the filter functions are almost identical, i.e., in the region, $0 < \kappa R < 4$, then the identity will hold. If the other functions have large contributions for $\kappa R > 4$ then the synonymity will break down.

To more quantitatively define the regions of applicability for the angle of arrival synonymity we define $\varepsilon(R)$, the error between the two functions relative to the small aperture correlation function,

$$(51) \qquad \varepsilon(R) = \frac{B_\beta(R) - \langle \alpha_x^2 \rangle}{B_\beta(R)} \quad .$$

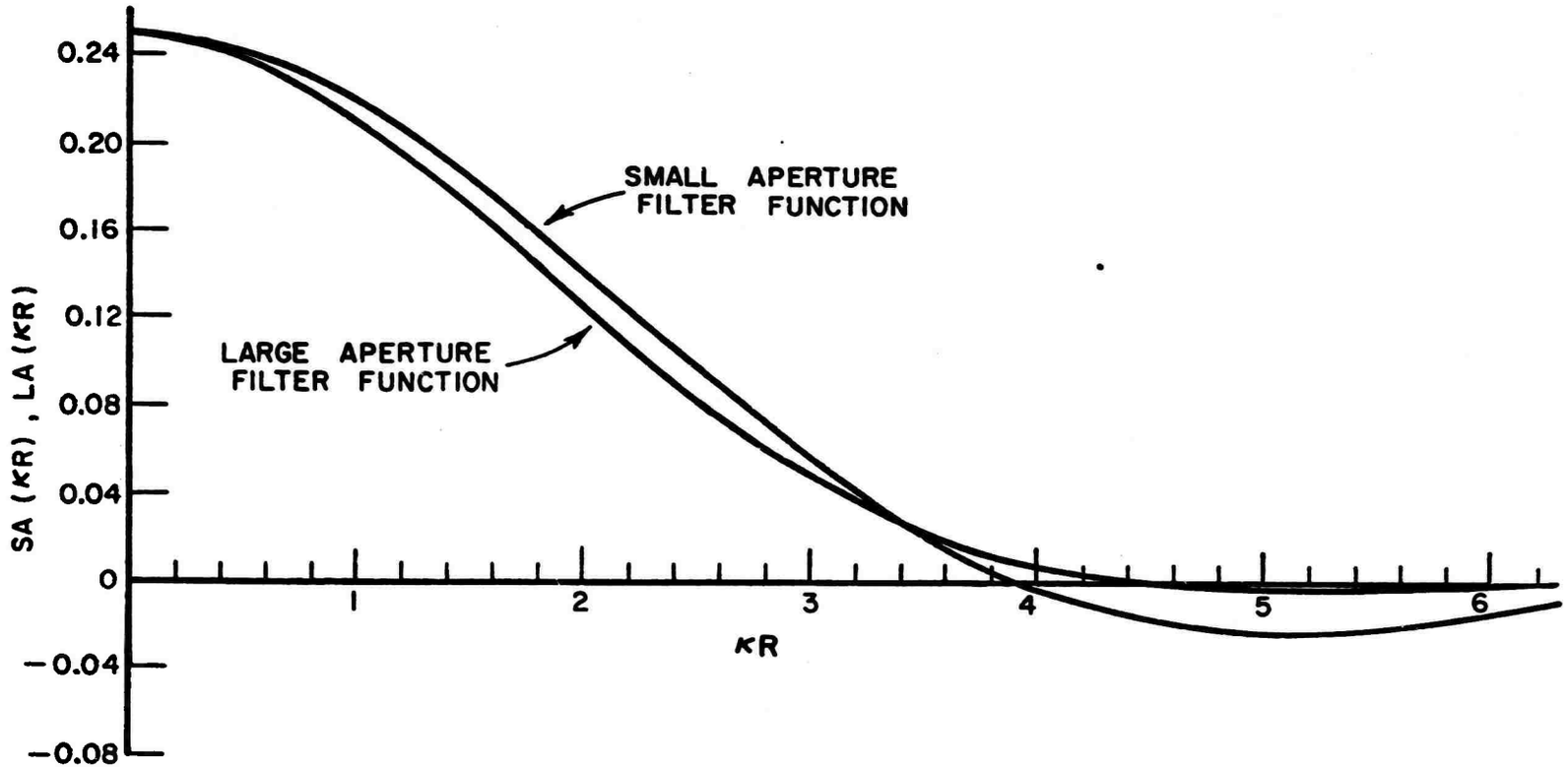

Fig. 41. Comparison of the large and small aperture angle of arrival filter functions.

The numerator of Eq. (51) is given by an integral, $I_D(\kappa R)$ of the difference between Eqs. (46) and (47). Using the difference function $\Delta(\kappa R)$ given in Eq. (52) and shown in Fig. 42,

$$\Delta(\kappa R) = SA(\kappa R) - LA(\kappa R) \tag{52}$$

the numerator integral is

$$I_D(\kappa R) = 4\pi^2 L \int_0^\infty \Delta(\kappa R)\, F_s(\kappa)\, \Phi_N(\kappa)\, \kappa^3\, d\kappa. \tag{53}$$

For a plane wave, $F_s(\kappa)$ varies between 1 and 2 and has little effect, thus, making $\Delta(\kappa R)$ and $\kappa^3\, \Phi_N(\kappa)$ the two functions of most interest.

We now proceed to examine $\varepsilon(R)$ qualitatively, but in some detail to determine the approximate functional dependence. This is to be done by examining the curves for $SA(\kappa R)$, $LA(\kappa R)$, $\Delta(\kappa R)$, and $\kappa^3\, \Phi_N(\kappa)$ and the various ways they can combine for various values of R. These curves are plotted quite precisely in Figs. 41, 42, and 43, using for $\Phi_N(\kappa)$ the Von Karman spectrum given in Eq. (33). The various functions are compared in Fig. 44 for several values of R. The effect of choosing various values of R is to select particular horizontal scales for the filter functions $SA(\kappa R)$, $LA(\kappa R)$ and $\Delta(\kappa R)$. Thus, as seen in Fig. 41, $LA(\kappa R)$ goes essentially to zero at $\kappa = 4.4/R$ and $SA(\kappa R)$ has its first zero at $\kappa = 3.9/R$. Fig. 42 shows that the difference function, $\Delta(\kappa R)$ has its first zero at $\kappa = 3.4/R$, pretty much in the same region. Examining curves in Fig. 44a and we see that for $R \ll \ell_o$ the small and large aperture filter functions are nearly constant over the complete range of $\kappa^3\, \Phi_N(\kappa)$ so that $B_\beta(R)$ and $\langle \alpha_x^2(R) \rangle$ are identical, each being given by that integral over $\kappa^3\, \Phi_N(\kappa)$. For $R = 4.4/\ell_o$, comparing Figs. 44a and 44c, we see that both $LA(\kappa R)$ and $SA(\kappa R)$ go to zero at about the same place that $\kappa^3\, \Phi_N(\kappa)$ becomes very small. For that case both curves are finite over the range $0\text{-}1/L_o$, the product at any point being less than the value of either curve. The integral over the product is then starting to decrease. This is the region of R where the curves of $B_\beta(\rho)$ and $\langle \alpha_x^2(R) \rangle$ start to decrease, as shown on graphs of these functions. Further the value of the error $\int \Delta(\kappa R)\, \kappa^3\, \Phi_N(\kappa)\, d\kappa$ has been increasing with R and has possibly a local maximum because $\Delta(\kappa R)$ has a negative portion where $\kappa^3\, \Phi_N(\kappa)$ is still finite.

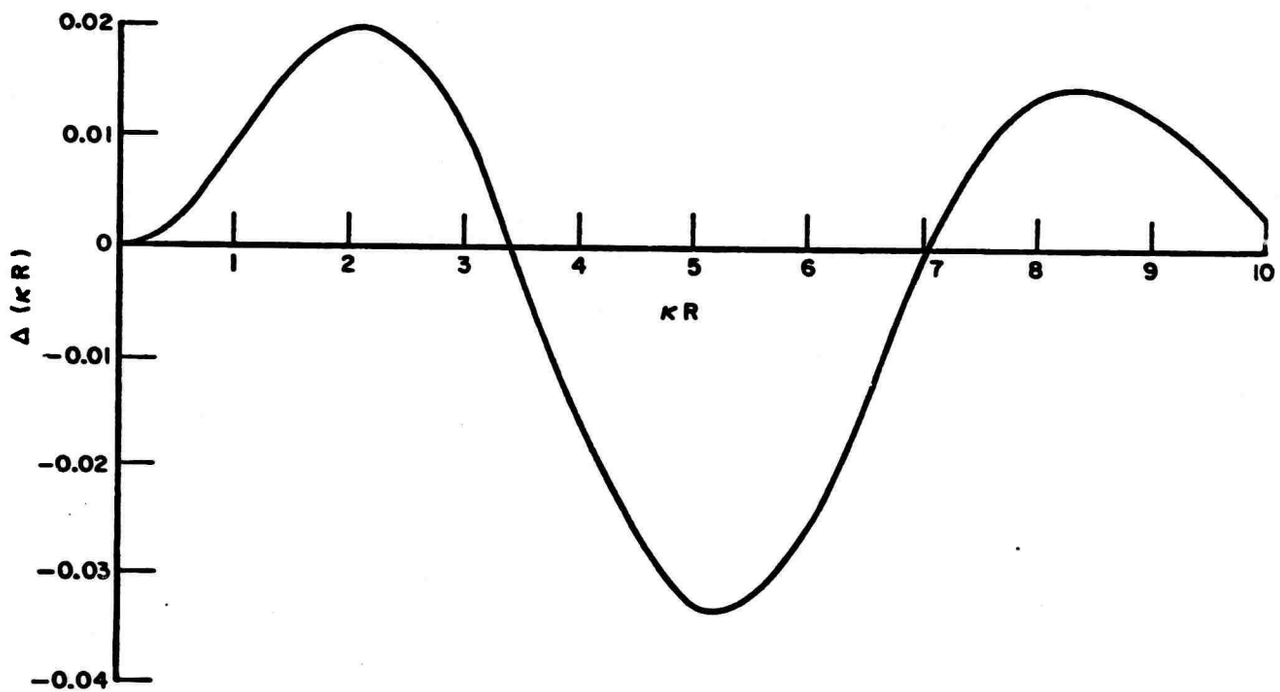

Fig. 42. Large and small aperture angle of arrival difference function versus spatial frequency.

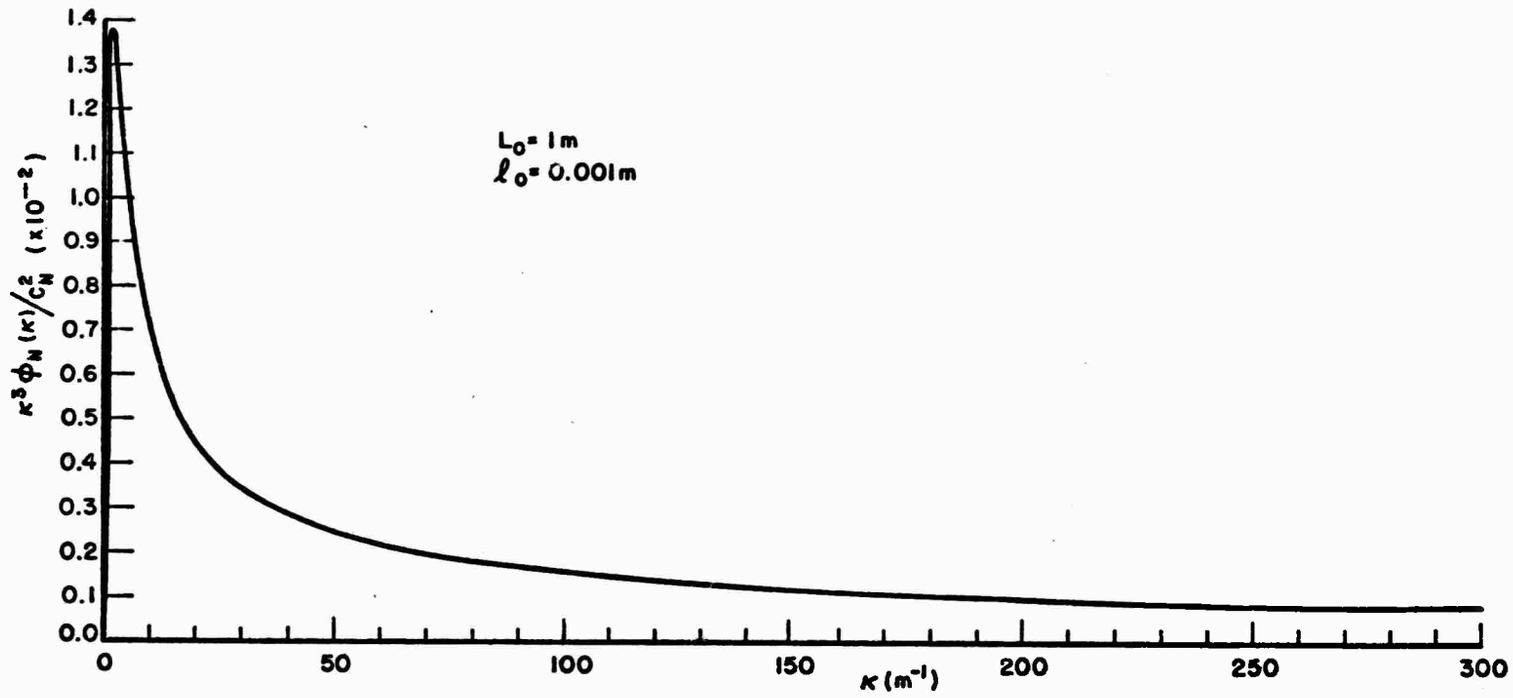

(a)

Fig. 43. Modified refractive index fluctuation spectrum for finite outer scale versus spatial frequency.

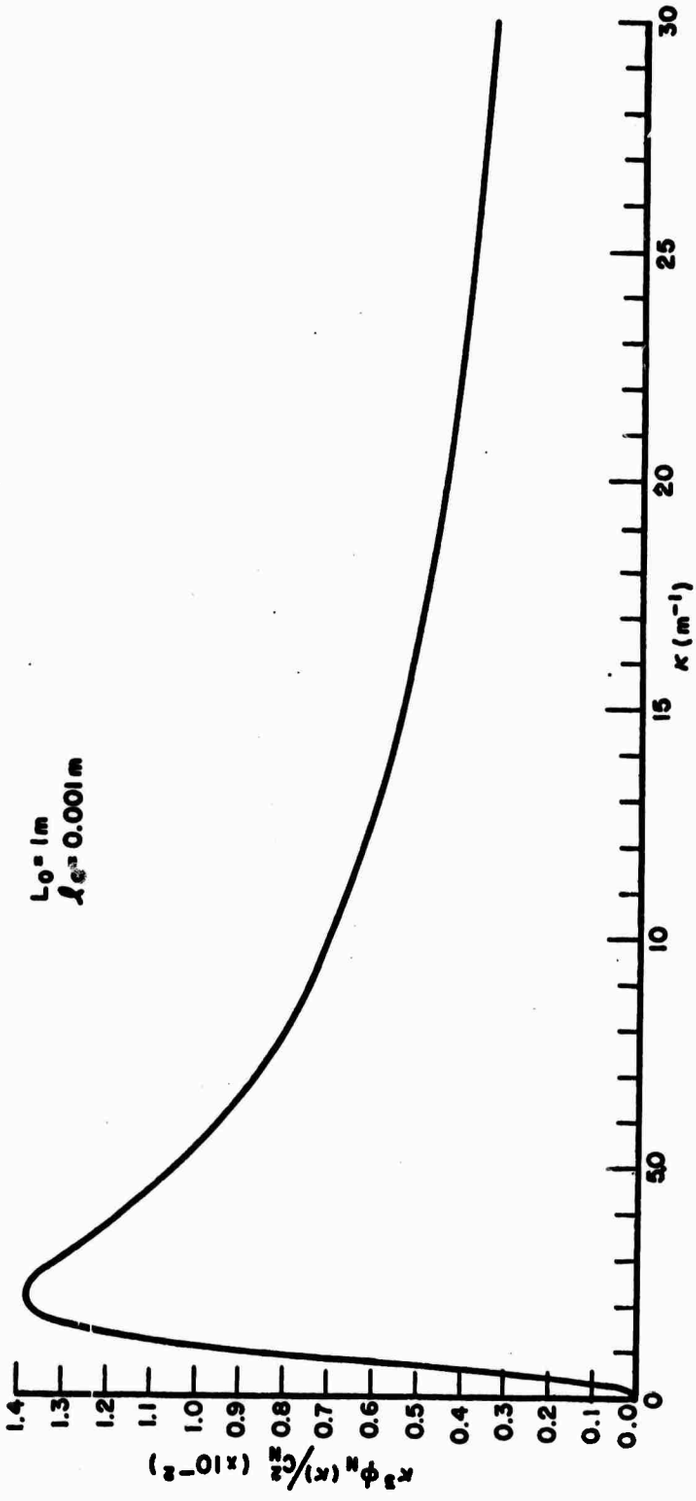

(b)

Fig. 43. (Contd.)

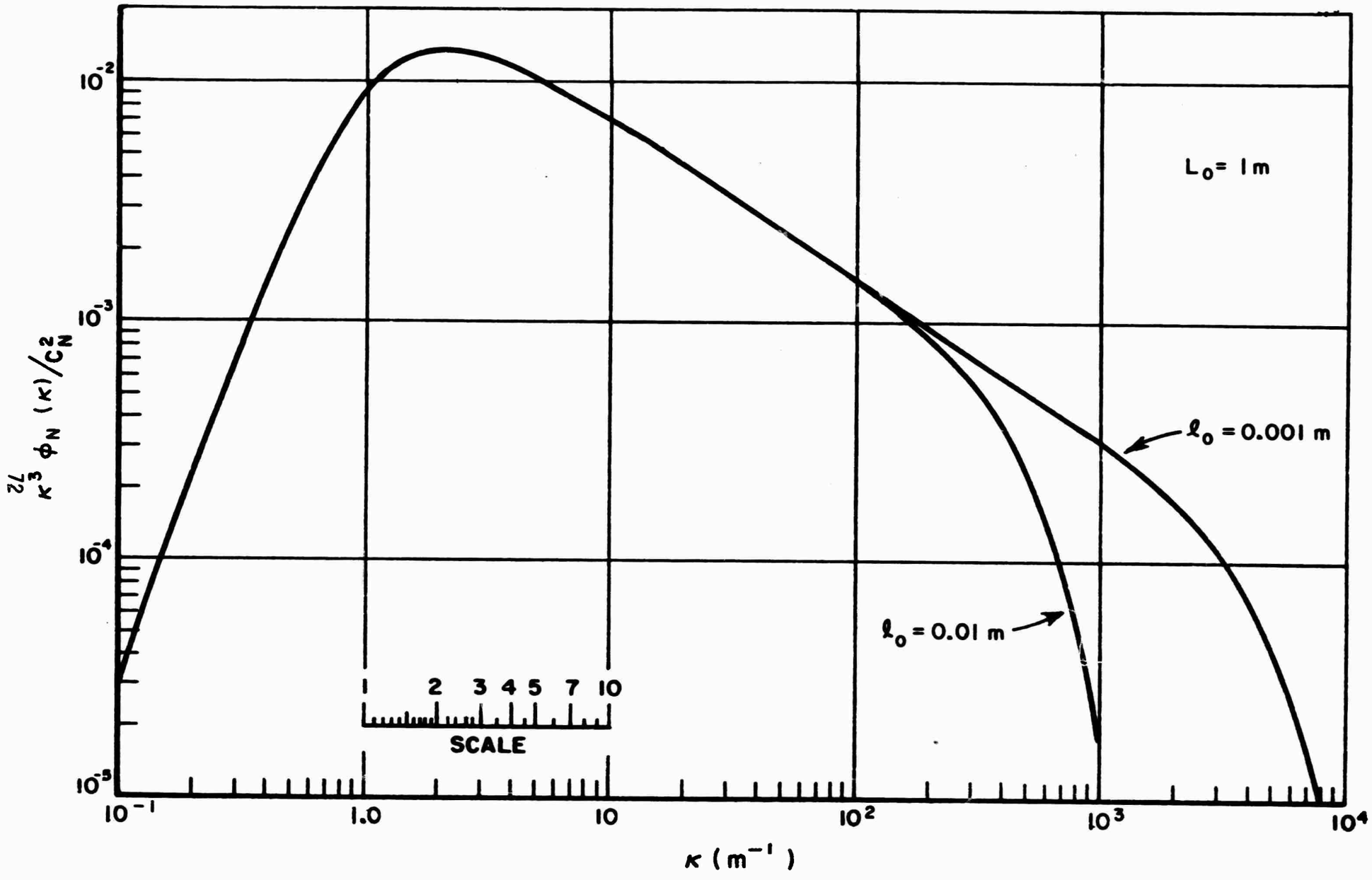

(c)

Fig. 43. (Contd.)

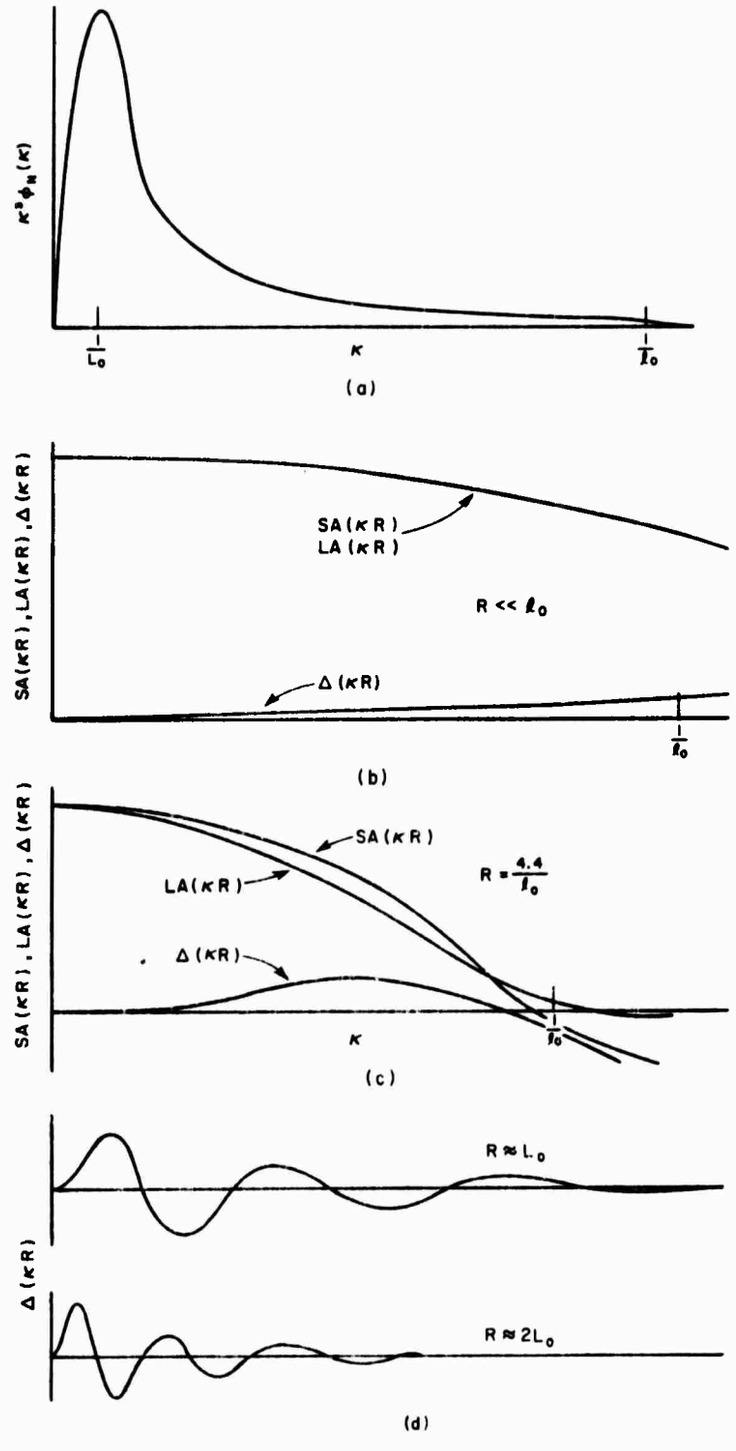

Fig. 44. Comparison of large and small aperture filter functions with the modified refractive index fluctuation spectrum.

For R in the region of L_o, comparing Figs. 44a and 44d shows that $\Delta(\kappa R)$ and $\kappa^3 \Phi_N(\kappa)$ both have large positive portions in the region of $\kappa \simeq 1/L_o$. One would expect a local maximum in the error around this region. As R increases slightly past L_o, the first zero of the $\Delta(\kappa R)$ curve approximately coincides with the peak of the $\kappa^3 \Phi_N(\kappa)$ curve so that the product is positive for $\kappa < 1/L_o$ and negative for $\kappa > 1/L_o$. One would expect the error to decrease for this region of R. Finally as R becomes still larger, the error curve will oscillate. This expected qualitative behavior is sketched in Fig. 45.

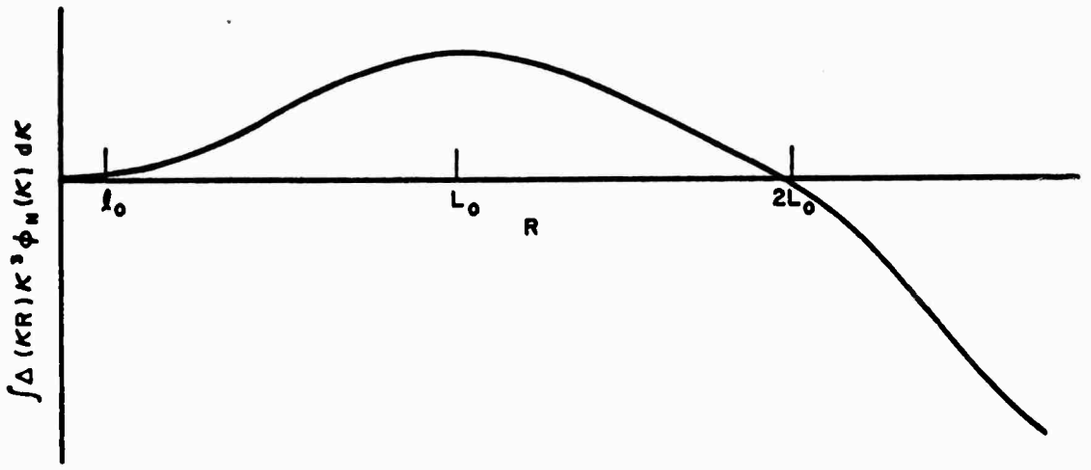

Fig. 45. Integrated large and small aperture angle of arrival difference function.

One can further examine the relative error, ε, defined in Eq. (51). In particular for the case where $R < L_o$ the product of $LA(\kappa R)$ and $\kappa^3 \Phi_N(\kappa)$ becomes quite small, being limited for small κ by $\kappa^3 \Phi_N(\kappa)$ and for large κ by $LA(\kappa R)$. Then $\langle \alpha_x^2(R) \rangle$ in Eq. (51) is relatively small and $\varepsilon(R)$ approaches unity. Thus the assymptotic value of $|\varepsilon(R)|$ is 1.00, i.e., 100% error. The expected qualitative behavior for $\varepsilon(R)$ is then plotted using the data on $\Delta(\kappa R)$, $SA(\kappa R)$ and the assymptotic value. The plot is given in Fig. 46.

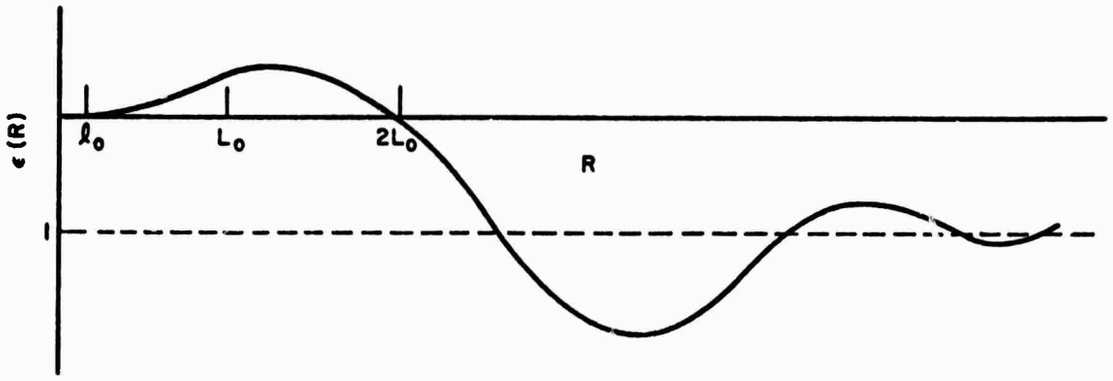

Fig. 46. Angle of arrival synonymity error function showing asymptotic behavior.

These qualitative results are confirmed by the quantitative numeric evaluation in Eq. (53), (including $F_S(\kappa)$) shown in Fig. 47. These numeric calculations required considerable computation time so only enough points were calculated to show the nature of the curves. Thus, some oscillations have more than likely been suppressed and the final value of $\varepsilon(R)$ was not reached. Accuracy in these calculations was difficult to obtain, however, the results are certainly correct to at least order of magnitude and demonstrate the behavior predicted earlier.

Three cases are shown in Fig. 47 corresponding to earlier calculations. The first characteristic we note is that $\varepsilon(R)$ is fairly small for $R < L_o$. This implies that for aperture diameters less than twice the outer scale, the large aperture mean square angle of arrival can be approximated by the small aperture azimuth correlation function. From Fig. 47 we see that this error will be on the order of 10%. Second, we note the range has very little effect as is to be expected. What effect the range, L, does have is incorporated in $F_S(\kappa)$.

To summarize, in this section, we have stated that the large aperture angle of arrival mean square value and the small aperture azimuthal angle of arrival correlation function are synonymous. The functional dependence was demonstrated to be very nearly equal for typical cases. The relationship was examined in the spectral domain both qualitatively and quantitatively showing that the results should be expected to be well within ten percent for values of the argument up to the outer scale.

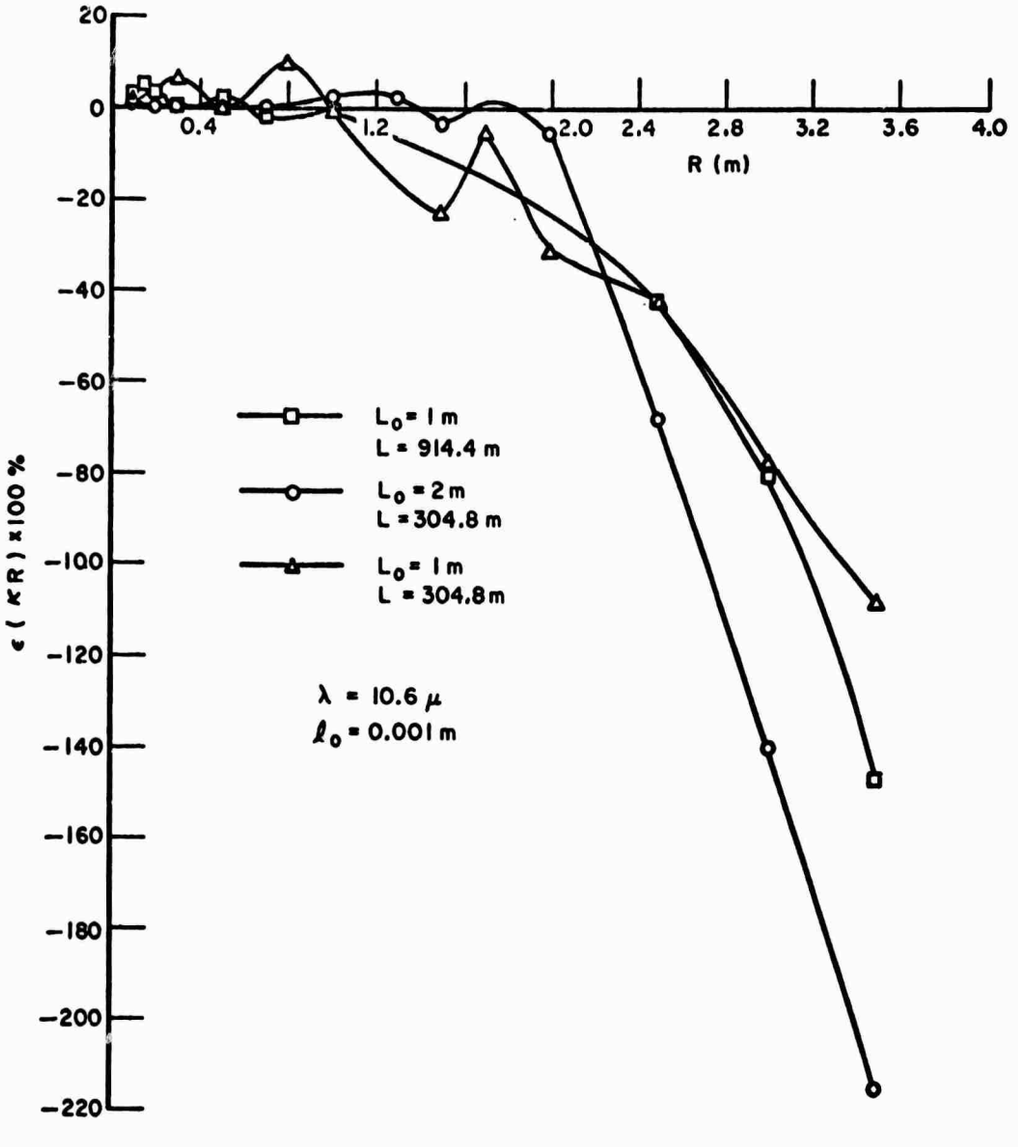

Fig. 47. Angle of arrival synonymity error function for two outer scales and two ranges.

VII. SUMMARY

In this report the subject of angle of arrival of light beams degraded by propagation through atmospheric turbulence has been considered. Data on arrival angle experiments was calculated for two types of experiments for a wide variety of cases and an equivalence between two types of angle of arrival experiments was demonstrated. In Chapter II the subject was introduced and reviewed, and the literature enumerated. It was pointed out that there were two approaches to angle of arrival considerations, one using a pair of pinhole apertures and the other using a single large aperture. In Chapter III the area of small aperture angle of arrival calculations was reviewed in detail, the basic theoretical expressions being derived. The calculation of large aperture angle of arrival was discussed in Chapter IV. In Chapter V the analytic expressions derived in Chapters III and IV were evaluated using a particular expression for the refractive index spatial spectrum, namely the Von Karman spectrum. The results were presented graphically for the two angle of arrival situations for variety of cases including various inner and outer scales. The Rytov approximation used in the derivation of the phase structure function used was considered and a graph given showing the expected range of validity the calculations. In Chapter VI a synonymity was presented between the large aperture angle of arrival mean square value expressed as a function of aperture radius and the small aperture azimuth angle of arrival correlation function taken as a function of aperture separation. This synonymity was used in Chapter V to simplify calculations and also offers the possibility of simplification of experimental measurements. The limitations on the synonymity were demonstrated.

APPENDIX A
DISCUSSION OF REFRACTIVE INDEX FLUCTUATION SPECTRA

Various forms of the refractive index fluctuation spectra have been used to find solutions of the wave equation for an inhomogeneous random media. Two forms which have been used recently are compared in this appendix. The choice of one of the constants is explained and several interesting characteristics noted. The derivations of these spectra are not presented since they are outside the scope of this report.

Kolmogorov theory predicts that the refractive index structure functions should have the following asymptotic behavior

$$(A1) \qquad D_N(r) = \begin{cases} C_N^2 \, \ell_o^{2/3} \, (\frac{r}{\ell_o})^2 & 0 < r << \ell_o \\ C_N^2 \, r^{2/3} & \ell_o << r << L_o \end{cases}$$

where

ℓ_o = inner scale of turbulence

L_o = outer scale of turbulence

C_N^2 = structure constant of the turbulence.

It can be shown that the Kolmogorov spectrum as used by Tatarski in [5] and given in Eq. (A2)

$$(A2) \qquad \Phi_N(\kappa) = .033 \, C_N^2 \, e^{-\kappa^2/\kappa_m^2} \, \kappa^{-11/3}$$

$$\kappa_m = \frac{5.92}{\ell_o}$$

has a structure function of the form

$$(A3) \qquad D_N(r) = 1.67\, C_N^2\, \kappa_m^{-2/3} \left[{}_1F_1\left(-\frac{1}{3}, \frac{3}{2}, -\frac{\kappa_m^2 r^2}{4}\right) - 1 \right]$$

where ${}_1F_1$ signifies a confluent hypergeometric function. Further, it can be shown the confluent hypergeometric function has the proper asymptotic behavior such that Eq. (A1) is satisfied.

Another form of $\Phi_N(\kappa)$ is the Von Karmann spectrum which includes outer and inner scale effects. Several algebraic forms have been used but they can be generalized to

$$(A4) \qquad \Phi_N(\kappa) = \frac{.033\, C_N^2\, e^{-\kappa^2/\kappa_m^2}}{(\kappa^2 + \kappa_0^2)^{11/6}}$$

with

$$\kappa_0 = \frac{A}{L_0}$$

where A is a normalization constant. The value of A has been chosen as 1 in [17] and 2π in [28]. For $L_0 = \infty$, Eq. (A4) reduces to Eq. (A3) as expected.

The value of A used in this report is 1. The reason for this choice will now be explained. We note that when $A = 2\pi$, the effect is to normalize L_0 to a new value L_0' such that

$$(A5) \qquad L_0' = \frac{L_0}{2\pi} .$$

The physical interpretation of L_0 is that it is a characteristic dimension of saturation effects. To examine this situation the refractive index spectrum and structure function calculated from Eq. (A3) and Eq. (A4) and the resulting phase structure function are shown in Figs. A1-A3 respectively. Dashed lines have been added at $\rho = 1/\kappa = L_0$ for $L_0 = 1$ and $L_0' = 1/2\pi$.

Two interesting characteristics are noted. First, all of the curves tend to saturate at a value predicted approximately by

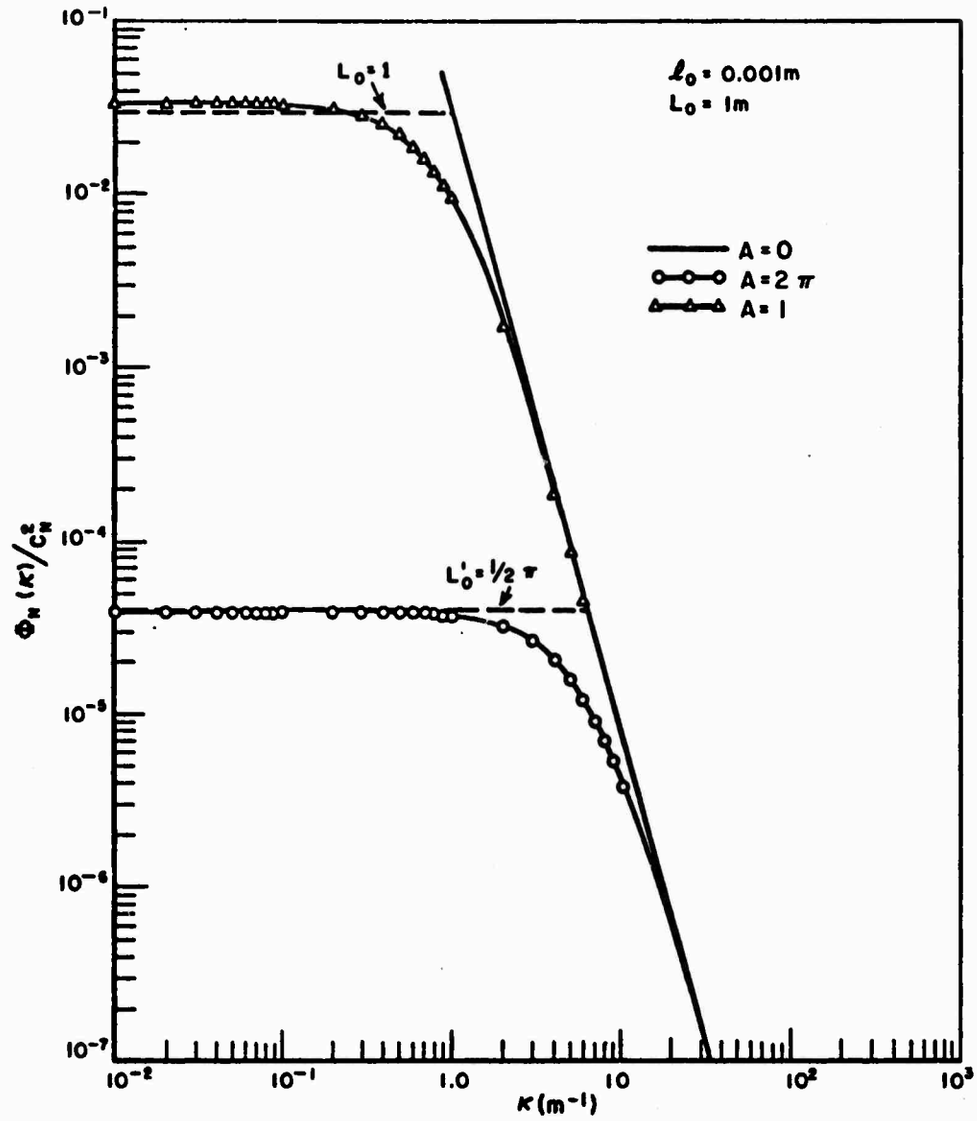

Fig. A1. Refractive index fluctuation spectrum versus spatial frequency.

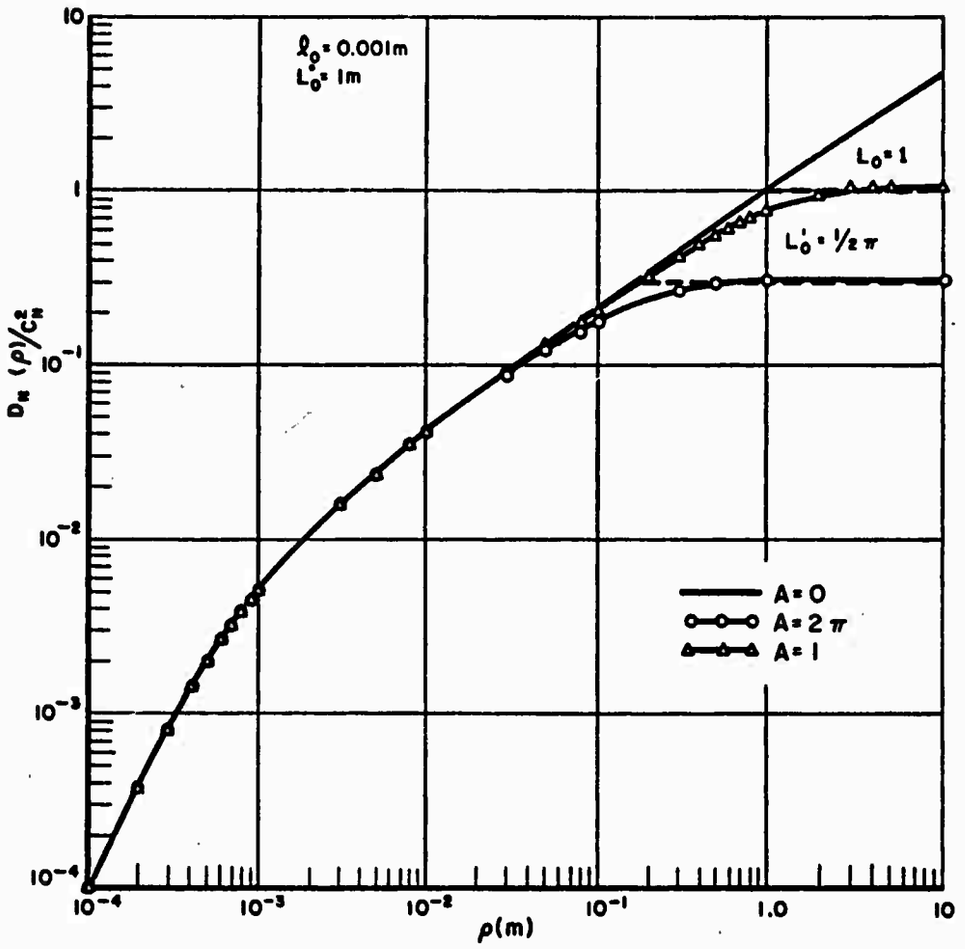

Fig. A2. Refractive index fluctuation structure function versus separation.

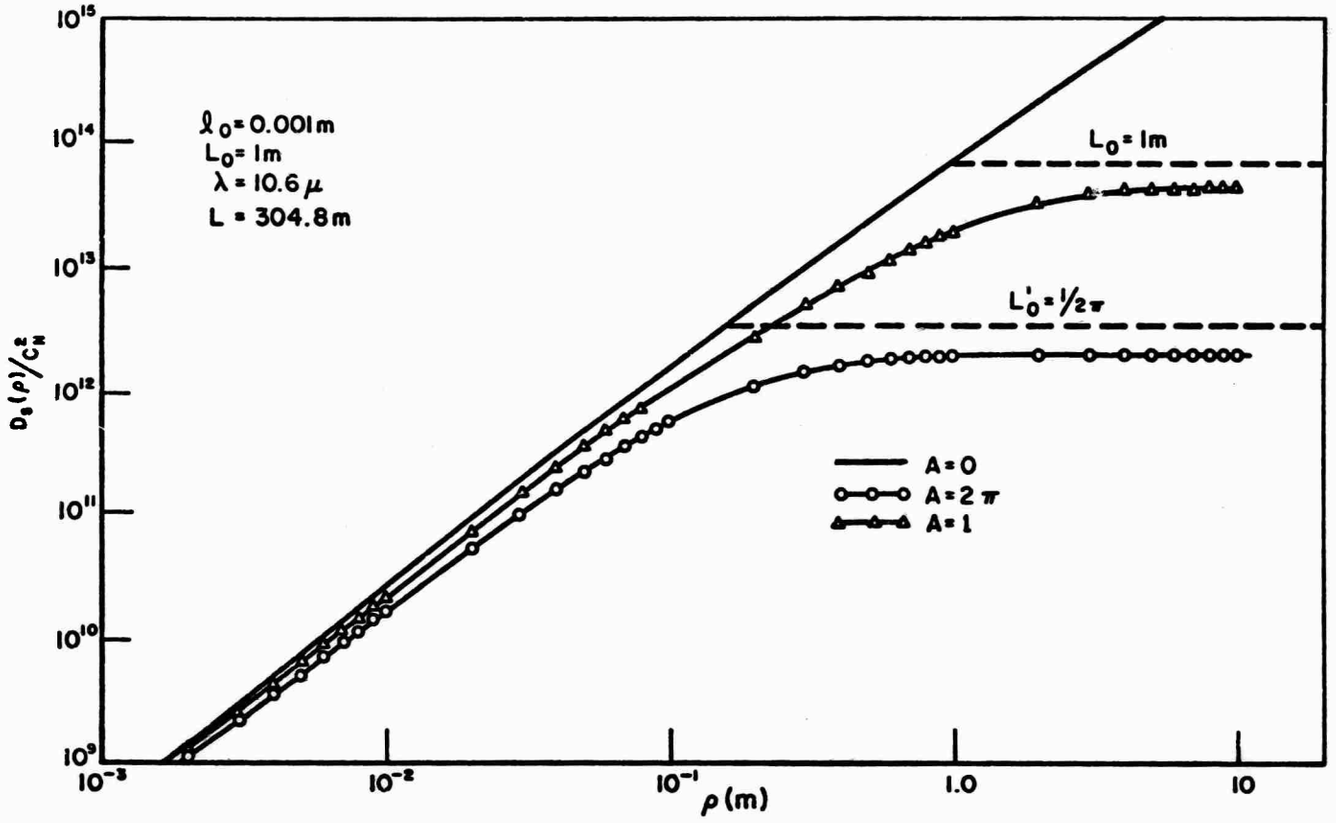

Fig. A3. Phase structure function versus separation.

the Kolmogorov spectrum at $\rho = 1/\kappa = L_0$. Secondly, the break point of the saturation occurs at the same point. These two characteristics are consistent with the original definition of the outer scale, L_0, and the use of $A = 2\pi$ merely clouds the issue. Thus, for this report A is chosen to be one.

Another interesting characteristic is seen in Fig. A3. The slope of the phase structure function in the inertial subrange is not unique. Since the effect of the outer scale is to cause saturation the slope must change continuously from that of square law to zero. Only for the special case of $L_0 = \infty$ is the slope a constant. Therefore, the outer scale makes it difficult to predict a unique slope of the phase structure function in the inertial subrange.

Concluding, two refractive index fluctuation spectra have been described and the criteria used to determine one of the constants explained. Several interesting characteristics were demonstrated.

APPENDIX B
COMPUTER PROGRAM USED FOR NUMERIC CALCULATIONS

The computer programs used for numeric calculations in this report are presented in this appendix. Each program will be described briefly and data input explained. A listing of the source deck is also presented. All programs were written for use on an IBM 360/75 computer in FORTRAN IV(G). Some subroutines are contained in the IBM Scientific Subroutine Package (360-CM-03X) Version III.

1. Small Aperture Angle of Arrival Calculations

Three programs were written to make the small aperture calculations. The first program evaluates the analytic functions for the angle of arrival mean square and 2 pt. correlation function, using the Kolmogorov spectrum and plane wave input. The second program evaluates the integral expressions using the Von Karmann spectrum and plane wave input. The third program evaluates the integral expressions for spherical wave input. These programs also calculate the refractive index fluctuation spectrum and structure function, the phase structure function and the wave structure function. Each program has numerous comment cards to describe the program flow and the variable names correspond closely to variables used in the report.

(a). The computer program used to calculate the angle of arrival correlation functions for the Kolmogorov spectrum is shown in listing (B1). It evaluates the confluent hypergeometric functions for pure real or pure imaginary arguments using formulae taken from Tables of Functions, Jahnke and Emde.

The first card in the input data specifies the parameters, ℓ_o, L, and λ. The variables are punched into ten column fields in decimal form. They are:

Columns

1-10	XLO = ℓ_o,	the inner scale of the turbulence in meters
11-20	XL = L,	the range in meters
21-30	XLAMB = λ,	the wavelength in meters.

If XL = 0, execution is terminated. The following card specifies the starting point, increment, and number of increments for the separation distance. These variables are:

LISTING B-1

```
C **** 10.6 PROPAGATION PHENOMENON PROGRAM ****
C ***** SMALL APERTURE ANGLE OF ARRIVAL CALCULATION FOR
C        THE KOLMOGOROV SPECTRUM *****
C
      COMPLEX G,GD
      REAL*8 RDYP2,XDYP2,RDYP3,XDYP3,B1,B2
C INITIALIZE NORMALIZATION CONSTANTS
      BANORM=1.
      BBNORM=1.
      BAGORM=1.
      BBGORM=1.
C READ DATA
 25   READ(5,900)XLO,XL,XLAMB
      IF(XLO.EQ.0.)CALL EXIT
 50   READ(5,900)RHOS,DELRH,XNR
      IF(XNR.EQ.0.)GO TO 25
 900  FORMAT(3E10.3)
      WRITE(6,1001)
 1001 FORMAT('1')
C CALCULATE CONSTANTS
      XK=6.2821/XLAMB
      XKM=5.94/XLO
      D=XKM**2*XL/XK
      NR=XNR+1
      A1=1.088*XL*XKM**.333333
      A2=D**(-.1666667)
      A3=D**(-1.166667)
      B1=DCOS(3.1415927/12.)
      B2=DSIN(3.1415927/12.)
      WRITE(6,1002)XK,XKM,D
 1002 FORMAT(/' XK= ',1PE10.3,5X,'XKM= ',E10.3,5X,'D= ',E10.3)
C BEGIN ITERATION ON RHO
      DO 100 I=1,NR
      RHO=RHOS+DELRH*FLOAT(I-1)
      G=XKM**2*RHO**2/4.
      XGD=(RHO**2*XK)/(4.*XL)
      GD=(0.,1.)*XGD
C BRANCH TO ASYMPTOTIC CALCULATION
      IF(XGD.GT.100.)GO TO 75
C
C SMALL RHO FORMULATION
C
C CALCULATE CONFLUENT HYPERGEOMETRIC FUNCTIONS
      CALL HYPERG(.1666,2.,-G,RHYP1,XHYP1)
      CALL DHYPER(-.8333,2.,GD,RDYP2,XDYP2)
C PRINT VALUES OF CONFLUENT HYPERGEOMETRIC
      WRITE(6,1003)RHYP1,XHYP1,RDYP2,XDYP2
 1003 FORMAT(4(E10.3,5X))
```

```
C CALCULATE BETA CORRELATION
      BBETA=A1*(.834*RHYP1+(A2*(  B1*RDYP2+  B2*XDYP2)))
C CALCULATE CONFLUENT HYPERGEOMETRIC FUNCTIONS
      CALL HYPERG(1.1666,3.,-G,RHYP2,XHYP2)
      CALL DHYPER(.16667,3.,GD,RDYP3,XDYP3)
C PRINT VALUES OF CONFLUENT HYPERGEOMETRIC
      WRITE(6,1003)RHYP2,XHYP2,RDYP3,XDYP3
C CALCULATE ALPHA CORRELATION
      BALPHA=BBETA-.2260*RHO**2*XL*XKM**2.333*(.166667*RHYP2+A3*(-B1*XDY
     1P3+B2*RDYP3))
      GO TO 60
 75   CONTINUE
C
C ASYMPTOTIC FORMULATION FOR LARGE RHO
C
      CALL HYPERG(.1666,2.,-G,RHYP1,XHYP1)
      BBETA =1.81*XL*XKM**.3333*RHYP1
      CALL HYPERG(1.1666,3.,-G,RHYP2,XHYP2)
      BALPHA=BBETA -1.81*XL*XKM**2.33333*RHO**2/24.*RHYP2
 60   CONTINUE
C NORMALIZE TO MEAN SQUARE ANGLE OF ARRIVAL
      BBN=BBETA/BBNORM
      BAN=BALPHA/BANORM
C PRINT RESULTS
      WRITE(6,1000)RHO,BBETA,BALPHA
      WRITE(6,1004)
 1004 FORMAT(T65,'CORRELATION NORMALIZED TO MEAN SQUARE VALUE ')
      WRITE(6,1000)RHO,BBN,BAN
      IF(RHO.NE.0.)GO TO 100
      BBNORM=BBETA
      BANORM=BALPHA
      BBGORM=BBETAG
      BAGORM=BALPHG
 100  CONTINUE
 1000 FORMAT(T65,'RHO=',1PE10.3,5X,'BBETA=',E10.3,5X,'BALPHA= ',E10.3)
      GO TO 50
      END
```

```
      SUBROUTINE DHYPER(ALPHA,GAMMA,CZ,RHYP,IHYP)
C
C THIS SUBROUTINE CALCULATES THE CONFLUENT HYPERGEOMETRIC FUNCTION
C ARGUMENTS ARE ALPHA,GAMMA, AND CZ. RESULT IS (RHYP,IHYP) (COMPLEX)
C CZ IS ASSUMED TO BE PURE IMAGINARY
C
      IMPLICIT COMPLEX(C),REAL*8 (A-B,D-I,O-Z)
      REAL*4 ALPHA,GAMMA,ARGZ,ARZG,A,B,BMA,SIGN,Z
      COMPLEX*16 CDZ,CRSUM,CSSUM,CRTERM,CSTERM,CF,DCONJG
      INTEGER I
      ARG(CZZ)=ATAN2(AIMAG(CZZ),REAL(CZZ))
 1000 FORMAT('ONO CONVERGENCE'/' CHYP=',2(1PE10.3,2X),5X,'CHYPO=',2(E10.
     13,2X))
 1001 FORMAT(' I= ',I5,5X,'ALPHA= ',F10.5,5X,'GAMMA= ',F10.5,5X,'CZ= ',2
     1(1PE10.3,2X),3X,'RHYP= ',E10.3,5X,'IHYP= ',E10.3)
      ARGZ=ARG(CZ)
C
C SMALL ARGUMENT EXPANSION
C
C SET UPPER LIMIT ON THE NUMBER OF TERMS
      LMT=200
  100 I=2
C
C CALCULATE REAL PART
C
      RHYP=1.
      IHYP=0.
      Z=AIMAG(CZ)
C TEST FOR ZERO
      IF( ABS(Z).LT.1.E-50)RETURN
C TEST FOR LARGE ARGUMENT
      IF(ABS(AIMAG(CZ)).GT.3.)GO TO 500
      RHYPO=ALPHA/GAMMA*Z*(ALPHA+1.)/(GAMMA+1.)*Z/2.*(-1.)
      SRHYP=RHYPO
  120 I=I+2
C CHECK NUMBER OF TERMS
      IF(I.GT.LMT)GO TO 140
      K=I-1
      RHYP=-RHYPO*(ALPHA+K-1.)/(GAMMA+K-1.)*Z/FLOAT(I-1)*(ALPHA+K)/(GAMM
     1A+K)*Z/FLOAT(I)
      SRHYP=SRHYP+RHYP
C TEST FOR CONVERGENCE
      IF(DABS(RHYP-RHYPO).LT.1.E-05)GO TO 130
      RHYPO=RHYP
      GO TO 120
C WRITE ERROR MESSAGE
  140 WRITE(6,1000)RHYP,RHYPO,CHYPO
      WRITE(6,1001)I,ALPHA,GAMMA,CZ,RHYP,IHYP
```

```
 130  IHYPO=0.
C
C CALCULATE IMAGINARY PART
C
      RHYP=SRHYP+1.
      I=1
      IHYPO=ALPHA/GAMMA*Z
      SIHYP=IHYPO
 220  I=I+2
C CHECK NUMBER OF TERMS
      IF(I.GT.LMT)GO TO 240
      IHYP=-IHYPO*(ALPHA+K-1.)/(GAMMA+K-1.)*Z/FLOAT(I-1)*(ALPHA+K)/(GAMM
     1A+K)*Z/FLOAT(I)
      SIHYP=IHYP+SIHYP
C TEST FOR CONVERGENCE
      IF(DABS(IHYP-IHYPO).LT.1.E-05)GO TO 230
      IHYPO=IHYP
      GO TO 220
C WRITE ERROR MESSAGE
 240  WRITE(6,1000)IHYP,IHYPO,CHYPO
      WRITE(6,1001)I,ALPHA,GAMMA,CZ,RHYP,IHYP
 230  IHYP=SIHYP
      RETURN
 500  CONTINUE
C
C ASYMPTOTIC EXPANSION FOR LARGE ARGUMENT
C
      CDZ=CZ
      CRSUM=1.
      CSSUM=1.
      CRTERM=1.
      CSTERM=1.
C SET UPPER LIMIT ON THE NUMBER OF TERMS
      LMT=5
      IF(ABS(Z).GT. 20.)LMT=1
      DO 600 I=1,LMT
      K=I-1
      CRTERM=(ALPHA+K)*(ALPHA-GAMMA+1.+K)/(FLOAT(I)*(-CDZ))*CRTERM
      CRSUM=CRSUM+CRTERM
      CSTERM=(GAMMA-ALPHA+K)*(1.-ALPHA+K)/(FLOAT(I)*CDZ)*CSTERM
      CSSUM=CSSUM+CSTERM
 600  CONTINUE
      SIGN=+1.
      IF(AIMAG(CZ).LE.0.)SIGN=-1.
      CALL GAMMB(ALPHA,GAMMA,A,B,BMA)
      ARGZ=3.141592/2.
      CF=CDABS(CDZ)**(-ALPHA)*CEXP((0.,1.)*ALPHA*SIGN*ARGZ)/BMA*CRSUM
      IF(ABS(Z).GT.20.)GO TO 650
```

```
      CF=CF+ CABS(CZ)**(ALPHA-GAMMA)*CEXP((0.,1.)*(ALPHA-GAMMA)*ARGZ+CZ)
     1/A*CSSUM
650   CONTINUE
      CF=CF*B
      RHYP=.5*(DCONJG(CF)+CF)
      IHYP=(0.,.5)*(DCONJG(CF)-CF)
      RETURN
      END
```

```
      SUBROUTINE HYPERG(ALPHA,GAMMA,CZ,RHYP,IHYP)
C
C THIS SUBROUTINE CALCULATES THE CONFLUENT HYPERGEOMETRIC FUNCTION
C ARGUMENTS ARE ALPHA,GAMMA, AND CZ. RESULT IS (RHYP,IHYP) (COMPLEX)
C CZ IS ASSUMED TO BE PURE REAL
C
      IMPLICIT COMPLEX (C)
      REAL IHYP,IHYPO
      ARG(CZZ)=ATAN2(AIMAG(CZZ),REAL(CZZ))
C SET UPPER LIMIT ON NUMBER OF TERMS
      LMT=500
      ARZG=ARG(-CZ)
      ARGZ=ARG(CZ)
 1000 FORMAT('ONC CONVERGENCE'/' CHYP=',2(1PE10.3,2X),5X,'CHYPO=',2(E10
     13,2X))
 1001 FORMAT(' I= ',I5,5X,'ALPHA= ',F10.5,5X,'GAMMA= ',F10.5,5X,'CZ= ',2
     1(1PE10.3,2X),3X,'RHYP= ',E10.3,5X,'IHYP= ',E10.3)
  300 CHYPO=(1.,0.)
      I=1
      Z=REAL(CZ)
C TEST FOR LARGE ARGUMENT
      IF(CABS(CZ).GT.3.)GO TO 500
C
C SMALL ARGUMENT EXPANSION
C
      IHYP=0.
      RHYPO=ALPHA/GAMMA*Z
      SRHYP=RHYPO
  320 I=I+1
C CHECK NUMBER OF TERMS
      IF(I.GT.LMT)GO TO 340
      K=I-1
      RHYP=RHYPO*(ALPHA+K)/(GAMMA+K)*Z/FLOAT(I)
      SRHYP=SRHYP+RHYP
C TEST FOR CONVERGENCE
      IF(ABS(RHYP-RHYPO).LT.1.E-05)GO TO 330
      RHYPO=RHYP
      GO TO 320
C WRITE ERROR MESSAGE
  340 WRITE(6,1000)RHYP,RHYPO,CHYPO
      WRITE(6,1001)I,ALPHA,GAMMA,CZ,RHYP,IHYP
  330 RHYP=SRHYP+1.
      RETURN
  500 CONTINUE
C
C ASYMPTOTIC EXPANSION FOR LARGE ARGUMENT
C
      RSUM=1.
```

```
      SSUM=1.
      RTERMO=1.
      STERMO=1.
      CALL GAMMB(ALPHA,GAMMA,A,B,BMA)
C SET UPPER LIMIT ON NUMBER OF TERMS
      LMT=5
      DO 600 I=1,LMT
      K=I-1
      RTERM=(ALPHA+K)*(ALPHA-GAMMA+1+K)/(FLOAT(I)*( -Z))*RTERMO
      RSUM=RSUM+RTERM
      RTERMO=RTERM
      STERM=(GAMMA-ALPHA+K)*(1.-ALPHA+K)/(FLOAT(I)* Z)*STERMO
      SSUM=SSUM+STERM
      STERMO=STERM
 600  CONTINUE
      CF=CABS(CZ)**(-ALPHA)*CEXP((0.,1.)*(-ALPHA)*ARZG)/BMA*RSUM
      IF(CABS(CZ).GT.99.)GO TO 700
      CF=CF+CABS(CZ)**(ALPHA-GAMMA)*CEXP((0.,1.)*(ALPHA-GAMMA)*ARGZ+CZ)/
     1A*SSUM
 700  CONTINUE
      RHYP=REAL(CF)*B
      IHYP=AIMAG(CF)*B
      RETURN
      END



      SUBROUTINE GAMMB(A,B,A1,B1,BMA)
C
C THIS SUBROUTINE CALCULATES GAMMA FUNCTIONS FOR CONFLUENT HYPERGEOMETRIC
C FUNCTION'S LARGE EXPANSIONS
C
      B1=GAMMA(B)
      IF(A.GT.B)GO TO 200
      BMA=GAMMA(B-A)
 150  CONTINUE
      IF(A.LT.0.)GO TO 100
      A1=GAMMA(A)
      RETURN
 100  A1=-3.141592/(GAMMA(-A+1.)*SIN(-3.14159*A))
      RETURN
 200  BMA=-3.141592/(GAMMA(A-B+1.)*SIN(3.141592*(A-B)))
      GO TO 150
      END
```

Columns

1-10	RHOS	= the first value of ρ
11-20	DELRH	= the increment of ρ
21-30	XNR	= the total number of increments.

Again the variables are punched in ten column fields in decimal form. If XNR = 0, then the program reads a new parameter card.

(b). The Von Karmann spectrum calculations of the mean square angle of arrival, two point correlation functions, and structure functions mentioned earlier are performed by numerical integration. The programs for both plane and spherical wave input are shown in listings (B-2) and (B-3), respectively. The integrations are performed by using a 96 point Gaussian quadrature algorithm. The Bessel functions were evaluated using a polynomial expansion from Handbook of Mathematical Functions by Abramowitz and Stegun.

The weighting factors and arguments for the Gaussian integration are read as input data and are shown in listing (B-4). All user input data should follow these cards. Since both programs use the same input data only one data deck will be explained.

The first user input data card specifies the parameters for the angle of arrival correlation function calculation. The data is again punched in ten column fields in decimal form. The input variables are:

Columns

1-10	XLO	= ℓ_o, the inner scale in meters
11-20	XL	= L, the range in meters
21-30	XLAMB	= λ, the wavelength in meters
31-40	XCAPLO	= L_o, the outer scale in meters
41-50	A	= A, the outer scale normalizing constant.

If XL = 0, the correlation function calculations are terminated and the program begins the structure function calculations.

Otherwise, the program reads the separation parameters: starting value, increment, and total number of increments. These variables are punched in ten column fields in decimal form. They are

LISTING B-2

```
C **** 10.6 MICRON PROPAGATION PHENOMENA PROGRAM ****
C ***** ANGLE OF ARRIVAL AND RELATED STRUCTURE FUNCTION CALCULATION
C         FOR THE VON KARMANN SPECTRUM, AND PLANE INPUT *****
      EXTERNAL FCT,FCT0,FCT1,FCT2,FCT3
      REAL*8 YINT,YINTG,FCT,YL,XU,YINT1,YINT2,XKAP
      COMMON RHO,XL,XK,XKM,XKO
      COMMON /INTG/TEST
      CALL GAUSZ
      TEST=0.
C READ INPUT DATA
  100 READ(5,900)XLO,XL,XLAMB,XCAPLO,A
  900 FORMAT(5E10.3)
      IF(XL.EQ.0.)GO TO 201
C CALCULATE CONSTANTS
      XKM=5.94/XLO
      XKO=A/XCAPLO
      PI=3.1415927
      XK=6.283184/XLAMB
C READ ARGUMENT VALUES
  150 READ(5,900)RHOS,DELRHO,XNR
      IF(XNR.EQ.0.)GO TO 100
C CALCULATE ANGLE OF ARRIVAL CORRELATION
      NR=XNR
      WRITE(6,1002)
 1002 FORMAT('1ANGLE OF ARRIVAL CORRELATION FUNCTION ')
      WRITE(6,1005)XL,XLO,XCAPLO,A,XLAMB
 1005 FORMAT(' RANGE=',1PE11.3,' M',5X,'INNER SCALE= ',E10.3,' M',5X,
     1'OUTER SCALE= ',E10.3,' M',5X,'A= ',E10.3,5X,'LAMBDA= ',E10.3,' M'
     2)
      DO 200 I=1,NR
      RHO=RHOS+DELRHO*FLOAT(I-1)
C ELEVATION ANGLE OF ARRIVAL CORRELATION
      CALL INTGRL(0.,1.E-3,8,FCT,YINT)
      BALPHA=2.*PI**2*XL*YINT
      IF(RHO.EQ.0.)BAN=BALPHA
      BALPHN=BALPHA/BAN
      WRITE(6,1000)RHO,BALPHA,BALPHN
 1000 FORMAT('0RHO= ',1PE10.3,5X,'BALPHA= ',E10.3,5X,'BALPHAN= ',E10.3)
C AZIMUTH ANGLE OF ARRIVAL CORRELATION
      CALL INTGRL(0.,1.E-3,8,FCT0,YINT)
      BBETA=2.*PI**2*XL*YINT
      IF(RHO.EQ.0.)BBN=BBETA
      BBETAN=BBETA/BBN
 1001 FORMAT(21X,'BBETA=  ',1PE10.3,5X,'BBETAN=  ',E10.3)
  200 WRITE(6,1001)BBETA,BBETAN
      GO TO 150
C CALCULATE STRUCTURE FUNCTIONS
C READ INPUT DATA
```

```
 201  READ(5,900)XLO,XL,XLAMB,XCAPLO,A
      IF(XL.EQ.0.)CALL EXIT
C CALCULATE CONSTANTS
      XK=6.2831484/XLAMB
      XKM=5.94/XLO
      XKC=A/XCAPLO
      WRITE(6,1003)
 1003 FORMAT('1STRUCTURE FUNCTIONS AND SPECTRA ')
      WRITE(6,1005)XL,XLO,XCAPLO,A,XLAMB
C READ ARGUMENT VALUES
 230  READ(5,900)RHOS,DELRHO,XNR
      IF(XNR.EQ.0.)GO TO 201
      NR=XNR+1.
      DO 220 I=1,NR
      RHO=RHOS+DELRHO*FLOAT(I-1)
      XKAP=RHO
C REFRACTIVE INDEX FLUCTUATION SPECTRUM
      PHIK=PHIEPS(XKAP,XKM,XKO)
C REFRACTIVE INDEX FLUCTUATION STRUCTURE FUNCTION
      CALL INTGRL(1.E-03,1.E-02,8,FCT1,YINT1)
      DN=8.*PI*YINT1
C PHASE STRUCTURE FUNCTION
      CALL INTGRL(1.E-02,1.0E-01,6,FCT2,YINT2)
      DS=4.*PI**2*XK**2*XL*YINT2
C WAVE STRUCTURE FUNCTION
      CALL INTGRL(1.E-03,1.E-02,7,FCT3,YINT2)
      DSW=8.*PI**2*XK**2*XL*YINT2
 220  WRITE(6,1004)RHO,PHIK,DN,DS,DSW
 1004 FORMAT('0ARGUMENT= ',1PE10.3,/,' REFRACTIVE INDEX FLUCTUATUION SPE
     1CTRUM= ',E10.3,5X,'STRUCTURE FUNCTION= ',E10.3,/,' PHASE STRUCTURE
     2 FUNCTION= ',E10.3,5X,'WAVE STRUCTURE FUNCTION= ',E10.3)
      GO TO 230
      END



      DOUBLE PRECISION FUNCTION FCT(XKAP)
C INTEGRAND FOR CALCULATING ELEVATION ANGLE OF ARRIVAL CORRELATION
      REAL*8 ARG1,FCT,XKAP
      COMMON RHO,XL,XK,XKM,XKO
      ARG3=(XKAP/XKM)**2
      IF(ARG3.GT.174.)GOTO 100
      ARG2=XKAP*RHO
      ARG1=XKAP**2*XL/XK
      IF(ARG1.EQ.0.)GO TO 100
      FCT=(1.+DSIN(ARG1)/ARG1)*(BESO(ARG2)-BES1X(ARG2))*XKAP**3*PHIEPS(X
     1KAP,XKM,XKO)
      RETURN
 100  FCT=0.
      RETURN
      END
```

```
      DOUBLE PRECISION FUNCTION FCTO(XKAP)
C INTEGRAND FOR CALCULATING AZIMUTH ANGLE OF ARRIVAL
      REAL*8 ARG1,FCTO,XKAP
      COMMON RHO,XL,XK,XKM,XKO
      ARG3=(XKAP/XKM)**2
      IF(ARG3.GT.174.)GOTO 100
      ARG2=XKAP*RHO
      ARG1=XKAP**2*XL/XK
      IF(ARG1.EQ.0.)GO TO 100
      FCTO=(1.+DSIN(ARG1)/ARG1)*BES1X(ARG2)*XKAP**3*PHIEPS(XKAP,XKM,XKO)
      RETURN
  100 FCTO=0.
      RETURN
      END



      DOUBLE PRECISION FUNCTION FCT1(XKAP)
C INTEGRAND FOR CALCULATING INDEX STRUCTURE FUNCTION
      REAL*8 ARG2,FCT1,XKAP
      COMMON RHO,XL,XK,XKM,XKO
      ARG1=XKAP**2*XL/XK
      ARG2=XKAP*RHO
      ARG3=(XKAP/XKM)**2
      IF(ARG3.GT.174.)GOTO 100
      IF(ARG1.EQ.0.)GO TO 100
      FCT1=(1.-DSIN(ARG2)/ARG2)*PHIEPS(XKAP,XKM,XKO)*XKAP**2
      RETURN
  100 FCT1=0.
      RETURN
      END



      DOUBLE PRECISION FUNCTION FCT2(XKAP)
C INTEGRAND FOR CALCULATING PHASE STRUCTURE FUNCTION
      REAL*8 ARG1,FCT2,XKAP
      COMMON RHO,XL,XK,XKM,XKO
      ARG3=(XKAP/XKM)**2
      IF(ARG3.GT.174.)GOTO 100
      ARG1=XKAP**2*XL/XK
      ARG2=XKAP*RHO
      IF(ARG1.EQ.0.)GO TO 100
      FCT2=(1.-BESO(ARG2))*(1.+DSIN(ARG1)/ARG1)*PHIEPS(XKAP,XKM,XKO)*XKA
     1P
      RETURN
  100 FCT2=0.
      RETURN
      END
```

```
      DOUBLE PRECISION FUNCTION FCT3(XKAP)
C INTEGRAND FOR CALCULATING THE WAVE STRUCTURE FUNCTION
      REAL*8 XKAP,FCT3
      COMMON RHO,XL,XK,XKM,XKO
      ARG2=XKAP*RHO
      ARG3=(XKAP/XKM)**2
      IF(ARG3.GT.174.)GOTO 100
      FCT3=(1.-BESO(ARG2))*PHIEPS(XKAP,XKM,XKO)*XKAP
      RETURN
  100 FCT3=0.
      RETURN
      END
```

```
      FUNCTION PHIEPS(XK,XKM,XKO)
C REFRACTIVE INDEX FLUCTUATION SPECTRUM
      REAL*8 XK
      TEST1=(XK/XKM)**2
      IF(TEST1.GT.174.)GO TO 100
      A=EXP(-TEST1)
      B=(XK**2+XKO**2)**(11./6.)
      TEST2=ALOG10(A)-ALOG10(B)
      IF(ABS(TEST2).GT.60.)GO TO 100
      PHIEPS=.033*A/B
      RETURN
  100 PHIEPS=0.
      RETURN
      END
```

```
      SUBROUTINE INTGRL(XLS,XUS,NINT,FCT,YINT)
C ORDER OF MAGNITUDE INTEGRATION ROUTINE
      COMMON /INTG/TEST
      REAL*8 YINT,YINTG,FCT,XL,XU
      EXTERNAL FCT
 1003 FORMAT(' INTEGRAL= ',1PE10.3,5X,'LOWER LIMIT= ',E10.3,5X,
     1'UPPER LIMIT= ',E10.3)
 1002 FORMAT(//)
      IF(TEST.GT.0.)WRITE(6,1002)
      XL=XLS
      XU=XUS
      CALL DGG96(XL,XU,FCT,YINT)
      IF(TEST.GT.0.)WRITE(6,1003)YINT,XL,XU
      DO 300 J=1,NINT
      XL=XU
      XU=XU*10.
      CALL DGG96(XL,XU,FCT,YINTG)
      YINT=YINT+YINTG
      IF(TEST.GT.0.)WRITE(6,1003)YINTG,XL,XU
  300 CONTINUE
      RETURN
      END
```

```
      SUBROUTINE DGG96(XL,XU,FCT,YINT)
C 96 POINT GAUSSIAN QUADRATURE INTEGRATION ROUTINE
      IMPLICIT REAL*8 (A-H,O-Z)
      COMMON /GAUSS/X(48),W(48)
      SUM=(XU+XL)/2.
      DIF=(XU-XL)/2.
      YINT=0.
      DO 100 I=1,48
      ARG1=DIF*X(I)+SUM
      ARG2=-DIF*X(I)+SUM
  100 YINT=W(I)*(FCT(ARG1)+FCT(ARG2))+YINT
      YINT=YINT*DIF
      RETURN
      END
```

```
      SUBROUTINE GAUSZ
C READ AND STORE GAUSSIAN INTEGRATION ARGUMENTS AND WEIGHTS
      IMPLICIT REAL*8 (A-H,O-Z)
      COMMON /GAUSS/X(48),W(48)
      READ(5,999)X
      READ(5,999)W
  999 FORMAT(5F16.15)
      WRITE(6,1111)X
      WRITE(6,1111)W
 1111 FORMAT(1X,6(F17.15,3X)/)
      RETURN
      END



      FUNCTION BES0(X)
      REAL*8 THETA
C J0(X)
      IF(X.GT.3.)GO TO 100
      Y=X/3.
      BES0=1.0-2.24999*Y**2+1.26562*Y**4-.316387*Y**6+.044447*Y**8-3.944
     14E-3*Y**10+2.10000E-4*Y**12
      RETURN
  100 Y=3./X
      THETA=X-.785398-.041663*Y-3.954E-05*Y**2+2.62573E-3*Y**3-5.4125E-4
     1*Y**4-2.9333E-4*Y**5+1.3558E-4*Y**6
      F0=.7978846-7.7E-7*Y-5.5274E-3*Y**2-9.512E-5*Y**3+1.37237E-3*Y**4-
     17.2805E-4*Y**5+1.4476E-4*Y**6
      BES0=F0*DCOS(THETA)/SQRT(X)
      RETURN
      END



      FUNCTION BES1X(X)
      REAL*8 THETA
C J1(X)/X
      IF(X.GT.3.)GO TO 100
      Y=X/3.
      BES1X=.50-.562499*Y**2+.210935*Y**4-3.95428E-2*Y**6+4.43319E-3*Y**
     18-3.1761E-4*Y**10+1.109E-5*Y**12
      RETURN
  100 Y=3./X
      THETA=X-2.35619+.124996*Y+5.650E-05*Y**2-6.37879E-3*Y**3+7.4348E-4
     1*Y**4+7.9824E-4*Y**5-2.9166E-4*Y**6
      F1=.797884+1.56E-6*Y+1.65966E-2*Y**2-1.7105E-4*Y**3-2.49511E-3*Y**
     14+1.13653E-3*Y**5-2.0033E-4*Y**6
      BES1X=F1*DCOS(THETA)/(X*SQRT(X))
      RETURN
      END
```

LISTING B-3

```
C **** 10.6 MICRON PROPAGATION PHENOMENA PROGRAM ****
C ***** ANGLE OF ARRIVAL AND RELATED STRUCTURE FUNCTION CALCULATION
C        FOR THE VON KARMANN SPECTRUM, AND SPHERICAL WAVE INPUT *****
      EXTERNAL FCT,FCT0,FCT1,FCT2,FCT3
      REAL*8 YINT,YINTG,FCT,YL,XU,YINT1,YINT2,XKAP
      COMMON RHO,XL,XK,XKM,XKO
      COMMON /INTG/TEST
      CALL GAUSZ
      TEST=0.
C READ INPUT DATA
  100 READ(5,900)XLO,XL,XLAMB,XCAPLO,A
  900 FORMAT(5E10.3)
      IF(XL.EQ.0.)GO TO 201
C CALCULATE CONSTANTS
      XKM=5.94/XLO
      XKO=A/XCAPLO
      PI=3.1415927
      XK=6.283184/XLAMB
C READ ARGUMENT VALUES
  150 READ(5,900)RHOS,DELRHO,XNR
      IF(XNR.EQ.0.)GO TO 100
C CALCULATE ANGLE OF ARRIVAL CORRELATION
      XNR=XNR-1.
      NR=XNR
      WRITE(6,1002)
 1002 FORMAT('1ANGLE OF ARRIVAL CORRELATION FUNCTION ')
      WRITE(6,1005)XL,XLO,XCAPLO,A,XLAMB
 1005 FORMAT(' RANGE=',1PE11.3,' M',5X,'INNER SCALE= ',E10.3,' M',5X,
     1'OUTER SCALE= ',E10.3,' M',5X,'A= ',E10.3,5X,'LAMBDA= ',E10.3,' M'
     2)
      DO 200 I=1,NR
      RHO=RHOS+DELRHO*FLOAT(I-1)
C ELEVATION ANGLE OF ARRIVAL CORRELATION
      CALL INTGRL(0.,1.E-3,8,FCT,YINT)
      BALPHA=.5*PI**2*8.*YINT
      IF(RHO.EQ.0.)BAN=BALPHA
      BALPHN=BALPHA/BAN
      WRITE(6,1000)RHO,BALPHA,BALPHN
 1000 FORMAT('0RHO= ',1PE10.3,5X,'BALPHA= ',E10.3,5X,'BALPHAN= ',E10.3)
C AZIMUTH ANGLE OF ARRIVAL CORRELATION
      CALL INTGRL(0.,1.E-3,8,FCT0,YINT)
      BBETA=.5*PI**2*8.*YINT
      IF(RHO.EQ.0.)BBN=BBETA
      BBETAN=BBETA/BBN
 1001 FORMAT(21X,'BBETA=  ',1PE10.3,5X,'BBETAN=  ',E10.3)
  200 WRITE(6,1001)BBETA,BBETAN
      GO TO 150
C CALCULATE STRUCTURE FUNCTIONS
```

```
C READ INPUT DATA
 201  READ(5,900)XLO,XL,XLAMB,XCAPLO,A
      IF(XL.EQ.0.)CALL EXIT
C CALCULATE CONSTANTS
      XK=6.2831484/XLAMB
      XKM=5.94/XLO
      XKO=A/XCAPLO
      WRITE(6,1003)
 1003 FORMAT('1STRUCTURE FUNCTIONS AND SPECTRA ')
C READ ARGUMENT VALUES
 230  READ(5,900)RHOS,DELRHO,XNR
      IF(XNR.EQ.0.)GO TO 201
      NR=XNR+1.
      DO 220 I=1,NR
      RHO=RHOS+DELRHO*FLOAT(I-1)
      XKAP=RHO
C REFRACTIVE INDEX FLUCTUATION SPECTRUM
      PHIK=PHIEPS(XKAP,XKM,XKO)
C REFRACTIVE INDEX FLUCTUATION STRUCTURE FUNCTION
      CALL INTGRL(1.E-03,1.E-02,8,FCT1,YINT1)
      DN=8.*PI*YINT1
C PHASE STRUCTURE FUNCTION
      CALL INTGRL(1.E-02,1.0E-01,6,FCT2,YINT2)
      DS=YINT2*PI**2*XK**2*8.
 220  WRITE(6,1004)RHO,PHIK,DN,DS
 1004 FORMAT('0ARGUMENT= ',1PE10.3,/,' REFRACTIVE INDEX FLUCTUATUION SPE
     1CTRUM= ',E10.3,5X,'STRUCTURE FUNCTION= ',E10.3,/,' PHASE STRUCTURE
     2FUNCTION= ',E10.3)
      GO TO 230
      END
```

```
      DOUBLE PRECISION FUNCTION FCT(XKAPPA)
C INTEGRAND FOR CALCULATING ELEVATION ANGLE OF ARRIVAL CORRELATION
      EXTERNAL FCT4
      REAL*8 ARG1,FCT,XKAP,DXL,DSPHR,XKAPPA,FCT4
      COMMON RHO,XL,XK,XKM,XKO
      COMMON /SPHERE/XKAP
      XKAP=XKAPPA
      DXL=XL
      ARG2=XKAP*RHO
      CALL DCG8 (0.,DXL,FCT4,DSPHR)
      FCT=(BESO(ARG2)-BES1X(ARG2))*XKAP**3*DSPHR
      RETURN
      END
```

```
      DOUBLE PRECISION FUNCTION FCT0(XKAPPA)
C INTEGRAND FOR CALCULATING AZIMUTH ANGLE OF ARRIVAL
      EXTERNAL FCT4
      REAL*8 ARG1,FCT0,XKAP,DXL,DSPHR,XKAPPA,FCT4
      COMMON RHO,XL,XK,XKM,XKO
      COMMON /SPHERE/XKAP
      XKAP=XKAPPA
      ARG2=XKAP*RHO
      DXL=XL
      CALL DCG8 (0.,DXL,FCT4,DSPHR)
      FCT0=BESJX(ARG2)*XKAP**3*DSPHR
      RETURN
      END



      DOUBLE PRECISION FUNCTION FCT1(XKAP)
C INTEGRAND FOR CALCULATING INDEX STRUCTURE FUNCTION
      REAL*8 ARG2,FCT1,XKAP
      COMMON RHO,XL,XK,XKM,XKO
      ARG1=XKAP**2*XL/XK
      ARG2=XKAP*RHO
      ARG3=(XKAP/XKM)**2
      IF(ARG3.GT.174.)GOTO 100
      IF(ARG1.EQ.0.)GO TO 100
      FCT1=(1.-DSIN(ARG2)/ARG2)*PHIEPS(XKAP,XKM,XKO)*XKAP**2
      RETURN
  100 FCT1=0.
      RETURN
      END



      DOUBLE PRECISION FUNCTION FCT2(XKAPPA)
C INTEGRAND FOR CALCULATING PHASE STRUCTURE FUNCTION
      EXTERNAL FCT4
      REAL*8 ARG1,FCT2,XKAP,DSPHR,DXL,XKAPPA,FCT4
      COMMON RHO,XL,XK,XKM,XKO
      COMMON /SPHERE/XKAP
      XKAP=XKAPPA
      ARG2=XKAP*RHO
      DXL=XL
      CALL DCG8 (0.,DXL,FCT4,DSPHR)
      FCT2=(1.-BESO(ARG2))*DSPHR*XKAP
      RETURN
      END
```

```
      DOUBLE PRECISION FUNCTION FCT3(XKAP)
C INTEGRAND FOR CALCULATING THE WAVE STRUCTURE FUNCTION
      REAL*8 XKAP,FCT3
      COMMON RHO,XL,XK,XKM,XKO
      ARG2=XKAP*RHO
      ARG3=(XKAP/XKM)**2
      IF(ARG3.GT.174.)GOTO 100
      FCT3=(1.-BESO(ARG2))*PHIEPS(XKAP,XKM,XKO)*XKAP
      RETURN
  100 FCT3=0.
      RETURN
      END



      DOUBLE PRECISION FUNCTION FCT4(DETA)
      REAL*8 XKAP,DETA,FCT4
      COMMON RHO,XL,XK,XKM,XKO
      COMMON /SPHERE/XKAP
      ARG1=XKAP*XL/DETA
      FCT4=(XL/DETA*DCOS(XL*(XL-DETA)*XKAP**2/(2.*XK*DETA)))**2*PHIEPS(
     1ARG1,XKM,XKO)
      RETURN
      END




      FUNCTION PHIEPS(XK,XKM,XKO)
C REFRACTIVE INDEX FLUCTUATION SPECTRUM
      REAL*8 XK
      TEST1=(XK/XKM)**2
      IF(TEST1.GT.174.)GO TO 100
      A=EXP(-TEST1)
      B=(XK**2+XKO**2)**(11./6.)
      TEST2=ALOG10(A)-ALOG10(B)
      IF(ABS(TEST2).GT.60.)GO TO 100
      PHIEPS=.033*A/B
      RETURN
  100 PHIEPS=0.
      RETURN
      END
```

```
      SUBROUTINE INTGRL(XLS,XUS,NINT,FCT,YINT)
C ORDER OF MAGNITUDE INTEGRATION ROUTINE
      COMMON /INTG/TEST
      REAL*8 YINT,YINTG,FCT,XL,XU
      EXTERNAL FCT
 1003 FORMAT(' INTEGRAL= ',1PE10.3,5X,'LOWER LIMIT= ',E10.3,5X,
     1'UPPER LIMIT= ',E10.3)
 1002 FORMAT(//)
      IF(TEST.GT.0.)WRITE(6,1002)
      XL=XLS
      XU=XUS
      CALL DGG96(XL,XU,FCT,YINT)
      IF(TEST.GT.0.)WRITE(6,1003)YINT,XL,XU
      DO 300 J=1,NINT
      XL=XU
      XU=XU*10.
      CALL DGG96(XL,XU,FCT,YINTG)
      YINT=YINT+YINTG
      IF(TEST.GT.0.)WRITE(6,1003)YINTG,XL,XU
  300 CONTINUE
      RETURN
      END



      SUBROUTINE DGG96(XL,XU,FCT,YINT)
C 96 POINT GAUSSIAN QUADRATURE INTEGRATION ROUTINE
      IMPLICIT REAL*8 (A-H,O-Z)
      COMMON /GAUSS/X(48),W(48)
      SUM=(XU+XL)/2.
      DIF=(XU-XL)/2.
      YINT=0.
      DO 100 I=1,48
      ARG1=DIF*X(I)+SUM
      ARG2=-DIF*X(I)+SUM
  100 YINT=W(I)*(FCT(ARG1)+FCT(ARG2))+YINT
      YINT=YINT*DIF
      RETURN
      END



      SUBROUTINE GAUSZ
C READ AND STORE GAUSSIAN INTEGRATION ARGUMENTS AND WEIGHTS
      IMPLICIT REAL*8 (A-H,O-Z)
      COMMON /GAUSS/X(48),W(48)
      READ(5,999)X
      READ(5,999)W
  999 FORMAT(5F16.15)
      WRITE(6,1111)X
      WRITE(6,1111)W
 1111 FORMAT(1X,6(F17.15,3X)/)
      RETURN
      END
```

```
      FUNCTION BESO(X)
C  JO(X)
      IF(X.GT.3.)GO TO 100
      Y=X/3.
      BESO=1.0-2.24999*Y**2+1.26562*Y**4-.316387*Y**6+.044447*Y**8-3.944
     14E-3*Y**10+2.10000E-4*Y**12
      RETURN
  100 Y=3./X
      THETA=X-.785398-.041663*Y-3.954E-05*Y**2+2.62573E-3*Y**3-5.4125E-4
     1*Y**4-2.9333E-4*Y**5+1.3558E-4*Y**6
      FO=.7978846-7.7E-7*Y-5.5274E-3*Y**2-9.512E-5*Y**3+1.37237E-3*Y**4-
     17.2805E-4*Y**5+1.4476E-4*Y**6
      BESO=FO*COS(THETA)/SQRT(X)
      RETURN
      END



      FUNCTION BES1X(X)
      REAL*8 THETA
C  J1(X)/X
      IF(X.GT.3.)GO TO 100
      Y=X/3.
      BES1X=.50-.562499*Y**2+.210935*Y**4-3.95428E-2*Y**6+4.43319E-3*Y**
     18-3.1761E-4*Y**10+1.109E-5*Y**12
      RETURN
  100 Y=3./X
      THETA=X-2.35619+.124996*Y+5.650E-05*Y**2-6.37879E-3*Y**3+7.4348E-4
     1*Y**4+7.9824E-4*Y**5-2.9166E-4*Y**6
      F1=.797884+1.56E-6*Y+1.65966E-2*Y**2-1.7105E-4*Y**3-2.49511E-3*Y**
     14+1.13653E-3*Y**5-2.0033E-4*Y**6
      BES1X=F1*DCOS(THETA)/(X*SQRT(X))
      RETURN
      END
```

LISTING B-4

```
.016276744849652.046812985135049.081297495464425.113695855110555.145973714654395
.176096882367618.210031310460557.241743155163640.273198812591049.304364944354496
.335208522892625.355696851472313.395797649828908.425347898840730.454709422167745
.483457973420596.511594177154557.539388108324357.566510415561397.593032364777572
.516925840125458.644163403784957.655718310043916.692564556642171.715676812345967
.738030643744400.759602341176647.780369043867433.800308744139140.819400310737931
.837623511228187.854959033434651.871356855909296.886394317402420.901406035315852
.915071423120898.927712456722305.939370339752735.950032717784437.959655291445742
.968326826463264.975939174555135.982517253563014.988054125329523.992543900323752
.995981842987209.998364375863151.999689503383230.                                .
.032850614492353.032516113713858.032447163714064.032343822558575.032205204794030
.032034456231992.031826750894411.031589330770727.031316425596851.031010332580515
.030671376123559.030299915420827.029896344135328.029461059958107.028994514150555
.028497411096508.027970607516845.027412952725029.026532686672591.026212340735672
.025570036005349.024900633222453.024204841792354.023483399085926.022737069650329
.021966644435744.021172939892191.020356707154333.019519031140145.018660679627411
.017782502316045.016885479064245.015970562952552.015038721020994.014090941772314
.013128229566961.012151604571088.011162102099838.010160776835088.009148671230735
.008126876925698.007096470791153.006058545504235.005014202842927.003964554335444
.002910731817934.001853956738946.000796792065552.                                .
```

Columns

1-10	RHOS	= starting value of ρ
11-20	DELRHO	= increment
21-30	XNR	= total number of increments.

If XNR = 0, a new parameter card is read, otherwise another set of separation parameters is expected.

The data deck for the structure function calculations is identical to the correlation data deck. The same variables are used and the same action is taken for XNR = 0. When XL = 0, the program is terminated.

2. Large Aperture Calculations

Two programs were written to perform the calculation of the large aperture results. One calculates the large aperture angle of arrival and linear phase error; the other calculates the error between the large and small aperture results. Both programs use the Von Karmann spectrum.

The large aperture angle of arrival program shown in listing (B5) performs four nested integrations to calculate κ_{0x}, $\langle\alpha_x^2\rangle$ and $\langle\Delta^2\kappa\rangle$. Gaussian quadrature integration of different orders is used in each case. The Gaussian subroutines are contained in the IBM Scientific Subroutine Package. They are essentially the same as DQG96 used earlier except the weighting factors and arguments, are contained in the subprograms. The large aperture error program evaluates the error function $\Delta(\kappa R)$ in a similar manner.

The input data for both programs is read with a namelist format. The variables are

XCAPLO	= L_0,	the outer scale in meters
XLO	= ℓ_0,	the inner scale in meters
RCAP	= R,	the aperture radius in meters
A	= A,	normalizing constant in Von Karmann spectrum
XLAMB	= λ,	wavelength in meters
XL	= L,	range in meters.

After each calculation a new data card is read. The program is terminated by setting XLAMB = 0.

LISTING B-5

```
C **** 10.6 MICRON PROPAGATION PHENOMENA PROGRAM ****
C **** ANGLE OF ARRIVAL AND ERROR CALCULATION
C       USING THE PHASE STRUCTURE FUNCTION ****
      IMPLICIT REAL*8 (D)
      COMMON R,RHO,GAMMA,RCAP
      COMMON /PHI/XKM,XKO
      COMMON /PHASE/XK,XL
      COMMON /APRAD/DDCAP
      EXTERNAL DINT1,DDEN,DERFCT
      NAMELIST/INPUT/XCAPLO,XLO,RCAP,A,XLAMB,XL
      PI=3.1415927
      WRITE(6,1000)
 1000 FORMAT('1ANGLE OF ARRIVAL CALCULATION USING PHASE STRUCTURE FUNCTI
     1ON'/' (RESULTS NORMALIZED TO CN**2)')
 1005 FORMAT(' RANGE=',1PE11.3,' M',5X,'INNER SCALE= ',E10.3,' M',5X,
     1'OUTER SCALE= ',E10.3,' M',5X,'A= ',E10.3,5X,'LAMBDA= ',E10.3,' M'
     2)
  100  READ(5,INPUT)
      WRITE(6,1005)XL,XLO,XCAPLO,A,XLAMB
      IF(XLAMB.EQ.0.)CALL EXIT
      XK=6.28318/XLAMB
      XKM=5.92/XLO
      DRCAP=RCAP
      XKO=A/XCAPLO
      CALLDQG12(0.D0,DRCAP,DINT1,DRINT1)
      CALLDQG12(0.D0,DRCAP,DDEN,DRDEN)
      GXO=-4.*PI**2*XK**2*XL*DRINT1/(PI*DRDEN**2)
      AOA=GXO/XK**2
      DDCAP=2.*DRCAP
      CALL DQG12(0.,DDCAP,DERFCT,DRNT1)
      DERROR=4.*PI*XK**2*XL*DRNT1/DRCAP**2
      DPSERR=DERROR/XK**2
      WRITE(6,1001)DRCAP,GXO,DERROR,AOA,DPSERR
 1001 FORMAT(' APERTURE RADIUS= ',1PE10.3,5X,'KAPPA X= ',E10.3,5X,'ERROR
     1= ',E10.3/33X,'MEAN SQUARE ANGLE OF ARRIVAL= ',E10.3,5X,'ERROR= ',
     2E10.3)
      GO TO 100
      END
```

```
      DOUBLE PRECISION FUNCTION DERFCT(DR)
C LINEAR PHASE ERROR FUNCTION
      IMPLICIT REAL*8 (D)
      EXTERNAL DFCT1
      COMMON R,RHO,GAMMA,RCAP
      COMMON /APRAD/DDCAP
      RHO=DR
      DARG=DR/DDCAP
      CALL INTGRL(1.E-02,1.0E-01,6,DFCT1,DINT1)
      DFL=6.*DARCOS(DARG)-(14.*DARG-8.*DARG**3)* DSQRT(1.-DARG**2)
      DERFCT=DR*DFL*DINT1
      RETURN
      END


      DOUBLE PRECISION FUNCTION DFCT1(DXKAP)
C INTEGRAND FOR CALCULATING PHASE STRUCTURE FUNCTION FOR DERFCT
      IMPLICIT REAL*8 (D)
      COMMON R,RHO,GAMMA,RCAP
      COMMON /PHI/XKM,XKO
      COMMON /PHASE/XK,XL
      ARG3=(DXKAP/XKM)**2
      IF(ARG3.GT.174.)GOTO 100
      DARG1=DXKAP**2*XL/XK
      ARG2=DXKAP*RHO
      IF(DARG1.EQ.0.)GO TO 100
      XKAP=DXKAP
      DFCT1=(1.-BESO(ARG2))*(1.+DSIN(DARG1)/DARG1)*PHIN(XKAP,XKM,XKO)*
     1DXKAP
      RETURN
  100 DFCT1=0.
      RETURN
      END


      DOUBLE PRECISION FUNCTION DINT1(DR)
C R INTERGRAND
      IMPLICIT REAL*8 (D)
      COMMON R,RHO,GAMMA,RCAP
      EXTERNAL DINT2
      R=DR
      DRCAP=RCAP
      CALL DQG8 (0.D0,DRCAP,DINT2,DRINT2)
      DINT1=DRINT2*R*R*W(R)
      RETURN
      END
```

```
      DOUBLE PRECISION FUNCTION DINT2(DRHO)
C RHO INTEGRAND
      IMPLICIT REAL*8 (D)
      COMMON R,RHO,GAMMA,RCAP
      EXTERNAL DINT3
      RHO=DRHO
      CALL DQG4 (0.D0,3.1415927D0,DINT3,DRINT3)
      DINT2=DRINT3*RHO*RHO*W(RHO)
      RETURN
      END



      DOUBLE PRECISION FUNCTION DINT3(DGAMMA)
C GAMMA INTEGRAND
      IMPLICIT REAL*8 (D)
      COMMON R,RHO,GAMMA,RCAP
      EXTERNAL DFCT
      GAMMA=DGAMMA
      CALL INTGRL(1.0E-03,1.E-02,7,DFCT,DPHASE)
      DINT3=DPHASE*COS(GAMMA)
      RETURN
      END



      DOUBLE PRECISION FUNCTION DFCT(DKAP)
C PHASE STRUCTURE FUNCTION INTEGRAND
      IMPLICIT REAL*8 (D)
      COMMON R,RHO,GAMMA,RCAP
      COMMON /PHASE/XK,XL
      COMMON /PHI/XKM,XKO
      ARG=DKAP*SQRT(R*R+RHO*RHO-2.*RHO*R*COS(GAMMA))
      XKAP=DKAP
      DARG1=XKAP**2*XL/XK
      DFCT=(1.-BESO(ARG))* PHIN(XKAP,XKM,XKO)*XKAP*(1.+DSIN(DARG1)/DARG1
     1)
      RETURN
      END
```

```
      FUNCTION PHIN(XKAP,XKM,XKO)
C REFRACTIVE INDEX FLUCTATION SPECTRUM
      TEST=(XKAP/XKM)**2
      IF(TEST.GT.174.)GO TO 100
      A=EXP(-TEST)
      B=(XKAP**2+XKO**2)**(11./6.)
      TEST1=ALOG10(A)-ALOG10(B)
      IF(ABS(TEST1).GT.30.)GO TO 100
      PHIN=.033*A/B
      RETURN
  100 PHIN=0.
      RETURN
      END



      FUNCTION W(R)
C APERTURE WEIGHTING FUNCTION
      W=1.
      RETURN
      END



      DOUBLE PRECISION FUNCTION DDEN(DR)
C DENOMINATOR INTEGRAND
      IMPLICIT REAL*8 (D)
      R=DR
      DDEN=DR**3*W(R)
      RETURN
      END



      SUBROUTINE INTGRL(XLS,XUS,NINT,FCT,YINT)
C ORDER OF MAGNITUDE INTEGRATION ROUTINE
      REAL*8 YINT,YINTG,FCT,XL,XU
      EXTERNAL FCT
      XL=XLS
      XU=XUS
      CALL DQG32(XL,XU,FCT,YINT)
      DO 300 J=1,NINT
      XL=XU
      XU=XU*10.
      CALL DQG32(XL,XU,FCT,YINTG)
      YINT=YINT+YINTG
  300 CONTINUE
      RETURN
      END
```

```
      FUNCTION BESO(X)
C J0(X)
      IF(X.GT.3.)GO TO 100
      Y=X/3.
      BESO=1.0-2.24999*Y**2+1.26562*Y**4-.316387*Y**6+.044447*Y**8-3.944
     14E-3*Y**10+2.10000E-4*Y**12
      RETURN
 100  Y=3./X
      THETA=X-.785398-.041663*Y-3.954E-05*Y**2+2.62573E-3*Y**3-5.4125E-4
     1*Y**4-2.9333E-4*Y**5+1.3558E-4*Y**6
      FO=.7978846-7.7E-7*Y-5.5274E-3*Y**2-9.512E-5*Y**3+1.37237E-3*Y**4-
     17.2805E-4*Y**5+1.4476E-4*Y**6
      BESO=FO*COS(THETA)/SQRT(X)
      RETURN
      END
```

LISTING B-6

```
C **** 10.6 MICRON PROPAGATION PHENOMENA PROGRAM ****
C **** ANGLE OF ARRIVAL      ERROR CALCULATION
C       USING THE PHASE STRUCTURE FUNCTION ****
      IMPLICIT REAL*8 (D)
      COMMON R,RHO,GAMMA,RCAP,XKAP
      COMMON /PHI/XKM,XKO
      COMMON /PHASE/XK,XL
      EXTERNAL DFCT
      NAMELIST/INPUT/XCAPLO,XLO,RCAP,A,XLAMB,XL
      PI=3.1415927
      WRITE(6,1000)
 1000 FORMAT('1ANGLE OF ARRIVAL CALCULATION USING PHASE STRUCTURE FUNCTI
     1ON'/' (RESULTS NORMALIZED TO CN**2)')
 1005 FORMAT('0RANGE=',1PE11.3,' M',5X,'INNER SCALE= ',E10.3,' M',5X,
     1'OUTER SCALE= ',E10.3,' M',5X,'A= ',E10.3,5X,'LAMBDA= ',E10.3,' M'
     2)
  100  READ(5,INPUT)
      WRITE(6,1005)XL,XLO,XCAPLO,A,XLAMB
      XK=6.28318/XLAMB
      XKM=5.92/XLO
      XKO=A/XCAPLO
      DRCAP=RCAP
      CALL INTGRL(1.0E-03,1.E-02,7,DFCT,DELAOA)
      DELTAA= 4.*PI**2*XL*DELAOA
      WRITE(6,1001)DRCAP,DELTAA
 1001 FORMAT(' APERTURE RADIUS= ',1PE10.3,5X,'DELTA AOA= ',E10.3,/)
      GO TO 100
      END



      DOUBLE PRECISION FUNCTION DFCT(DKAP)
C PHASE STRUCTURE FUNCTION INTEGRAND
      IMPLICIT REAL*8 (D)
      REAL*8 AOASA,AOALA,BES1X,AOAL
      COMMON R,RHO,GAMMA,RCAP,XKAP
      COMMON /PHASE/XK,XL
      COMMON /PHI/XKM,XKO
      EXTERNAL DINT1
      XKAP=DKAP
      DARG1=XKAP**2*XL/XK
      DRCAP=RCAP
      CALLDQG12(0.D0,DRCAP,DINT1,DRINT1)
      AOALA=-16.*DRINT1/(3.141592*DRCAP**8)
      AOAL=AOALA/DKAP**2
      AOASA=BES1X(DKAP*DRCAP)/2.0000000000000D0
      DIF=AOASA-AOAL
      DFCT=DIF*DKAP**3*PHIN(XKAP,XKM,XKO)*(1.+DSIN(DARG1)/DARG1)
      RETURN
      END
```

```
      DOUBLE PRECISION FUNCTION DINT1(DR)
C R INTERGRAND
      IMPLICIT REAL*8 (D)
      COMMON R,RHO,GAMMA,RCAP,XKAP
      EXTERNAL DINT2
      R=DR
      DRCAP=RCAP
      CALL DQG8 (0.D0,DRCAP,DINT2,DRINT2)
      DINT1=DRINT2*R*R
      RETURN
      END



      DOUBLE PRECISION FUNCTION DINT2(DRHO)
C RHO INTEGRAND
      IMPLICIT REAL*8 (D)
      COMMON R,RHO,GAMMA,RCAP,XKAP
      EXTERNAL DINT3
      RHO=DRHO
      CALL DQG4 (0.D0,3.1415927D0,DINT3,DRINT3)
      DINT2=DRINT3*RHO*RHO
      RETURN
      END



     DOUBLE PRECISION FUNCTION DINT3(DGAMMA)
C GAMMA INTEGRAND
      IMPLICIT REAL*8 (D)
      REAL*8 BESO
      COMMON R,RHO,GAMMA,RCAP,XKAP
      EXTERNAL DFCT
      GAMMA=DGAMMA
      DPHASE=1.000000000000000-BESO(XKAP*DSQRT(R**2+RHO**2-2.*R*RHO*
     1DCOS(DGAMMA)))
      DINT3=DPHASE*COS(GAMMA)
      RETURN
      END
```

```
      FUNCTION PHIN(XKAP,XKM,XKO)
C REFRACTIVE INDEX FLUCTATION SPECTRUM
      TEST=(XKAP/XKM)**2
      IF(TEST.GT.174.)GO TO 100
      A=EXP(-TEST)
      B=(XKAP**2+XKO**2)**(11./6.)
      TEST1=ALOG10(A)-ALOG10(B)
      IF(ABS(TEST1).GT.30.)GO TO 100
      PHIN=.033*A/B
      RETURN
  100 PHIN=0.
      RETURN
      END
```

```
        SUBROUTINE INTGRL(XLS,XUS,NINT,FCT,YINT)
  C ORDER OF MAGNITUDE INTEGRATION ROUTINE
        REAL*8 YINT,YINTG,FCT,XL,XU
        EXTERNAL FCT
        XL=XLS
        XU=XUS
        CALL DQG16(XL,XU,FCT,YINT)
        DO 300 J=1,NINT
        XL=XU
        XU=XU*10.
        CALL DQG16(XL,XU,FCT,YINTG)
        YINT=YINT+YINTG
    300 CONTINUE
        RETURN
        END
```

```
      FUNCTION BESO(X)
      REAL*8 BESO,X,Y,FO,THETA
C JO(X)
      IF(X.GT.3.)GO TO 100
      Y=X/3.
      BESO=1.0-2.24999*Y**2+1.26562*Y**4-.316387*Y**6+.044447*Y**8-3.944
     14E-3*Y**10+2.10000E-4*Y**12
      RETURN
  100 Y=3./X
      THETA=X-.785398-.041663*Y-3.954E-05*Y**2+2.62573E-3*Y**3-5.4125E-4
     1*Y**4-2.9333E-4*Y**5+1.3558E-4*Y**6
      FO=.7978846-7.7E-7*Y-5.5274E-3*Y**2-9.512E-5*Y**3+1.37237E-3*Y**4
     17.2805E-4*Y**5+1.4476E-4*Y**6
      BESO=FO*DCOS(THETA)/DSQRT(X)
      RETURN
      END
```

```
      FUNCTION BESIX(X)
      REAL*8 THETA,F1,Y,BESIX,X
C J1(X)/X
      IF(X.GT.3.)GO TO 100
      Y=X/3.
      BESIX=.50-.562499*Y**2+.210935*Y**4-3.95428E-2*Y**6+4.43319E-3*Y**
     18-3.1761E-4*Y**10+1.109E-5*Y**12
      RETURN
  100 Y=3./X
      THETA=X-2.35619+.124996*Y+5.650E-05*Y**2-6.37879E-3*Y**3+7.4348E-4
     1*Y**4+7.9824E-4*Y**5-2.9166E-4*Y**6
      F1=.797884+1.56E-6*Y+1.65966E-2*Y**2-1.7105E-4*Y**3-2.49511E-3*Y**
     14+1.13653E-3*Y**5-2.0033E-4*Y**6
      BESIX=F1*DCOS(THETA)/(X*DSQRT(X))
      RETURN
      END
```

REFERENCES

1. Muchmore, R.B. and Wheelon, A.D., "Line of Sight Propagation Phenomenon 1, Ray Treatment," Proc. IEEE, 43, p. 1437, (1955).

2. Chernov, L.A., Wave Propagation in a Medium with Random Homogeneities, McGraw Hill, (1960).

3. Beckmann, P., "Signal Degeneration in Laser Beams Propagated Through a Turbulent Atmosphere," U.S. Nat. Bureau Stand. Jour. Res. in Radio Science, 69, p. 629, (1965).

4. Tatarski, V.I., Wave Propagation in a Turbulent Medium, Dover, (1967).

5. Tatarski, V.I., Wave Propagation in a Turbulent Atmosphere, Nanka, Moscow, (1967).

6. Strobehn, J.W., "Line of Sight Propagation Through the Turbulent Atmosphere," Proc. IEEE, 56, p. 1301, (1968).

7. Strobehn, J.W. and Clifford, S.F., "Polarization and Angle of Arrival Fluctuations for a Plane Wave Propagated Through a Turbulent Medium," IEEE PGAP, 15, p. 416, (1967).

8. Hufnagel, R.E. and Stanely, N.R., "Modulation Transfer Function Associated with Image Transmission Through Turbulent Media," J. Opt. Soc. Am., 54, p. 52, (1964).

9. Fried, D.L., "Statistics of a Geometric Representation of Wavefront Distortion," J. Opt. Soc. Am., 56, p. 1372, (1966).

10. Heidbreder, G.R., "Image Degradation with Random Wavefront Tilt Compensation," IEEE PGAP, 15, p. 90, (1967).

11. Kallistratova, M.A. and Kon, A.I., "Fluctuations in the Angle of Arrival of Light Waves from an Extended Source in a Turbulent Atmosphere," Radio Phys., 9, p. 636, (1966), (9, p. 1100, (1966)).

12. Kallistratova, M.A., "Fluctuations in the Direction of Propagation of Light Waves in an Inhomogeneous Turbulent Medium," Radio Phys., 9, p. 33, (1966), (9, p. 50, (1966)).

13. Chernov, L.A., op. cit., p. 18.

14. Coulman, C.E., "Dependence of Image Quality on Horizontal Range in a Turbulent Atmosphere," J. Opt. Soc. Am., 56, p. 1232, (1966).

15. Coulman, C.E. and Hall, D.N., "Optical Effects of Thermal Structure in the Lower Atmosphere," Appl. Opt., 6, p. 497, (1967).

16. Carlson, F.P. and Ishimaru, A., "Propagation of Spherical Waves in Locally Homogeneous Random Media," J. Opt. Soc. Am., 59, p. 319, (1969).

17. Strobehn, J.W., "The Feasibility of Laser Experiments for Measuring the Permitivity Spectrum of the Turbulent Atmosphere," Journal Geophysical Res., 75, p. 1067, (1970).

18. Tatarski, V.I., "Second Approximation in the Problem of Wave Propagation in a Medium with Random Inhomogeneities," Iz. VUZ Radio Fig. 5, p. 490, (1962).

19. DeWolf, D.A., "Wave Propagation Through Quasi-Optical Irregularities," J. Opt. Soc. Am., 55, p. 812, (1965).

20. Brown, W.P., Jr., "Validity of the Rytov Approximation in Optical Propagation Calculations," J. Opt. Soc. Am., 56, p. 1045, (1966).

21. Fried, D.L., "Test of Rytov Approximation," J. Opt. Soc. Am., 57, p. 268, (1967).

22. DeWolf, D.A., "Validity of Rytov's Approximation," J. Opt. Soc. Am., 57, p. 1067, (1967).

23. Brown, W.P., Jr., "Validity of Rytov's Approximation," J. Opt. Soc. Am., 57, p. 1539, (1967).

24. Strobehn, J.W., "Comments on Rytov's Method," J. Opt. Soc. Am., 58, p. 139, (1968).

25. Keller, J.B., "Accuracy and Validity of the Born and Rytov Approximations," J. Opt. Soc. Am., 59, p. 1003, (1969).

26. Sancer, M.I. and Varvatsis, A.D., "A Comparison of the Born and Rytov Methods," IEEE, 58, p. 140, (1970).

27. Bouricius, G.M.B. and Clifford, S.F., "Experimental Study of Atmospherically-Induced Phase Fluctuations in an Optical Signal," to be published, J. Opt. Soc. Am., November, 1970.

28. Lutomirski, R.F. and Yura, H.T., "Modulation Transfer Function and Phase Structure Function of an Optical Wave in a Turbulent Medium," J. Opt. Soc. Am., 59, p. 999, (1969).